Traffic Management in Mixed Autonomy with CAVs: Sensing, Signal Optimization, and Trajectory Control

by

Fan Wu

A thesis submitted in partial fulfillment of the requirements for the degree of

Doctor of Philosophy

in

Transportation Engineering

Department of Civil and Environmental Engineering

University of Alberta

Abstract

Global vehicle numbers continue to climb alongside population growth and economic expansion, resulting in increased traffic congestion, air pollution, and accidents. Major cities worldwide estimate that drivers lose considerable working hours annually to congestion, leading to wasted time, fuel, and increased air pollution levels which impact road users' comfort. Consequently, addressing traffic congestion, reducing vehicle emissions, and ensuring road safety are imperative for sustainable urban development. Intelligent transportation systems (ITS) are vital for smart cities and sustainable urban development, leveraging emerging technologies such as the connected vehicle (CV) technology, the automated vehicle (AV) technology, the connected and automated vehicle (CAV) technology, the vehicle-to-everything (V2X) communication, and the mobile edge computing (MEC). These innovations integrate vehicle automation, real-time communication, and extensive computing resources, offering opportunities for improved traffic management and more efficient real-time traffic control.

Conventional human-driven vehicles (HDVs) and pedestrians are still key players in shaping traffic dynamics today. As such, we must acknowledge the reality of an extended coexistence among various road users, including conventional HDVs, connected vehicles (CVs), connected automated vehicles (CAVs), pedestrians, and cyclists, creating what is termed as a 'mixed-autonomy' or 'mixed-traffic' system. However, there is a tendency to overlook the benefits

of pedestrians or conventional vehicles when adopting new CAV technology. Therefore, while emerging technologies hold promise, integrating them into real-world transportation scenarios is essential for effectively managing this dynamic traffic system.

Given the complexities of mixed-autonomy traffic and the advancements of CAV technology, this dissertation focuses on enhancing traffic management strategies. It aims to achieve this through the development of methods for predicting and sensing traffic states, optimizing traffic signal control, and implementing trajectory control approaches for CAVs. The overall goal is to ensure road users' safety, improve traffic efficiency, reduce vehicular emissions within mixed-autonomy traffic scenarios, and consider the benefits of emerging technologies for all types of road users in mixed traffic. To achieve this goal, the research is structured into three main parts:

The first part develops a precise and efficient method for estimating traffic states using sparse trajectory data from CVs on mixed traffic scenarios involving conventional HDVs and CVs or CAVs, suitable for various road segments such as freeways, highways, or urban arterials. The goal is to predict comprehensive traffic states for both HDVs and CVs, supporting subsequent signal optimization and trajectory control. The study introduces a novel model that utilizes Gaussian processes (GP). By employing a kernel rotation re-parametrization scheme, a standard isotropic GP kernel is transformed into an anisotropic one, allowing for better modeling of traffic wave propagation in flow data. This method effectively estimates traffic states from sparse sensing data collected from fixed sensors, probe vehicles, and CVs. The results demonstrate superior performance of the estimating model in terms of accuracy, efficiency, and robustness.

The second part introduces adaptive signal optimization methods for mid-

block crossings, tailored for scenarios involving conventional HDVs and pedestrians, as well as scenarios with a mix of HDVs, CVs, and pedestrians. This aims to enhance traffic efficiency along an arterial road, particularly focusing on the urban arterial level with a midblock crossing. It ensures pedestrians' safety while minimize the impact of frequent crossing requests on the arterial traffic flow. The proposed models utilize the signal control status of adjacent intersections and leverage real-time vehicle location information obtained from CVs to optimize pedestrian waiting time. The optimization model ensures pedestrian safety while enhancing signal coordination between the midblock crossing and downstream intersections. The approach effectively reduces both vehicle and pedestrian delays.

The final section provides an innovative approach to trajectory control specifically tailored for CAVs, with a focus on improving fuel efficiency, safety, and overall traffic performance. This method is developed to handle diverse traffic scenarios involving a combination of HDVs, CAVs, and pedestrians at intersections. The trajectory planning framework integrates a deep reinforcement learning (DRL) algorithm with a multi-agent control strategy. Using the deep deterministic policy gradient (DDPG) algorithm, the proposed method enables CAVs to learn optimal control policies within the complexities of mixed traffic environments. Through thorough evaluations, the proposed framework demonstrates significant enhancements in traffic efficiency, a reduction in vehicle emissions, and an improvement in traffic safety.

The dissertation presents comprehensive research on traffic management within mixed-autonomy traffic environments. The models and algorithms introduced offer effective means to enhance traffic efficiency, minimize vehicle emissions, and prioritize safety. The findings contribute to methodological and practical insights into sustainable and efficient mixed traffic management.

Preface

The content covered in Chapters 3 through 5 encompasses three articles that have been published, or are under review in mainstream peer-reviewed journals within the field of transportation engineering, and have been presented at conferences. I declare that I am the first author of these articles, having contributed to various aspects including idea proposing, model and experiment design, model implementation and testing, and manuscript composition. Prof. Tony Qiu is my supervisor and provides guidance, comments, and editorial revisions to the articles. The list detailing the published, or presented articles relevant to the dissertation is provided below.

1. **Refereed Journal Articles:**

- **Wu, F.**, Cheng, Z., Chen, H., Qiu, T. Z.*, and Sun, L. (2024). Traffic State Estimation from Vehicle Trajectories with Anisotropic Gaussian Processes. *Transportation Research Part C: Emerging Technologies, 163, 104646.* DOI: 10.1016/j.trc.2024.104646. (Prepared data, code and demo are available at https://github.com/Lucky-Fan/GP_TSE)

- **Wu, F.**, Chen, H., Hou, K., Cheng, Z., and Qiu, T. Z*. (2022). Adaptive Pushbutton Control for Signalized Pedestrian Midblock Crossings. *Journal of Transportation Engineering, Part A: Systems, 148(4), 04022011.* DOI: 10.1061/JTEPBS.0000659. (Prepared data, code and demo are available at https://github.com/Lucky-Fan/AMCCs)

- **Wu, F.**, Chen, H., and Qiu, T. Z*. CAV Trajectory Control at Mixed-traffic Intersection: a Deep Reinforcement Learning Approach. *Under Review in IEEE Transactions on Intelligent Transportation Systems.*

2. Refereed Conference Articles:

- **Wu, F.**, Cheng, Z., Chen, H., Qiu, T. Z.*, and Sun, L. Traffic State Estimation from Vehicle Trajectories with Anisotropic Gaussian Processes, in *Transportation Research Board 103rd Annual Meeting*, Washington, D.C., January 2024.

- **Wu, F.**, Chen, H., Hou, K., Qiu, T. Z*. Adaptive Pushbutton Control for Signalized Pedestrian Midblock Crossings: toward an Arterial Traffic-efficient Scheme, in *Transportation Research Board 101st Annual Meeting*, Washington, D.C., January 2022.

Acknowledgements

Time has flown by, and as I reflect on the past five years, I can't help but feel a sense of nostalgia for my time at the University of Alberta. Despite the challenges and busy days, I cherish the memories of my struggles, efforts, time of happiness, moments of bitterness, flashes of brilliance, and even the occasional foolishness. I am deeply grateful for the opportunity to pursue my Ph.D. degree and extend my heartfelt thanks to everyone who has supported me throughout this journey.

First and foremost, I wish to extend my heartfelt gratitude to my supervisor, Prof. Tony Qiu, for his unwavering guidance and support throughout my Ph.D. journey. Prof. Qiu's dedication to his work and tireless efforts have motivated me to strive for excellence in my doctoral studies. I am particularly grateful for his flexibility and understanding, which have allowed me to explore my research interests and hone my skills effectively. Prof. Qiu's expertise and remarkable achievements have played a pivotal role in securing substantial funding for our research endeavors. I consider myself incredibly fortunate to have had the opportunity to work under his mentorship.

I would like to extend my appreciation to my supervisor and supervisory committee members, Dr. Tae J. Kwon and Dr. Karim EI-Basyouny, for their feedback during our annual meetings. Additionally, I would like to thank Dr. Mahdi Shahbakhti, Dr. Stephen Wong, Dr. Tae J. Kwon, Dr. Karim EI-Basyouny, and Dr. Tony Qiu for their participation in my candidacy exam. Their collective expertise and input have played a crucial role in shaping my research. I am also grateful to Dr. Qipei Mei for chairing my candidacy exam.

Furthermore, I extend my heartfelt thanks to my defense examiners: my

Contents

List of Tables

List of Figures

List of Acronyms

ACC	Adaptive Cruise Control
ADAS	Advanced Driver Assistance System
AIM	Autonomous Intersection Management
AI	Artificial Intelligence
AMCC	Adaptive Midblock Crossing Control
AOG	Arrival On Green
AOR	Arrival On Red
ARD	Automatic Relevance Determination
ASM	Adaptive Smoothing Interpolation
AV	Automated Vehicle
BSM	Basic Safety Message
CACC	Cooperative Adaptive Cruise Control
CAV	Connected and Automated Vehicle
CDF	Cumulative Distribution Function
CV	Connected Vehicle
C-V2X	Cellular-Vehicle to Everything
DPG	Deterministic Policy Gradient
DDPG	Deep Deterministic Policy Gradient
DL	Deep Learning
DQN	Deep Q-Network
DRL	Deep Reinforcement Learning
DSRC	Dedicated Short-Range Communication
ELBO	Evidence Lower Bound
EPA	Environmental Protection Agency
FCFS	First Come First Serve
Fixed	Fixed Phase and Timing Control

GHG	Greenhouse Gas
GLOSA	Green Light Optimized Speed Advisory
GP	Gaussian Process
GP-ARD	Gaussian Process regression with standard Automatic Relevance Determination kernels
GP-rotated	Gaussian Process based on rotated kernels
HDV	Human-Driven Vehicle
HighD	Highway Drone Dataset
HAWK	High Intensity Activated CrossWalK
ICT	Information and Communication Technology
IDM	Intelligent Driver Model
IEEE	Institute of Electrical and Electronics Engineers
IoT	Internect of Things
IoV	Internect of Vehicles
ITS	Intelligent Transportation System
LKAS	Lane Keeping Assist System
LTE	Long Term Evolution
MAE	Mean Absolute Error
MBVE	Model-Based Value Estimation
MDP	Markov Decision Process
MEC	Mobiel Edge Computing
MILP	Mixed-interger Linear Programing
ML	Machine Learning
MML	Maximum Marginal Likelihood
MPC	Model Predictive Control
MUTCD	Manual on Uniform Traffic Control Devices
NGSIM	Next Generation Simulation dataset
OBU	On-Board Unit
PA	Pedestrian Actuated
PCD	Purdue Coordination Diagram
PC5	Direct communication interface, terminal-to-terminal
Pelican	Pedestrian light-controlled
PET	Post Encroachment Time
P-GP-rotated	Pre-trained Gaussian Process based on rotated kernels
PHB	Pedestrian Hybrid Beacon

POG	Percent On Green
Puffin	Pedestrian user-friendly intelligent
PWT	Pedestrian Waiting Time
RL	Reinforcement Learning
RMSE	Root Mean Square Error
RSU	Road-Side Unit
SAE	Society of Automotive Engineers
SOFT	Smoothness Of the Flow of Traffic
SPaT	Signal Phase and Timing
STH-LRTC	Spatiotemporal Hankel Low-Rank Tensor Completion
SUMO	Simulation of Urban MObility
TMC	Traffic Management Center
TMS	Traffic Management System
TSE	Traffic State Estimation
TTC	Time-To-Collision
Uu	Cellular network communication interface, terminal and base station
VSGP	Variational Sparse Gaussian Process
V2C	Vehicle-to-Cloud
V2I	Vehicle-to-Infrastructure
V2X	Vehicle-to-Everything
V2V	Vehicle-to-Vehicle
3GPP	The 3rd Generation Partnership Project

Chapter 1

Introduction

1.1 Background

The transportation system holds a significant role in the life of residents, economic growth, and urban development. Comprising various modes like road, rail, air, and water, it forms a complex network vital for societal functioning. Among these modes, road transportation stands as the most widely utilized, facilitating daily travel for residents worldwide. By 2023, the global vehicle count stands at approximately 1.475 billion, impacting a vast portion of the world's population [1]. This number continues to rise alongside with the population growth and the economic expansion. However, the increasing number of vehicles also brings a series of problems, such as traffic congestion, air pollution, and traffic accidents. For instance, in Canada, the nation's largest city, Toronto, endured an annual loss of 118 hours, ranking as the 6th highest delay city in 2022 due to traffic congestion [2]. This congestion not only results in time and fuel wastage but also contributes to increased air pollution levels. According to the United States Environmental Protection Agency (EPA), the transportation sector emerged as the largest contributor to greenhouse gas (GHG) emissions in 2021, accounting for approximately 29% of total emissions [3]. Therefore, traffic congestion mitigation, vehicle emission reduction, and the protection of all road participants' safety are crucial for sustainable urban development.

Many cities worldwide launched the smart city initiative to address these

challenges. Smart cities leverage information and communication technologies (ICT) to enhance urban management and services, aiming to improve the quality of life for residents, reduce environmental impact, and promote economic growth [4]. The transportation sector is a key focus of smart city initiatives, to improve traffic efficiency, reduce emissions, and enhance road safety. To achieve these objectives, smart cities have implemented various technologies, such as intelligent transportation systems (ITS) utilizing some emerging technologies. These technologies encompass a range of advancements, such as connected vehicle (CV), automated vehicle (AV), connected and automated vehicle (CAV), vehicle-to-everything (V2X) communication, and mobile edge computing (MEC). These innovations integrate vehicle automation, communication, computing resources, and road infrastructure, paving the way for the next generation of ITS.

Traffic management system (TMS) represents a crucial branch of ITS, garnering significant attention from both researchers and engineers. For example, signal coordination and optimization has been one of the main techniques for improving the performance of arterial traffic management. In the past decades, much research has been done to improve the performance of signal coordination, such as actuated coordinated control. Most traffic management strategies rely on loop detectors and cameras to collect data and improve the performance of signal timing, and most methods are based on offline optimizations. Therefore, existing methods are insufficient in capturing real-time information of each vehicle along an arterial and only give attention to simplified scenarios like macroscopic arterial traffic smoothness. There is still a long way to go for real-time traffic management.

Emerging technologies generate a substantial volume of data, including real-time trajectory data, which serves as a valuable resource for developing advanced traffic management strategies. Examples include optimizing traffic signal control and estimating traffic states using sensor data. Effective and real-time traffic management requires accurate and timely knowledge of traffic state over the entire network. However, current fixed sensors like loop detec-

2

tors are point sensors and are unable to provide global vehicle information. Although we can collect data from mobile vehicles and infrastructure with the support of V2X technology, the challenge is that not all vehicles are equipped with V2X devices. Therefore, it is essential to develop efficient and robust sensing methods to capture the full map of real-time traffic information and improve traffic management strategies from limited sensing trajectories from probe vehicles or connected vehicles (CVs).

Moreover, it's important to note that the scope of ITS extends beyond CAV alone. Conventional human-driven vehicles (HDVs) and pedestrians also play pivotal roles in influencing traffic dynamics and transportation infrastructure today, and they should be served equally. According to [5], automated vehicles (AVs) or connected and automated vehicles (CAVs) may not dominate the traffic stream until the 2040s to 2050s, indicating a prolonged period of coexistence between conventional HDVs, CVs, CAVs and other road users within what can be termed a 'mixed autonomy' traffic system.

While these emerging technologies offer great potential for revolutionizing the transportation system, their integration also presents new challenges. Therefore, it is essential to seamlessly integrate these new techniques with existing transportation domain knowledge to thoroughly comprehend and address traffic issues. This study includes tackling the complexities of mixed-autonomy traffic systems and developing more efficient and sustainable traffic management and control strategies to adapt to these transformative changes.

1.2   Research Motivations and Questions

CVs have introduced the convenience of accessing real-time vehicle data and hold promise for enhancing traffic management strategies. However, their deployment is still in its early stages, with a low penetration rate. Additionally, the coexistence of CAVs, CVs, and HDVs within the same traffic environment is an ongoing reality that must be addressed. Managing this dynamic traffic ecosystem is crucial. In essence, while emerging technologies offer potential

solutions, it is imperative to integrate them with transportation engineering knowledge to effectively address traffic challenges. This approach ensures the optimization of traffic systems. Consequently, this section outlines the research motivations and questions.

1.2.1 Research motivations

- **Understanding the mixed autonomy traffic system with CAVs.** Most of the research about CAV controls is based on individual vehicle control, which is not enough for the real-world traffic system which covers multiple vehicles; most of the research about intersection/segment traffic operation or driving behavior is based on the assumption that all vehicles are CAVs, which is also not practical for the real-world traffic system. Consequently, most current traffic management algorithms are based on the assumption of a 100% CAV market penetration rate or a fully traditional traffic environment. According to [5] and [6], HDVs, CVs, and CAVs will coexist for the next 20-30 years, with the market penetration rate of CAVs not expected to reach 100% until the 2040s to 2050s. Therefore, it is crucial to comprehend the mixed autonomy traffic system to inform data sensing, signal optimization, and vehicle control strategies effectively in real-world traffic scenarios.

- **Describing the heterogeneous and dynamic nature of the mixed autonomy traffic system.** The mixed autonomy traffic system comprises a multitude of interacting agents, representing various types of road users. These agents range from intelligent entities like CAVs and traffic signals to physical entities such as HDVs, pedestrians, and cyclists (smart entities as well but less controllable than intelligent entities), contributing to the system's diversity. Additionally, each agent or road user possesses distinct preferences, leading to dynamic interactions within the transportation system. As highlighted by Wu et al. [7], the mixed autonomy system exhibits characteristics such as high stochasticity, cascading effects, nonlinearity, discontinuity, hybridity, and network

dynamics. Understanding the heterogeneity and dynamism of the mixed autonomy traffic system is essential for further development of efficient and sustainable traffic management strategies to improve mobility.

- **Leveraging limited sensing data from CVs and the limited intelligence from controllable AVs.** ITS heavily relies on traffic information collected from various detectors like loop detectors, video cameras, probe vehicles, and more recently, CVs. However, each detector type has its limitations regarding coverage and data completeness, often due to installation costs or data processing constraints. Despite advancements allowing flexible data collection from CVs and infrastructure through V2X technology, not all vehicles are equipped with V2X devices, limiting sensing data availability. However, comprehensive traffic information is essential for real-time and accurate traffic operation. Additionally, in a mixed autonomy traffic scenario with CAVs, the intelligent agents are constrained due to the low penetration rate of CAVs. These challenges impede the comprehensive capture of real-time traffic information and hinder the enhancement of traffic management strategies. Therefore, developing estimation methods to glean traffic state information from limited sensing data and devising intelligent control approaches leveraging the presence of limited CAVs are imperative for enabling more precise traffic control and management within ITS.

- **Enhancing advanced, efficient, and robust signal optimization and control methods for mixed autonomy traffic.** CAVs offer real-time trajectory data, providing a distinct advantage over aggregated data from fixed detectors. With their information access from multiple sensors and control capabilities, CAVs enable the perception of traffic flow, enhancing traffic signal optimization and trajectory control. Consequently, research on signal optimization and traffic control in CAV environments has gained traction. Studies by [8] argued that most work has primarily focused on traffic signal control within fully CAV environ-

ments, while some researchers have explored potential models for mixed traffic control, only emphasizing vehicle-side factors such as CAV driving policies and non-CAV driving behaviors. Control methods aimed at enhancing mixed traffic efficiency often entail a significant computational burden. Meanwhile, distributed control methods have been introduced to optimize the advantages of individual CAVs, however, the studies are even without due consideration for the benefits of non-CAVs [9]. Artificial intelligence (AI) can facilitate the approach development and solve complex real-world traffic scenarios better than analytical traffic models. Therefore, developing advanced, efficient, and robust signal optimization and control methods that adapt the mixed autonomy traffic system leveraging AI techniques is essential.

- **Ensuring the benefits extend to various types of road users in mixed autonomy traffic.** Among the advancements in ITS, particularly with the introduction of CV and AV, there's a clear acknowledgment of the benefits these vehicles can derive from advanced strategies. Their ability to sense, process, and act on information holds promise for enhancing performance. However, as we transition into a prolonged period of mixed autonomy traffic systems, encompassing HDVs, CVs, CAVs, and pedestrians, it's imperative to consider the diverse needs of all road users. Most of the concepts focus on tailoring policies and approaches to better serve CAVs, such as initiatives of dedicated lanes, however, we must not overlook the significance of pedestrians and HDVs in shaping traffic dynamics. Despite lacking the special characteristics to perceive and decide like connected and automated vehicles, these road users have their own rights in the transportation system. As such, the scope of ITS should not be limited to CAVs alone but should consider all entities on the road, both physical and intelligent, in order to better manage the traffic system. ITS should strive to enhance overall traffic management and try to ensure the benefits of emerging technologies for all road users involved.

1.2.2 Research questions

In light of the challenges and motivations outlined in the preceding section, this study aims to address the key research question: **How to achieve efficient and sustainable traffic management strategies covering sensing, signal optimization and trajectory control in the mixed autonomy with HDVs, CVs, CAVs, and pedestrians?** To better solve this research problem, it can be divided into the following sub-questions:

- How can we accurately predict comprehensive traffic states using sparse or limited vehicle trajectories gathered from CVs to facilitate signal optimization and trajectory control?

- How can real-time trajectory data from CVs, combined with V2I communication, effectively optimize signal control and enhance traffic efficiency along an arterial with a pedestrian crossing?

- How to propose an intelligent distributed trajectory control for effectively implementing CAV driving through an intersection with minimized delay, conflicts and emission?

- How can we achieve traffic efficiency and sustainability in a mixed autonomy environment with CAVs through traffic management strategies that consider various types of road users?

1.3 Research Scope and Objectives

To address the research questions outlined earlier, the dissertation defines its scope and objectives.

1.3.1 Research scope

- The research focuses on **mixed autonomy traffic scenarios**, encompassing HDVs, CVs, CAVs, and pedestrians. The methodology in Chapter 3 applies to mixed traffic with HDVs and CVs or HDVs and CAVs,

extending beyond CV trajectory data to include sparse data from other detectors. Chapter 4 addresses mixed traffic with HDVs, CVs, and pedestrians, along with proposing a method for scenarios with HDVs and pedestrians. The approach developed in Chapter 5 is designed for mixed traffic involving HDVs, CAVs, and pedestrians.

- The research addresses both **segment and intersection levels**. Chapter 3 introduces a methodology suitable for traffic flow on road segments of freeways, highways, or urban arterials. Chapter 4 concentrates on the urban arterial level, encompassing a road segment with two adjacent intersections. Chapter 5 delves into the intersection level.

- The research underscores **methodological innovations incorporating traffic characteristics**, drawing inspiration from artificial intelligence techniques. While not all chapters focus solely on control-based approaches, Chapter 5 advances an intelligent distributed trajectory control method rooted in reinforcement learning (RL). Chapter 3 employs a machine learning (ML) approach, specifically an anisotropic Gaussian process, for traffic state estimation. In Chapter 4, two adaptive push-button traffic signal optimization methods are introduced, grounded in optimization theory.

- The research primarily aims to **enhance traffic efficiency and sustainability**, particularly by reducing traffic delays, and vehicular emissions, and improving pedestrian crossing efficiency while ensuring safety. It is noticeable the focus is not on improving safety or reducing traffic accidents. Chapter 4 contributes to reducing traffic delays and enhancing pedestrian crossing efficiency while maintaining safety standards. Similarly, Chapter 5 focuses on reducing traffic delays and vehicular emissions while improving traffic safety.

- The research operates under the assumption that all CVs consistently provide **accurate information without communication loss**, a premise

applied in Chapter 3 and Chapter 4. Additionally, CAVs are presumed to be controllable and capable of adhering to control commands from the traffic management system, with the communication assumption mentioned above simultaneously.

- The research does not design the microscopic driving behaviors of HDVs, CVs, and CAVs, such as car-following and lane-changing behaviors. The research focuses on the **macroscopic traffic management** strategies like traffic operation and control.

1.3.2   Research objectives

This dissertation aims to enhance traffic sensing, improve traffic efficiency, and reduce vehicular emissions in mixed autonomy traffic scenarios. The specific objectives related to Chapter 3, 4 and 5 will be achieved by implementing traffic state estimation, traffic signal optimization, and vehicle trajectory control, leveraging V2X communication and CAV technology. The summary of objectives, structure, and primary contributions of the dissertation is diagrammed in Fig. 1.1.

- **Develop a precise and efficient traffic state estimation method** using sparse trajectory data from CVs to predict comprehensive traffic states for both HDVs and CVs, supporting subsequent signal optimization and trajectory control efforts.

- **Propose adaptive midblock crossing signal optimization methods** for scenarios featuring exclusively HDVs and pedestrians, as well as scenarios involving HDVs, CVs, and pedestrians to enhance traffic efficiency along an arterial, improving pedestrian crossing efficiency.

- **Provide an intelligent distributed trajectory control method** for CAVs in a mixed traffic of CAVs, HDVs and pedestrians to improve performance in terms of fuel consumption, safety, and efficiency to enable efficient intersection control.
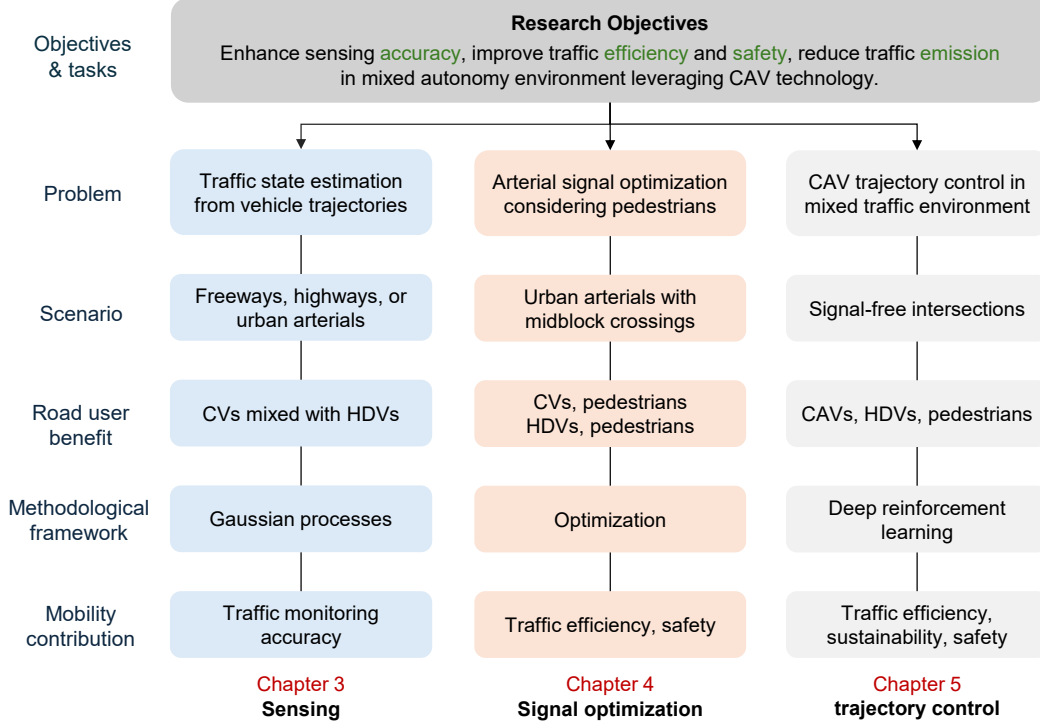
Figure 1.1: Summary of objectives, tasks, and dissertation organization.

1.4 Dissertation Contribution

Each chapter of the dissertation contributes methodologies, algorithms, and integrates domain knowledge with emerging technologies to the existing literature. The traffic management strategies for mixed autonomy traffic developed in this research offer valuable insights and practical guidance for implementation. The detailed contributions of the three main chapters in this dissertation are outlined as follows.

- **Contribution i: Sensing.** This dissertation delves into the challenges and requirements of sensing in mixed autonomy traffic systems. While only a fraction of vehicles is equipped as CVs or CAVs, accurately estimating real-time traffic states for all components is essential for effective traffic management. Chapter 3 proposes a novel method leveraging Gaussian processes (GP) to tackle this challenge. Through a kernel rotation re-parametrization scheme, a standard isotropic GP kernel is transformed into an anisotropic one, better modeling traffic wave prop-

agation in flow data. This method can effectively estimate traffic states from sparse sensing data obtained from fixed sensors, probe vehicles, and CVs. Additionally, it provides statistical uncertainty quantification, enhancing reliability. Extension to a multi-output GP allows simultaneous estimation of traffic states for multiple lanes. Results demonstrate superior performance compared to state-of-the-art methods in accuracy, efficiency, and robustness. Applicable to segments of freeways, highways, or arterials, this approach contributes to the mixed autonomy traffic system involving HDVs, CVs, and CAVs. The work in this chapter has been published in Wu et al. [10]. The contributions of this work carry significant implications for real-time and cost-effective traffic monitoring, particularly in the near-term mixed autonomy traffic.

- **Contribution ii: Optimization.** Given the fundamental role of signal control in V2I applications, this dissertation tackles the complexities of traffic signal optimization within mixed autonomy traffic systems. Specifically, it addresses challenges posed by scenarios involving HDVs, CVs, and pedestrians. A typical real-world scenario illustrating this complexity is an arterial road with two adjacent intersections and a midblock crossing between them. In such scenarios, pushbutton control is often employed for midblock crossings, resulting in significant traffic flow interruptions due to frequent pedestrian crossing requests. Chapter 4 introduces two adaptive midblock crossing control methods (AMCC-band and AMCC-vehicle). The AMCC-band method utilizes the signal control status of adjacent intersections, such as signal phase and timing (SPaT), while AMCC-vehicle leverages real-time vehicle location information, such as that obtained from CVs. Compared with baseline models, these methods, while ensuring pedestrian safety, improve signal coordination between the midblock crossing and downstream intersections, thereby effectively reducing both vehicle and pedestrian delays. The work in this chapter has been published in Wu et al. [11]. The contributions of this work broaden the application scope of conventional

pushbutton control methods and offer insights into designing a more efficient mixed autonomy traffic system that caters to the needs of both vehicles and pedestrians.

- **Contribution iii: Control.** The dissertation illustrates that the presence of a mixed traffic composition, including both CAVs and HDVs, introduces distinct system dynamics compared to homogeneous traffic scenarios. Focusing on intersections accommodating HDVs, CAVs, and pedestrians—an increasingly common scenario—the dissertation addresses the complexities of vehicle trajectory control in mixed autonomy traffic systems. Chapter 5 introduces an intelligent distributed trajectory control method for CAVs, leveraging RL to enable intelligent decision-making at intersections. This method significantly reduces traffic delays, traffic conflicts, and vehicular emissions, particularly in scenarios involving a mix of HDVs, CAVs, and pedestrians. The contributions of this research provide valuable insights into the development of effective and sustainable traffic management strategies for mixed autonomy traffic systems, particularly in the near-term context.

1.5 Dissertation Organization

This dissertation comprises six chapters, where Chapters 3 to Chapter 5 are based on articles that were either published or under review by peer-reviewed mainstream journals. Below is a concise overview of the chapter-level organization:

- **Chapter 1** outlines an introduction to the background, motivation, questions, scope, objectives, and contributions of this thesis. It also explains the connections between each chapter.

- **Chapter 2** gives a comprehensive literature review covering emerging technologies and related research, summarizing the state-of-the-art and identifying research gaps.

- **Chapter 3** presents a novel and efficient traffic state estimation method utilizing sparse trajectory data from CVs to predict comprehensive traffic states for both HDVs and CVs. This method surpasses state-of-the-art techniques in terms of estimation accuracy, efficiency, and robustness, thereby enhancing support for signal optimization and trajectory control.

- **Chapter 4** proposes two adaptive pushbutton traffic signal optimization methods: one tailored for scenarios involving only HDVs and pedestrians, while the other for HDVs, CVs, and pedestrians when trajectory from CVs is available. These methods enhance the traffic efficiency of an arterial and improve pedestrian crossing efficiency while ensuring safety.

- **Chapter 5** develops an intelligent distributed trajectory control method to facilitate CAV navigation through an intersection, effectively reducing traffic delays, traffic conflicts, and vehicular emissions in mixed autonomy traffic scenarios involving HDVs, CAVs, and pedestrians.

- **Chapter 6** summarizes the final conclusion, discusses research limitations, and outlines future directions.

1.6   Conclusion

This chapter serves as a foundation for the dissertation, providing an overview of the research background, motivations, questions, scopes, objectives, and contributions essential to navigating the dissertation. It briefly summarizes the challenges and technical opportunities in related research fields, laying the groundwork for the research goals. This chapter also serves as a connection between introductory concepts and forthcoming content. As subsequent chapters go deeper, this connection maintains a coherent narrative, facilitating a transition from conceptual groundwork to practical research.

Chapter 2

Literature Review

This chapter provides a comprehensive review of the literature on supported emerging technologies, traffic management and control. Through extensive exploration and analysis, it delineates the current state-of-the-art in intelligent traffic management within mixed autonomy environments. By collating relevant research articles and categorizing them based on methodological developments, this chapter aims to offer insights into the field, identify research gaps, and point out potential areas for further investigation, laying the groundwork for subsequent analyses and discussions.

The chapter is structured into five sections, each addressing key aspects of the literature review. The first section offers an overview of emerging technologies pivotal to the next generation of ITS, setting the groundwork for the research discussed in this dissertation. Following this, the second section delves into a review of state-of-the-art traffic state estimation methods, highlighting their data acquisition role in facilitating intelligent traffic management and control. In the subsequent section, the focus shifts to intelligent traffic control systems, particularly their applications in arterial traffic management, while also identifying the oversight of pedestrian considerations in such systems. To address this gap, the fourth section concentrates on signal optimization at mid-block crossings within arterials. Moving forward, the fifth section, investigates trajectory control in mixed autonomy scenarios, with a specific emphasis on the intersection level. Finally, the concluding section offers a concise summary of the literature review's key findings.

2.1 Emerging Technologies

As described in the previous section, the transportation system is undergoing a significant transformation due to the emergence of various technologies. Communication, vehicle automation, and computational resources integrated with fundamental road infrastructures form the next generation of ITS. This section provides an overview of the key technologies that are shaping the next generation of ITS.

2.1.1 Connected vehicle

CAVs have garnered widespread recognition for their transformative potential and have experienced rapid development, fueled by advancements in autonomous vehicle manufacturing and communication technologies. CAVs are an integration of CVs and AVs. In this section, we will discuss the CVs and their potential in the transportation system first.

CVs are equipped with wireless communication devices, enabling them to communicate with other vehicles, road infrastructure, and traffic management centers. This communication enables the exchange of real-time traffic information, such as vehicle speed, location, and acceleration. For example, CVs can provide real-time traffic information to drivers, alerting them to potential hazards and traffic congestion. CVs can also be used to improve traffic signal control, by providing real-time traffic information to traffic signal controllers, enabling them to adjust signal timing to reduce traffic congestion and improve traffic safety.

It is worth noting that the drivers in CVs are not necessarily replaced by automation, and human drivers can still control the vehicle. In other words, CVs refer more to the vehicle with only communication technology.

2.1.2 Vehicle-to-everything

V2X allows vehicles to communicate with any part of the surrounding traffic system, also known as connected vehicle-to-everything-communication. It

mainly includes vehicle-to-vehicle (V2V), vehicle-to-infrastructure (V2I), vehicle-to-pedestrian (V2P), vehicle-to-network (V2N), and other communication application scenarios. In this way, the real-time information exchange of related entities is realized. As a result, it supports the management of modern traffic systems, reduces traffic accidents, eases traffic congestion, reduces emissions, and provides related information services.

A related concept is the Internet of Vehicles (IoV), which originated from the Internet of Things (IoT). The IoV and V2X seem to be the same, and both represent the connection between the vehicle and the outside world. However, there are still some nuances. For example, the IoV is a concept at the upper layer, therefore, it is a manifestation of a network system. As for V2X, it is more of a slightly lower level of technical support. More precisely, we emphasize the connection method or communication technology to achieve beyond the line of sight, therefore we often call it V2X technology. Therefore, in this research, it is called V2X technology and referred as a specific communication support. Moreover, it is necessary to understand that Dedicated Short-Range Communication (DSRC) and Cellular-Vehicle to Everything (C-V2X) are two technical directions in V2X technology, or two sets of communication technology standards.

DSRC is a wireless communication technology that enables vehicles to communicate with each other directly without involving cellular or other infrastructure. Vehicle-to-vehicle and vehicle-to-road communication are its main applications. Each vehicle sends its position, direction, and speed ten times per second securely and anonymously, and all surrounding cars receive the message. This technology can realize the identification and two-way communication of high-speed moving objects (cars) in a specific area (usually tens of meters) and transmit information in real-time [12], [13]. The DSRC series of standards include Institute of Electrical and Electronics Engineers (IEEE) 802.11p [14], IEEE 1609 series, and Society of Automotive Engineers (SAE) J2735 and J2945 standards.

The DSRC series of standards include IEEE 802.11p [14], IEEE 1609 series,

and SAE J2735 and J2945 standards. The DSRC standardization process can be traced back to 2004. First, IEEE formulated new vehicle communication standards under the 802.11 wireless local area network standard series; around 2007, IEEE framed 1609.x series of standards as the security architecture of V2X. The above IEEE 802.11p and 1609.x were for safety. Then SAE J2735 and SAE J2945, which define the information carried in the message packet, including incoming position, the direction of travel, speed, and braking information, were motivated to improve the traffic efficiency.

C-V2X is a new generation of vehicle communication technology based on the evolution of cellular network communication technologies such as 3G/4G/5G. While DSRC was a mature technology for V2X communications in the past, C-V2X was proposed and gained attention recently [15], [16]. C-V2X is a cellular vehicle connection, a wireless communication technology for vehicles based on the evolution of cellular network communication technologies such as 3G/4G/5G. C-V2X is a communication technology based on the 3rd generation partnership project (3GPP) unified standard, broadly including long term evolution (LTE) (and enhanced LTE-V2X) and 5G-V2X.

C-V2X has two communication interfaces: one is to realize short-distance direct communication between people, vehicles and roads through PC5 (direct communication interface, terminal-to-terminal). The characteristics are low latency, high capacity and highly reliable communication; the other is based on Uu (cellular network communication interface, terminal and base station), characterized by realizing long-distance and larger-range reliable communication. When the terminal equipment supporting C-V2X is within the coverage of the cellular network of the base station, Uu can be used under the control of the cellular network. Still, the PC5 interface can be used regardless of whether there is cellular network coverage so that the Uu interface and the PC5 interface form an effective complementary.

The 3GPP R14 version standard supporting LTE-V2X was officially released in 2017; the 3GPP R15 version standard supporting LTE-V2X enhancement (LTE-eV2X) was formally completed in June 2018; the 3GPP R16+ ver-

17

sion standard supporting 5G-V2X was announced in research that began in June 2018 and will form a complementary relationship with LTE-V2X/LTE-eV2X.

Overall, it can be seen that DSRC is a relatively mature and stable technology with an earlier layout. Compared with LTE-V2X in C-V2X, it has a huge advantage of low latency, but the communication distance is short; the current version of C-V2X is LTE-V2X and the technical layout is late, but the interface is flexible and can support more scene applications. Compared with DSRC, it has the advantage of high bandwidth, which can support longer distance communication. Therefore, in this dissertation, we study all the problems based on a C-V2X scenario to support the traffic management.

2.1.3 Automated vehicle

An automated vehicle, also referred to as an autonomous vehicle or self-driving vehicle, possesses the capability to perceive its surroundings and operate without direct human intervention. In this study, the term "automated vehicle" is employed to denote such vehicles, emphasizing their focus on enhanced vehicle automation. Analysts point out that by the year 2025, approximately 8 million AVs or semi-AVs will traverse roadways. However, before fully integrating onto road networks, some AVs progress through six distinct levels of driver assistance technology advancements or some go directly to a certain level. These levels, delineated by SAE, span from no automation (Level 0) to full automation (Level 5) [17]. The hierarchical progression of automation levels is illustrated in the accompanying Fig. 2.1.

At Level 0, human drivers maintain complete control of the vehicle while remaining responsible for monitoring the driving environment. Progressing to Level 1, the vehicle introduces limited automated control, often in longitudinal or lateral modes. Level 2 marks a significant advancement, where the automated system assumes full control over both longitudinal and lateral functions, although drivers must remain alert and ready to intervene if needed. Moving forward, Level 3 builds upon Level 2 by incorporating an additional monitoring

Figure 2.1: SAE J3016 levels of automation. Source: SAE International [17].

agent to oversee the driving environment. At Level 4, the vehicle gains the ability to operate without driver intervention, albeit within specific environmental and conditional constraints. Finally, Level 5 represents the full automation, with the vehicle capable of operating autonomously in all environments and conditions, without any reliance on human intervention.

2.1.4 Connected and automated vehicle

In the preceding section, we outlined the six levels of automation for AVs. The level of automation correlates with the advanced driver-assist system (ADAS). Various ADAS functions are integrated into different levels of automation. For instance, adaptive cruise control (ACC) and lane keeping assist system (LKAS) are incorporated into Level 2 automation. A crucial marker of autonomy is the transition from ADAS to a fully automated driving system (ADS). Vehicles at Levels 0 to 2 are equipped with ADAS, while those at Levels 3 to 5 feature ADS. Currently, ADAS is widespread in vehicles, with many manufacturers like Tesla, BMW, Volvo, and GM equipping new vehicles with ADAS up to Level 1 or 2 [18]. The proliferation of AVs at Levels 4 and 5 is experiencing

rapid growth, and commercial deployment is transitioning from technological feasibility to reality. In this study, especially of trajectory control, we need AVs to be fully controlled, thus, Levels 0 to 2 represent vehicles that cannot transmit whole environmental data or are fully controlled by agents, precluding them from being defined as CAVs. Conversely, vehicles at Levels 3 to 5 possess the capability of V2X, thus qualifying as CAVs in this research.

CVs and AVs are combined to revolutionize transportation mobility. CVs utilize communication technologies to establish connections with both autonomous and non-autonomous vehicles, roadside infrastructures, and other road participants. This connectivity facilitates the sharing of driving information, aiding human or automated agents in making informed decisions by leveraging data collected through V2X communication. On the other hand, AVs perform driving tasks by relying on a variety of sensors and systems, gradually reducing the need for human intervention based on their autonomy level. Within the transportation community, to some degree, CVs can serve as enablers of AVs, with CV technology exerting a significant influence on the development and effectiveness of AVs [19]. The integration of both AV and CV technologies in CAVs offers manifold benefits, surpassing those achievable with either technology in isolation. Overall, this research focuses on CAVs with an autonomy level ranging from Level 3 to 5 and equipped with V2X communication capabilities.

2.1.5 Mobile edge computing

MEC, also known as Multi-access Edge Computing, is a transformative technology that relocates the cloud computing platform from the mobile core network to the edge. This "edge" refers to computing, storage, and network resources positioned along the path from data sources to the cloud computing center. Combining MEC with V2X can provide a more efficient and reliable communication environment for CAVs. MEC aggregates and stores vehicle-side and road-side data from various intelligent equipment, such as cameras, millimeter-wave radar, traffic lights, and lidar. By doing so, it reduces the

network burden on the traffic management center (TMC) while facilitating fast computing and message distribution to the on-board unit (OBU) and the road-side unit (RSU).

A critical connection between CAVs and traffic management lies in the underlying road infrastructure, enabling V2I communication. V2I functionalities, such as signal control and route guidance, necessitate real-time data processing, optimization, decision-making, and message distribution for CAVs. Traditionally, CAV data is sent to the cloud for processing, resulting in significant delays unsuitable for real-time applications. However, MEC offers a solution by enabling real-time data processing from both the vehicle and infrastructure sides. In the context of the next generation of ITS, each CAV is equipped with an OBU responsible for data storage, computing, and message distribution. Road-side units (RSUs) are deployed along the roadside to collect additional information such as signal timing and environmental data. These RSUs, acting as edge servers or MECs, play a crucial role in providing computational resources for processing real-time data from both vehicles and infrastructure, thus facilitating the advancement of traffic management strategies.

2.2 Traffic State Estimation Approaches

As highlighted earlier, traffic state estimation (TSE) stands as an important element in the evolution of ITS, particularly in extrapolating the comprehensive traffic dynamics of both HDVs and CAVs from sparse CV trajectories. TSE refers to the process of inferring the traffic state, such as vehicle speed, density, and flow, from the available traffic data. In this section, we will review the state-of-the-art TSE methods and discuss their potential applications in the next generation of ITS.

We can broadly classify existing TSE models into model-based and data-driven methods, specifically model-based, data-driven, and streaming data-driven strategies [20]. Model-based approaches adopt macroscopic traffic flow

models to depict the traffic states; these models include first-order traffic models like the Lighthill-Whitham-Richards (LWR) model [21], [22], high-order traffic models like Payne-Whitham (PW) model [23], [24] and the Aw-Rascle-Zhang (ARZ) model [25]–[27], and their extensions. The model-based approach often performs the Data Assimilation (DA) or estimation with the traffic observation via a filter-based method. The most utilized one is the Kalman filter (KF) and its variants - KF-like techniques (e.g., the extended/unscented/ ensembled Kalman filter) [28]–[33]. Other methods are not oriented from the Kalman filter, such as particle filter (PF) [34], adaptive smoothing filter (ASF) [35], or others. A comprehensive review of the above methods can be found in [20]. Although the model-based techniques can follow the traffic principles, these models rely heavily on the assumptions of traffic physics that can lead to numerical biases or approximation errors when the premises are not coherent with real-world data. In addition, model-based methods require substantial prior information on traffic dynamics, such as free flow speed, minimum gap, etc.

Due to the availability of massive traffic data and the development of machine learning techniques, data-driven models have received more attention. Data-driven models usually utilize statistical or machine-learning approaches to infer traffic states from the spatiotemporal characteristics extracted from historical data (e.g., from sensors like loop detectors, cameras, or connected vehicles). For example, various research incorporates the spatiotemporal features into data-driven models utilizing the following techniques like the auto-regressive integrated moving average (ARIMA) [36], Bayesian network (BN) [37], Kernel regression (KR) [38], k-nearest neighbors (kNN) [39], convolutional neural networks (CNN) and deep neural networks (DNN) [40]–[45], graph embedding generative adversarial network (GE-GAN) [46], tensor decomposition [47], and principal component analysis [48] et al. Besides, streaming-data-driven approaches are regarded as more robust against uncertainties while requiring a large amount of streaming data to perform the prediction. Some research contributes to the streaming-data-driven models, such

as [49] and [50]. One of the advantages of data-driven models is that they require less prior info on traffic dynamics and can be more accurate than model-based methods. The other advantage is that they do not need rigid assumptions for traffic principles, which may cause unexplainable estimation. Meanwhile, the data-driven models often depend on a large amount of training data.

In terms of data sources, most of the research discussed thus far utilized static data from fixed-location sensors like loop detectors or static data combined with mobile data obtained from probe vehicles [28], [51], [52]. Recently, more and more researchers investigated the trajectory-based TSE methods from trajectory data. For example, [51], [53], [54] utilizes the trajectory data of probe vehicles or CAVs to estimate the traffic state of freeways. Moreover, there is a trend that combines model-based and data-driven models to develop "physics-informed" machine learning models for TSE [44], [45], [55].

Traditional fixed sensors are expensive to install and maintain throughout the road. With the development of CV technology, there exists an opportunity that such moving sensors can provide data sources at a relatively cheaper cost all over the road. Therefore, we still have to deal with the scenario where data is sparse because not all cars are CVs that provide information. There is some research about the TSE using CV technology. Chen and Levin [56] estimated traffic states like flow, density, and speed by proposing an algorithm based on CV basic safety message (BSM) data. This study tested the Kalman Filter and cell transmission algorithm in a simulator. Fountoulakis et al. [57] proposed microscopic simulation research of the TSE with mixed traffic (CVs and conventional vehicles) via CV and spot-sensor data. At the same time, Bekiaris-Liberis et al. [58] developed a model-based TSE approach for per-lane density estimation and an on-ramp and off-ramp flow estimation in the presence of connected vehicles. There have also been works discussed online and offline TSE with CV data in a Bayesian model [54].

As presented here, the most similar research to our work in Chapter 3 is the adaptive smoothing interpolation (ASM) by Treiber et al. [59]. The au-

thors used the anisotropic features of traffic waves and developed a smoothing method to estimate the traffic speed profile. The interpolation of ASM is a weighted sum of a free-flow component and a congested component. Schreiter et al. [60] proposed two fast implementations of ASM by efficient matrix operations and Fast Fourier Transform (FFT), bringing improvements in computation time by two orders of magnitude. The classical ASM lacks a well-defined method to determine the model parameters. Yang et al. [61] reformulate ASM using matrix completion, which can estimate the weight parameter by the Alternating Direction Method of Multipliers (ADMM) algorithm. Yang et al. [62] proposed a neural network based on ASM, which can learn its parameters from sparse data of road sensors. In our study, the proposed GP approach is a probabilistic model that can learn the parameters and uncertainties from the data. Additionally, the proposed method can be applied to the TSE problem on a continuous space without defining grids.

2.3 Intelligent Traffic Control System

It is well known that a traffic control system is closely related to an intelligent transportation system. Many cities implemented various dynamic traffic signal control systems in the past decades. For example, the early developed SCOOT [63], [64] and SCAT [65] systems are variants of TRANSTY [66]; they are developed based on active traffic coordination. The above systems utilize traffic demand, optimize traffic signals in a network (arterials and a road network), and provide more green time for vehicles.

Although these systems work well, they also have some drawbacks. Firstly, implementing and maintaining these systems is costly. As mentioned above, these systems use current traffic demand, so in the past they relied heavily on loop detectors, which are expensive and hard to maintain. Now, it is more convenient to use high-resolution cameras, which are also high in cost. Secondly, these control systems are centralized control systems, which rely on an extensive communication system.

After the early versions of intelligent traffic control systems, various kinds of algorithms developed depending on different methods and data sets. For example, much work has been done with the coordination of actuated arterial signal control, such as [67]–[70]. Hu and Liu [71] utilized the high-resolution traffic signal data to optimize the actuated signal coordination along the arterial, and a data-driven model was developed to adjust the offset. Another kind of intelligent traffic signal control, like adaptive signal control, belongs to a smart traffic control system. The adaptive traffic signal control system is the most recently developed algorithm, and most of these studies aim to utilize real-time data to improve the system's efficiency [72]–[76]. Besides, an increasing number of researchers have concentrated on adaptive control and real-time offset optimization for the arterial coordination system, such as [77]–[81]. However, its implementations are rare now, because this kind of implementation requires a higher level of infrastructure like high-resolution data, and we can obtain corresponding vehicle data simultaneously.

2.4 Arterial Traffic Management

Arterial traffic management is a critical aspect of overall traffic management strategies. The research primarily focuses on arterials rather than networks, a common approach in traffic management strategies. It can be divided into two parts when it comes to arterial traffic management. The first part is how to improve arterial progression; there is no doubt that the signal coordination strategy is one of the most effective methods to solve arterial passage. The second part is evaluating the arterial progression effects or performance.

2.4.1 Arterial signal coordination strategies

Much research has been done to improve arterial progression and signal coordination that can be divided into two classifications. One can be generally called the band-based method; its function is to maximize the bandwidth along the arterial. The other is often called the flow profile method [82] (or is sometimes

referred to as delay-based method or other index-based method). The major objective of the flow profile method is to minimize the total delay or other indices like travel time of the system.

Some representative studies in band-based methods are as follows. In the 1960s, Morgan and Little [83], [84] advanced the signal coordination by developing a bandwidth maximization model using mixed-integer linear programming. In the 1970s, Messer et al. [85] developed a well-known band-based tool PASSER II. Later, Little et al. [86], Chang et al. [87] extended their previous work and formed MAXBAND and the variant MAXBAND-86 for networks. Next, to tackle the same band problem for all links of MAXBAND, Gartner et al. [88], Stamatiadis and Gartner [89] proposed the MULTIBAND package to generate progression bands with varying widths; they also proposed a variant called MULTIBAND-96 to realize network control. In recent years, Zhang et al. [90] introduced an AM-BAND model by relaxing the asymmetrical progression band.

Regarding flow profile methods, in the 1960s, Hillier and Rothery [91] collected arrival timing data for four neighboring intersections to minimize total delay and achieve the optimal offset. Gartner et al. [92] also tried to minimize average delay on coordinated roads. D'Acierno et al. [93] generated optimal offset by minimizing total delay in a two-way coordinated arterial.

Overall, these two categories include two steps: optimization at individual intersections and then coordination. Flow profile methods are more flexible than band-based methods in several respects. However, delay-based models are more difficult to solve.

2.4.2 Arterial traffic performance evaluation

The performance measures are essential for evaluating and analyzing traffic characteristics and progression quality along the corridor. Moreover, visualizing the performance measurement is important for engineering practice. The performance measure visualization changes according to the data source and requirements of reality. Day et al. [82] recently divided graphic performance

measure tools into three categories: time-space diagram, flow profile concept, and Purdue coordination diagram (PCD); the time-space diagram and PCD are the two primary performance measure visualization tools.

The time-space diagram became a long-standing standard method or tool for signal timing visualization, demonstrating the status between traffic movement and signal according to [82]. This graphic measure came into use because of data collection difficulties and cost in the 1960s by Gazis [94]. Anwar et al. [95] showed the time-space diagram and its significance in the era of data abundance with application in bus routes. What's more, time-space diagrams are utilized to help with different transportation research like evaluating signal coordination and traffic prediction, such as [96]–[99]. Flow profile is also widely used and dates back to [91], showing vehicle arrival information at the intersection.

The PCD originated from the concept of arrival type. Later, Day et al. [100], Brennan Jr et al. [101] developed the PCD combining advance detection data and signal timing. It was utilized to illustrate vehicle arrival on green (AOG) or arrival on red (AOR) characteristics cycle by cycle related to a signal at one intersection, intended to help visualize and diagnose the traffic control performance of the site. Then the original PCD was developed in different studies to better reveal the signal coordination performance. Wang and Abbas [102] introduced a colored PCD that can not only illustrate the arrival pattern but also show the speed passing detectors. They also proposed a new performance measure called VT number. As PCD is a cycle by cycle one-day measurement, Huang et al. [103] enhanced the PCD to aggregate PCD (APCD), applying it to a multi-day display using advanced data analytics. In order to quantify the continuous smoothness traveling along a corridor considering speed variation, Beak et al. [104] introduced smoothness of the flow of traffic (SOFT) replacing percent on green (POG), travel time, and delay. In addition, they introduced connected vehicle PCD (CV-PCD) since they utilized CV trajectories rather than advance detector data. Furthermore, PCD has been widely used for engineering and research about coordination

performance visualization and evaluation, such as [105]. The studies discussed here worked with advance detector data. However, the performance measure changed significantly with the coming of new data sources like vehicle positions. For current research, vehicle trajectory data which is spatialtemporal shows great potential according to [82].

In summary, PCD is the visualization for one intersection but is not enough for indicating continuous arterial evaluation. What has proven more difficult is the visualization of large quantities of data in a time-space diagram.

2.5   Signal Control at Midblock Crossings

Most research above discussing arterial traffic management has predominantly focused on vehicles or drivers. However, it's essential to recognize that all road users, including pedestrians and cyclists, play a crucial role in the arterial system. A significant scenario arises in arterials with midblock crossings, where pedestrians are active. Consequently, there is a pressing need to examine midblock crossing control strategies within arterials.

Firstly, let's delve into pushbutton control, renowned for its application in midblock crossings. The Forest City Electronic Company invented the first pushbutton system in 1931 [106]. Since then, various types of pushbutton control systems have been developed. Based on previous studies [107], [108], we categorize major midblock crossing signal control systems into six types: fixed phase and timing control, simple pushbutton (i.e., Forest City pushbutton), pedestrian light-controlled (Pelican), high intensity activated crosswalk (HAWK, also known as pedestrian hybrid beacon (PHB)), pedestrian user-friendly intelligent (Puffin), and pedestrian actuated (PA). Features of these midblock crossing signalizations are summarized in Fig. 2.2. PHB and PA are commonly utilized in North America, while Pelican and Puffin are found in Europe [109]. PHB is a modified version of Pelican to adapt for America and is recommended in the Manual on Uniform Traffic Control Devices (MUTCD) [110]. Both PHB and Pelican allow vehicles to pass the midblock

during the end of a pedestrian clearance phase (flashing period) if pedestrians have already crossed the street. Therefore, they are recommended for high vehicle demand situations [111]. In addition, Puffin and PA can detect if all pedestrians have crossed the street and extend the pedestrian phase when needed. Puffin relies on the pushbutton and detector, while PA depends solely on the detector.

Controls	PWT	Activation	Signal operation sequence			
Fixed phase	Depend on allocation	N/A	Vehicle	Green / Amber / Red / Green until next activation		
			Pedestrian			
Pelican	Fixed	Pushbutton	Vehicle	Green / Flashing amber		
			Pedestrian	Until activated / Flashing green		
HAWK/PHB	Fixed	Pushbutton	Vehicle	Dark until activation / Flashing amber / Flashing red / Dark until next activation		
			Pedestrian	Red until activated / Flashing red		
Puffin	Fixed	Pushbutton & detector	Vehicle	Green until activation		
			Pedestrian	Red until activation / Extended green (if remains detected)		
PA	Fixed	Detector	Vehicle			
			Pedestrian	Red until sensors actuated / Extended green (if remains detected)		

Figure 2.2: Visual differences of major midblock crossing signalizations.

Much research has studied the efficiency and the safety of pushbutton control at midblock crossings. For example, Lu and Noyce [112] utilized fuzzy logic to control the right-of-way at midblock crossings. The authors reported their method improves efficiency and safety over Puffin. Godavarthy [111] evaluated the unnecessary delay (vehicles unable to move even once pedestrians have crossed) at a midblock crossing. They found PHB can reduce unnecessary delay compared with other pushbutton control methods. Ma et al. [113] developed a signal optimization model for two-stage midblock crosswalks, where the two-stage pedestrian phases are coordinated. The cycle length and offset of the two pedestrian phases are optimized by mixed-integer linear programming (MILP). Kim et al. [108] compared fixed phase and timing controls with pushbutton controls at midblock crossings. They concluded that the pushbutton system is more efficient based on their case study. Recently, Yang et al. [114] proposed using pedestrian detectors at upstream sidewalks to reduce pedestrian wait time at a midblock crossing. However, their method increases

vehicle delay and is more suitable for situations with low pedestrian demand. Along with studies on midblock crossings, researchers have also extensively investigated signal optimization at an isolated intersection considering pedestrian phases [115]–[118].

The research discussed thus far analyzed the midblock crossing as an isolated system. However, Teketi and Pulugurtha [119] found that midblock crossing control (PHB in their paper) could significantly increase the delay and queue length at nearby intersections. Furthermore, only a few studies have jointly considered a midblock crossing with adjacent intersections. In two such studies, Ma and Yang [120] and Zheng et al. [121] proposed models to coordinate midblock crossings with adjacent intersections using fixed phase and timing controls. In addition, Yu et al. [122] proposed an optimization framework to simultaneously determine the quantity, location, and signalization of midblock crossings on an arterial, also adopting a fixed phase and timing control at midblock crossings. However, a notable gap in research of pushbutton-type midblock crossing control with consideration of adjacent intersections is still evident.

2.6 Trajectory Control with Full HDVs/CAVs

The evolution of vehicle trajectory control traces back to the car-following models, which describe longitudinal interactions among vehicles, such as car-following traffic flow, Newell's model, the Gipps model, and the Intelligent Driver Model (IDM) [123]–[126], demonstrating the progression over time. Initially tailored for HDVs rather than mixed autonomy scenarios, these models laid the groundwork for subsequent research in trajectory control aimed at enhancing traffic efficiency. One such strategy is eco-driving, which optimizes speed profiles to reduce vehicular emissions. Furthermore, the implementation of Green Light Optimized Speed Advisory (GLOSA) systems [127], [128] has emerged as a notable advancement, coordinating vehicle speeds with traffic lights to minimize stops and improve overall traffic flow. Subsequently, many

researchers have favored employing diverse optimal control methods to refine vehicle trajectory planning [129], [130]. These models typically treat acceleration/deceleration or vehicle speed as the primary control variables. This evolution highlights the development of vehicle trajectory control within a traditional traffic environment, predominantly comprising fully HDVs.

The rise of CAVs has increased significant interests in CAV trajectory control and optimization. ACC is a solution to dynamically adjust vehicle speed, ensuring a safe distance from preceding vehicles. This advanced driver-assistance system is now standard in most vehicles [131]. Additionally, with inter-vehicle communication facilitated by V2X communication, cooperative adaptive cruise control (CACC) has been introduced. CACC utilizes exchanged data to compute relative distance, speed, and acceleration, enabling more cooperative and responsive control [132]. These advancements primarily focus on optimizing for a full CAV environment.

Building upon the aforementioned studies, researchers have devised algorithms to enhance road traffic management at signalized intersections. Malakorn and Park [133] integrate CACC with intelligent traffic signals to optimize vehicle trajectories. The approach divides the trajectory into acceleration and cruising segments, ensuring vehicles arrive at green lights efficiently. He et al. [134] introduced a multi-stage optimal control framework aimed at optimizing vehicle speed trajectories, considering constraints such as queue impacts and traffic light statuses at intersections. Yao et al. [135] devised a trajectory smoothing method tailored for signalized intersections, coordinating variable speed limits with signal timing to enable vehicles to traverse the intersection without stops. Yu et al. [136] proposed a MILP model to optimize vehicle trajectories and traffic signals within a unified framework, accounting for all vehicle movements and optional lane changes in a CAV environment. Feng et al. [137] utilized optimal control theory to regulate the trajectory of platoon-leading vehicles, focusing on minimizing fuel consumption and emissions. Liu et al. [138] developed an intersection control algorithm comprising an optimal traffic signal control algorithm and a trajectory planning function. Their inter-

section controller aimed to maximize intersection throughput while enhancing vehicle energy efficiency. Collectively, these studies represent the advancement of trajectory planning designs integrating signal timing at signalized intersections within a full CAV environment.

Research has also explored intersections without signals in a full CAV environment, commonly referred to as 'signal-free' intersections which follow the all-way stop rule. Much of this research has centered on autonomous intersection management (AIM), often employing reservation-based schemes. A prevalent strategy is the 'first-come, first-serve' (FCFS) approach, where vehicles submit requests to a central controller for space and time allocations. This concept has been explored in various studies, including those in [139]–[142]. Other researchers have utilized optimization models or formulated optimal control problems to enhance AIM, aiming to maximize intersection throughput, minimize total delay, and reduce vehicle emissions [143]–[147]. Additionally, intelligent AIM approaches leveraging deep learning (DL) or RL have been proposed to enhance CAV control and enable learning from traffic environments at signal-free intersections, thereby improving traffic efficiency and collision avoidance [148]–[150]. While these methods enable CAVs to navigate intersections automatically, trajectory control often remains at the individual CAV level or is studied under low-traffic demand scenarios within a full CAV environment.

2.7 CAV Trajectory Control with Mixed Autonomy

The coexistence of HDVs, CVs, and CAVs has been a reality in recent years. Therefore, numerous research has been done to optimize CAV trajectories at the intersection. Studies in [151]–[153] have leveraged model predictive control (MPC) techniques to optimize CAV velocity or acceleration rates. By predicting HDV behavior and adjusting CAV trajectories accordingly, these approaches aim to enable CAVs to arrive during green signal phases with fewer

32

stops, thereby reducing fuel consumption. Pourmehrab et al. [154] proposed a joint optimization of incoming vehicle trajectories and SPaT, resulting in optimized trajectories and reduced travel time. Guo et al. [155] integrated dynamic programming with a shooting heuristic algorithm to optimize CAV trajectories, accounting for interactions between CAVs, human-driven vehicles, and intersection control, achieving fuel consumption savings. Other research has explored various centralized or decentralized control methods, as well as RL, to optimize CAV trajectories in mixed traffic at isolated signalized intersections, as evidenced by studies, such as [156]–[158]. While these studies have demonstrated the effectiveness of trajectory optimization strategies in reducing traffic delay and fuel consumption in mixed-traffic environments, it's important to note that they primarily focus on signalized intersection scenarios.

As described above, despite the extensive exploration of vehicle trajectory planning at unsignalized intersections within fully CAV environments, there remains a scarcity of studies addressing trajectory planning for CAVs at unsignalized intersections under mixed traffic conditions. This gap in research was highlighted in a recent review by Li et al. [9]. In the mixed traffic of CAVs and HDVs, the predominant approach has been to treat CAVs as individual control units, with a focus on maximizing their benefits. In [159], CAVs were tasked with adjusting their speed to prevent collisions with HDVs, assuming no cooperation between CAVs and HDVs at intersections. The effectiveness of this approach was demonstrated through the utilization of an MPC controller, which yielded positive outcomes for CAVs. Chen et al. [160] explored a different strategy, employing CAVs as traffic regulators to enhance overall efficiency in mixed traffic scenarios and built a MILP model to optimize the entry times of CAVs, strategically controlling subsequent HDVs to improve traffic efficiency. RL and graph neural networks (GNN) offer promising avenues for enhancing mixed traffic efficiency by mitigating vehicle delays, especially considering uncertainties in human drivers' intentions, as demonstrated in [161]. In addition to research on mixed traffic of CAVs and HDVs at unsignalized

intersections, there are also studies focusing on the interaction between CAVs and pedestrians or cyclists. Much of this research has centered on learning for autonomous driving control, with the objective of maximizing CAV benefits while considering human interaction; [162]–[164] are notable examples in this domain.

In summary, extensive research has addressed trajectory control in fully HDV or fully CAV environments. However, most optimal control approaches encounter computational challenges under high traffic demand, whether at signalized or unsignalized intersections. In mixed-traffic environments, studies have predominantly focused on optimizing CAV benefits alone, often in scenarios involving CAVs with HDVs or pedestrians. Notably, there exists a research gap wherein investigations into mixed traffic scenarios encompassing CAVs, HDVs, and pedestrians are imperative.

2.8 Conclusion

This chapter serves as a comprehensive exploration on emerging technologies, traffic state estimation, intelligent traffic control, signal optimization at mid-block crossings, and CAV trajectory control under mixed autonomy, which are important components of ITS.

The emergence of technologies such as CV, AV, CAV, V2X, and MEC signifies important advancements in transportation infrastructure. It is imperative to sketch the evolution of each of these technologies, underpinning the transition toward the next generation of ITS. This chapter explains the transformative impact of each technology and their interconnectedness and respective roles within the infrastructure landscape.

A comprehensive examination of TSE reveals that model-based approaches may fall short in accuracy due to their inability to fully capture the complex details of real-world traffic dynamics. Conversely, leveraging vast traffic data and machine learning methodologies opens avenues for achieving TSE in a purely data-driven fashion. Nonetheless, employing a data-driven approach

typically necessitates a substantial external training dataset and a comprehensive validation dataset. However, acquiring an appropriate training dataset may prove challenging, and the external dataset may not accurately represent road segments with missing data. Hence, this dissertation identifies a necessity to develop a data-driven TSE methodology in lack of external training datasets. In scenarios where observed data is exceedingly sparse, it becomes imperative for TSE to provide statistical uncertainty estimates. Especially, in the context of mixed traffic with CVs, trajectory data can be leveraged to enhance TSE accuracy and reliability.

This chapter also explores intelligent traffic control systems, including conventional ones like SCOOT and SCAT, which face challenges such as high economic costs and reliance on fixed loop detectors, leading to maintenance issues. Furthermore, effective intelligent traffic control algorithms require access to high-resolution data. Thus, this chapter identifies an opportunity to address these challenges by leveraging emerging communication technologies and trajectory data from CVs to enhance traffic control systems and develop more intelligent control algorithms.

Additionally, the chapter investigates the significance of arterial traffic management, stressing the importance of assessing arterial progression and performance. Moreover, the chapter highlights the critical role of signal control at midblock crossings, particularly in arterials with active pedestrian crossings, given the diverse mix of road users. Various pushbutton control systems and their applications in midblock crossings are discussed, emphasizing the importance of efficient and safe signal control strategies. Furthermore, the chapter identifies a research gap in the integrated consideration of midblock crossings with adjacent intersections, highlighting the necessity for enhanced arterial traffic management to accommodate mixed autonomy, including pedestrians.

Finally, the chapter concludes with a discussion on CAV trajectory control under mixed autonomy, highlighting the importance of developing trajectory control strategies capable of effectively managing mixed traffic scenarios. While existing studies primarily focus on CAV control strategies in either pure

CAV environments or in mixed autonomy scenarios involving CAVs and HDVs, this chapter identifies a research gap in the trajectory control of CAVs within a mixed autonomy environment, encompassing CVs, HDVs, and pedestrians. To address this gap, this dissertation aims to develop a trajectory control strategy for CAVs in such environments, leveraging CV data, V2X communication technologies, and AI algorithms to enhance traffic management strategies.

Chapter 3

Traffic State Estimation from Vehicle Trajectories utilizing Anisotropic Gaussian Processes

3.1 Introduction

Intelligent transportation systems rely heavily on traffic state information, which is typically collected using a variety of detectors, such as loop detectors, video cameras, probe vehicles, and, more recently, CVs. However, each type of detector has its limitations in terms of coverage and completeness of data. For instance, loop detectors are stationary sensors that only provide data at fixed locations, while video cameras require significant time and resources to process footage and must be installed on a high building or a gantry. As a result, these sensors are sparsely distributed in the traffic network, resulting in limited spatial coverage. In recent years, mobile sensors such as probe vehicles and CVs that can provide real-time traffic information, including speed and location, are playing an ever-important role in TSE. However, because of the low penetration rate of CVs, the trajectories of CVs are sparse in both space and time. Therefore, an imputation method is needed to obtain the traffic state information in the entire spatiotemporal space, which would enable more accurate traffic control and management in ITS.

Traffic state estimation refers to the inference of traffic state variables, such as density, speed, or other relevant variables, in a spatiotemporal domain by

37

utilizing partially observed traffic data from detectors [20]. Generally, there are two types of TSE approaches: model-based and data-driven. Model-based TSE methods rely on traffic flow models and require strong prior knowledge, such as the capacity of the road, to accurately infer traffic state variables. Typical methods include first-order Lighthill-Whitham-Richards (LWR) model [21], [22] and high-order Payne-Whitham (PW) model [23], [24]. However, a model-based TSE may not always be accurate because it may not fully capture the complexity of real-world traffic. Conversely, with massive traffic data and machine learning techniques available, TSE can be achieved in a purely data-driven manner, as demonstrated by some recent works [41], [47]. However, the training of a data-driven approach typically requires a large external training dataset and a validation dataset with full information. For example, many deep-learning-based TSE models [41] are first trained on a traffic simulation dataset, and then applied to a real-world TSE problem. However, it may not always be possible to obtain an appropriate training dataset, and the external dataset may not be representative of the road segment with missing values. Therefore, there is a need to develop a data-driven TSE method without any external training dataset. For cases where the observed data is extremely sparse, we expect the TSE could also be able to provide statistical uncertainty quantification for the estimation.

To address the above research gap, we propose using Gaussian processes (GPs) [165] for TSE. GPs are non-parametric Bayesian models that have been widely used for spatiotemporal kriging/imputation, providing a data-driven TSE approach that does not require an external training dataset. Additionally, GPs offer statistical uncertainty quantification for TSE. There are some studies that utilize the GPs in the calibration and evaluation of traffic flow models [166]–[170]. However, conventional GP models are inadequate in modeling traffic flow data due to the non-stationarity and anisotropy caused by traffic wave propagation. Taking Fig. 3.2 (a) as an example, the congestion wave propagates backward, generating directional spatiotemporal correlations that traditional GP kernels cannot model. To capture the anisotropic corre-

lation in traffic wave propagation, we re-parameterized the GP kernel with a rotation angle. The kernel rotation angle indicates the speed of congestion propagation in traffic waves and can be estimated from partially observed data. We address the scalability issue of the GP model with variational sparse GP. Moreover, we propose using a multi-output GP model to simultaneously enable TSE on multiple lanes, rather than using several individual GPs. To test the TSE performance, we compare the proposed rotated GP with other imputation methods in NGSIM and HighD datasets under different types and percentages of observed traffic information, which can also be regarded as CV penetration rates in the mixed traffic environment. We also use simulated data to test the TSE performance under a traffic bottleneck scenario. Experimental results demonstrate that the proposed rotated GP significantly outperforms other methods regarding accuracy and robustness for TSE under low CV penetration rates.

The contributions of this chapter are summarized as follows:

- A new approach is proposed for TSE using Gaussian process models with rotated anisotropic kernels that can capture the anisotropic correlation in traffic wave propagation. The rotation angle can be estimated from partially observed data, offering valuable insights into the speed of congestion propagation within traffic waves. Our approach elegantly merges statistical modeling with traffic flow theory.

- The proposed GP-based TSE method is a purely data-driven approach that does not require an external training dataset and provides statistical uncertainty quantification for the estimation, which is important for TSE under low CV penetration rates.

- The results from extensive experiments demonstrate the adaptability of our GP-based TSE method across different CV penetration rates and types of detectors, achieving state-of-the-art accuracy in scenarios with sparse observation rates.

- The multi-output GP model is proposed for TSE on multiple lanes, which leverages the correlation between the traffic states of different lanes to improve TSE accuracy.

3.2 Methodology

3.2.1 Problem formulation

We aim to estimate the traffic state (speed in this paper) of a highway segment over a period of time, using data collected from fixed or moving sensors such as loop detectors and CVs. For a single lane of the highway segment, we denote s as the spatial coordinate on the segment, t as the temporal coordinate, and $y(s,t)$ as the traffic speed at location s and time t. In practice, s and t are usually defined as discrete values on an $S \times T$ spatiotemporal grid. However, for our purposes, we can consider a general continuous space with a subscript i such that $y_i = y(\mathbf{x}_i)$, where $\mathbf{x}_i = [s_i, t_i]^\top$ is a vector representing the spatiotemporal coordinate.

Assume we can obtain the traffic speed $\mathbf{y}_o = \{y_i\}_{i=1}^{n}$ at a set of spatiotemporal locations $X_o = \{\mathbf{x}_i\}_{i=1}^{n}$ using loop detectors or probe vehicles, where n is the number of observations. Our goal is to estimate the traffic speed distribution of $\mathbf{y}_* = \{y_i\}_{i=n+1}^{n+u}$ at unknown spatiotemporal locations $X_* = \{\mathbf{x}_i\}_{i=n+1}^{n+u}$ given the observed data $\{X_o, \mathbf{y}_o\}$, where u is the number of points/locations whose traffic state is unknown. For a highway segment with multiple lanes, the problem becomes estimating the joint distribution $p\left(\mathbf{y}_*^1, \cdots, \mathbf{y}_*^L\right)$ from observations $\left\{X_o^1, \mathbf{y}_o^1, \cdots, X_o^L, \mathbf{y}_o^L\right\}$, where L is the number of lanes.

3.2.2 Gaussian process regression

For a single lane of the highway segment, we assume the observed traffic state y_i consists of a ground truth value f_i and a noise term ε_i:

$$y_i = f_i + \varepsilon_i, \tag{3.1}$$

where ε is an independent and identically distributed (i.i.d.) Gaussian noise with zero mean and variance σ_ε^2.

Assume the ground truth traffic state f is a function of the spatiotemporal coordinate $\mathbf{x}$. We can impose a GP prior [165] to the function $f(\mathbf{x}) \sim \mathcal{GP}(\mu, k)$. A GP is a distribution over functions (or in other words, a distribution with an infinite number of random variables). The ground truth traffic state that occurred within the spatiotemporal range being examined can be considered as a sample drawn from the GP. With the GP prior, any finite collection of $\mathbf{f} \in \mathbb{R}^N$ at spatiotemporal location X is assumed to follow a multivariate Gaussian distribution:

$$\mathbf{f} = f(X) = [f(\mathbf{x}_1), \cdots, f(\mathbf{x}_N)]^\top \sim \mathcal{N}(\boldsymbol{\mu}, K), \tag{3.2}$$

where the mean is often set to be zero $\boldsymbol{\mu} = \mathbf{0}$, and the covariance matrix K is defined by a kernel function k such that $K[i, j] = k(\mathbf{x}_i, \mathbf{x}_j)$. For example, the commonly used squared exponential (SE) kernel takes the form:

$$k_{\text{SE}}(\mathbf{x}_i, \mathbf{x}_j) = \sigma^2 \exp\left(-\frac{1}{2\ell^2}\|\mathbf{x}_i - \mathbf{x}_j\|^2\right), \tag{3.3}$$

where the length scale ℓ determines how far apart two points in the input space can still be considered similar; the kernel variance σ^2 determines how far the function values can be from the mean. The kernel hyper-parameters and the noise variance $\boldsymbol{\theta} = \{\sigma^2, \ell, \sigma_\varepsilon^2\}$ can be estimated from the observed data using Maximum Marginal likelihood (MML) estimation.

Taking advantage of the conditional Gaussian distribution, the posterior distribution of traffic state $\mathbf{f}_*$ at the unknown spatiotemporal locations $\mathbf{X}_*$ given observed data can be obtained by:

$$p(\mathbf{f}_*|X_*, X_o, \mathbf{y}_o) \sim \mathcal{N}(\bar{\mathbf{f}}_*, \text{cov}(\mathbf{f}_*)), \tag{3.4}$$

$$\bar{\mathbf{f}}_* = K_{n*}^\top \left(K_{nn} + \sigma_\varepsilon^2 I\right)^{-1} \mathbf{y}_o, \tag{3.5}$$

$$\text{cov}(\mathbf{f}_*) = K_{**} - K_{n*}^\top \left(K_{nn} + \sigma_\varepsilon^2 I\right)^{-1} K_{n*}, \tag{3.6}$$

where matrices K_{nn}, K_{**}, and K_{n*} represent the kernel matrices evaluated at observed locations (size $n \times n$), unknown locations (size $u \times u$), and between observed and unknown locations (size $n \times u$), respectively. Next, the distribution of $\mathbf{y}_*$ can be readily obtained by Eq. (3.1).

3.2.3 Rotated anisotropic kernel

Most GP kernels, such as the SE kernel in Eq. (3.3), are isotropic, meaning the covariance is only a function of $\|\mathbf{x}_i - \mathbf{x}_j\|$ and is invariant to the directions between $\mathbf{x}_i$ and $\mathbf{x}_j$. The traffic wave, however, exhibits anisotropic behavior as it propagates along a specific direction. Although an isotropic kernel can have anisotropic properties by using different length scales on different dimensions (i.e., implementing Automatic Relevance Determination (ARD) [171]), the ARD kernel is a very limited form and is still incapable of modeling the correlation propagates along a spatiotemporal direction.

Without loss of generality, let us consider the "squared distance" between $\mathbf{x}_i$ and $\mathbf{x}_j$ in an ARD kernel:

$$d(\mathbf{x}_i, \mathbf{x}_j)^2 = (\mathbf{x}_i - \mathbf{x}_j)^\top M (\mathbf{x}_i - \mathbf{x}_j), \tag{3.7}$$

where M is a diagonal matrix with the d-th diagonal element being ℓ_d^{-2}, specifying the dimension-specific length-scale. The diagonal structure of M makes the length-scale along the spatial and temporal directions independent. To account for the traffic wave propagation, we introduce a rotation angle α, a new hyper-parameter, which is the angle between the traffic wave and the space direction, as shown in Fig. 3.1. Then, we can measure the directional covariance using the following rotated squared distance:

$$
\begin{aligned}
d_{\mathrm{rot}}\left(\mathbf{x}_i, \mathbf{x}_j\right)^2 &= \left(R\left(\mathbf{x}_i - \mathbf{x}_j\right)\right)^\top M \left(R\left(\mathbf{x}_i - \mathbf{x}_j\right)\right) \\
&= (\mathbf{x}_i - \mathbf{x}_j)^\top \left(R^\top M R\right)(\mathbf{x}_i - \mathbf{x}_j),
\end{aligned}
\tag{3.8}
$$

$$
R = \begin{bmatrix} \cos\alpha & -\sin\alpha \\ \sin\alpha & \cos\alpha \end{bmatrix}. \tag{3.9}
$$

The matrix R is a rotation matrix. Eq. 3.8 can be used in general kernel functions. For example, the rotated squared distance can be used to define a rotated anisotropic squared exponential (SE) kernel:

$$
k_{\mathrm{SE}}(\mathbf{x}_i, \mathbf{x}_j) = \sigma^2 \exp\left(-\frac{1}{2} d_{\mathrm{rot}}(\mathbf{x}_i, \mathbf{x}_j)^2\right). \tag{3.10}
$$
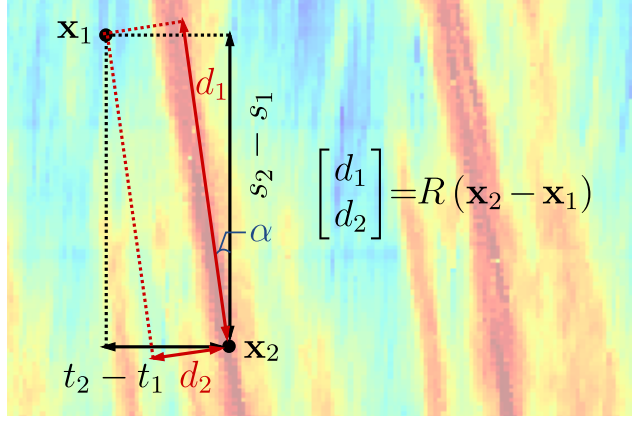
Figure 3.1: Illustration of the rotated coordinates.

The same transformation applies to other kernel functions, such as Matérn kernels and the rational quadratic kernel.

A graphical illustration of our method is shown in Fig. 3.1. The intuition behind the proposed kernel is the rotation of the coordinates. The rotation angle α can be used to measure the speed of congestion propagation in the traffic wave. Similar to other hyper-parameters, the angle α can be estimated from the observed data.

3.2.4 Model inference with variational sparse GP

The computational complexity of an MML estimation of GP scales cubically with the number of data points, which limits its applicability to large datasets. Therefore, we use the variational sparse GP (VSGP) [172] for scalable inference. VSGP introduces a set of m inducing points at $Z = \{\mathbf{z}_1, \cdots, \mathbf{z}_m\}$ that act as a sparse approximation to the full Gaussian process. The model assumes that the function values at the inducing points follow the same GP prior, and the posterior distribution of the function values is approximated by a Gaussian distribution conditioned on the inducing variables. The locations of inducing points can be optimized as other hyper-parameters.

The model parameters, including hyper-parameters $\boldsymbol{\theta}$ and the locations of inducing variables Z, are learned by maximizing the evidence lower bound (ELBO), which is a lower bound of the log marginal likelihood of the observed

data. The ELBO of VSGP derived by Titsias [172] is:

$$\log p(\mathbf{y}_o) \geq \log \mathcal{N}\left(\mathbf{y}_o | \mathbf{0}, Q_{nn} + \sigma_\varepsilon^2 I\right) - \frac{1}{2\sigma_\varepsilon^2} \operatorname{tr}\left(K_{nn} - Q_{nn}\right), \qquad (3.11)$$

where $Q_{nn} = K_{nm} K_{mm}^{-1} K_{nm}^\top$, matrices K_{mm} and K_{nm} are the kernel evaluated at the inducing points, and between the observed locations and inducing points, respectively. We can interpret the ELBO as the sum of the approximate log marginal likelihood and a regularization term $-\frac{1}{2\sigma_\varepsilon^2} \operatorname{tr}\left(K_{nn} - Q_{nn}\right)$. The regularization term minimizes the squared error of predicting the training latent function values $\mathbf{f}_n$ from the inducing variables. Eq. (3.11) can be simplified with the Woodbury matrix identity, and the time complexity of VSGP is $O(mn^2)$.

The posterior distribution of function values at unknown location $\mathbf{x}_*$ is given by the integral $p(\mathbf{f}_*) = \int p(\mathbf{f}_*|\mathbf{f}_z) p(\mathbf{f}_z) d\mathbf{f}_z$, which is a Gaussian distribution with the mean and covariance:

$$\bar{\mathbf{f}}_* = K_{*m} K_{mm}^{-1} \bar{\mathbf{f}}_z, \qquad (3.12)$$

$$\operatorname{cov}(\mathbf{f}_*) = K_{**} - K_{m*}^\top K_{mm}^{-1} K_{m*} + K_{m*}^\top K_{mm}^{-1} \Lambda K_{mm}^{-1} K_{m*}, \qquad (3.13)$$

where $\bar{\mathbf{f}}_z = \sigma_\varepsilon^{-2} \Lambda^{-1} K_{mm}^{-1} K_{mn} \mathbf{y}_o$ is the posterior mean of the inducing variables, and $\Lambda = K_{mm}^{-1} + \sigma_\varepsilon^{-2} K_{mm}^{-1} K_{mn} K_{nm} K_{mm}^{-1}$ is the posterior precision matrix of the inducing variables.

3.2.5 Multi-output GP

The traffic states of neighboring lanes of the same road are highly correlated, because drivers can choose a less congested lane to travel and thus the traffic state of the neighboring lane reaches a similar condition. The TSE in a highway segment with multiple lanes can be naturally modeled using a multi-output GP model [173], [174], also known as a coregionalized GP or co-kriging. Unlike using independent GP models for each lane, a multi-output GP model can leverage the correlation between the traffic states of different lanes to improve estimation accuracy. In Section 3.3.8, we will demonstrate that the multi-output GP model can estimate traffic speed during a long period that has no observations in a lane, by utilizing information from the other lane.

The probe vehicles from different lanes locate at different spatiotemporal locations, which is referred to as heterotopic data in the multi-output GP literature. We model the traffic states of L different lanes as a multi-output function $\boldsymbol{f}(\mathbf{x}) = \left[f^1(\mathbf{x}), \cdots, f^L(\mathbf{x}) \right]^{\top}$ with a GP prior. The covariance of the i-th output at $\mathbf{x}$ and the j-th output at $\mathbf{x}'$ is given by the kernel function:

$$k_{\text{multi}} \left(f^i(\mathbf{x}), f^j(\mathbf{x}') \right) = k(\mathbf{x}, \mathbf{x}') B \left[i, j \right], \qquad (3.14)$$

where B is an $L \times L$ symmetric and positive-definite matrix parametrized by $B = AA^{\top}$, and $A \in \mathbb{R}^{L \times r}$ is a parameter to learn, r is the rank of A. This kernel parametrization is also called the intrinsic model of coregionalization [173] in the geostatistics literature. One can view the multi-output kernel k_{multi} as functions on an extended input space with the index of the lane, which allows for using the same inference procedure as the single-output GP model.

3.3   Case Study

We evaluate the proposed GP-based TSE method on two real-world datasets and one simulated dataset: the NGSIM [175] traffic trajectory data and the HighD [176] naturalistic vehicle trajectory data and a simulated dataset for traffic bottleneck scenario. In Section 3.3.3, we compare the TSE performance of the proposed model with a set of benchmark models under different CV penetration rates. In Section 3.3.4, we evaluate the TSE performance when assuming using loop detector data. The uncertainty quantification and computational time of the proposed method are further analyzed in Section 3.3.6 and 3.3.7. Finally, we also explore the use of a multi-output rotated GP for TSE on multiple lanes. The code and data associated with this paper are available at https://github.com/Lucky-Fan/GP_TSE.

3.3.1   Data and experimental setup

We test the proposed rotated GP for TSE using the trajectories from two real-world datasets, namely NGSIM [175] and HighD [176] as well as a simulated

dataset. Both real-world datasets provide detailed information about each vehicle's trajectory, such as vehicle ID, recording frame, time, location, velocity, lane, etc. This allows us to use the ground truth traffic state to evaluate the accuracy of TSE. In the case of NGSIM, we focus on the traffic data from lane 2 of US Highway 101. For HighD, we utilize data from two lanes of a German highway. These lanes are selected as they display some very representative stop-and-go traffic waves. The simulated traffic data in a bottleneck scenario is utilized to ensure its effectiveness in broader contexts. The specific details of the three datasets are provided below:

- The NGSIM data: We use vehicle trajectories extracted from video cameras on lane 2 of US highway 101. In contrast to the previous work by Wang et al. [47], our experiment covers a longer road segment of 600 meters and a larger time range of 2500 seconds. We extract the complete data and focus on the traffic state at a 200×500 spatiotemporal grid with a resolution of 3 meters and 5 seconds, where the traffic state is defined as the average vehicle speed in each grid cell. Fig. 3.2 (a) and (b) show the traffic speed maps of the entire dataset and samples of observed trajectories under a 5% penetration rate, respectively.

- The HighD data: This dataset provides naturalistic vehicle trajectories recorded on German highways using drones. The dataset includes 60 recordings from six different locations; each recording is identified by track ID. In our study, we focus on the recording with track ID 25. Where the full drive length of vehicles during the road segment is 1120346.1 meters, and the time range is 80676.08 seconds. To make the most of the data, we extract traffic state in a spatiotemporal grid of size 100×220 with a resolution of 4 meters and 5 seconds, representing a domain of 400 meters and 1100 seconds. The average vehicle speed is calculated to describe the traffic state at each cell. We use the data from lane 4 for the TSE of a single lane in Table 3.2, and we use the data from lane 3 and lane 4 to test using multi-output GP for TSE.

46

- The simulated data: We construct and simulate a bottleneck scenario in SUMO [Simulation of Urban MObility, 177]. This scenario spans 1000 meters over 3600 seconds. Initially, the speed limit is 100 km/h for the first 750 meters, followed by a 250-meter bottleneck segment where the speed limit decreases to 20 km/h. Vehicle arrivals conform to a Poisson process with an expected rate of 720 veh/h. Moreover, we introduced two peak periods with vehicle demand set at 2160 veh/h and 1800 veh/h during the time intervals of 800 to 1000 seconds and 2000 to 2200 seconds, respectively, to induce shockwaves. Our focus is solely on the midsection, excluding the warm-up and end times. This simulated data serves as a means to assess the TSE performance in a traffic bottleneck scenario.

When using CVs as probe vehicles, we set 5%, 10%, 20%, 30%, 40%, and 50% as the penetration rate of CVs and assume only the trajectories of CVs are observed (i.e., the training data). Under each CV penetration rate, we repeat the experiment 10 times with different random draws of trajectories. Note that we define spatiotemporal grids to make an easy comparison with other models, although GP can make TSE on a continuous space without defining grids. Overall, the NGSIM, HighD datasets and the simulated dataset provide rich sources of data for evaluating the effectiveness and efficiency of our approach and baselines under different scenarios.

3.3.2 Baseline models and hyper-parameters

In the following, we refer to the proposed GP based on rotated kernels as "GP-rotated". We use the following baselines to compare the performance of GP-rotated with other methods:

- The adaptive smoothing interpolation method (ASM) [59]: It is an interpolation method for estimating traffic states. This method resembles the proposed rotated GP in terms of considering the traffic wave propagation using an anisotropic interpolation. We set the propagation speed of congestion traffic to be -19.87 km/h and -17.86 km/h for the NGSIM

47

and HighD datasets, respectively, which is based on the estimated hyper-parameters of the GP-rotated method (see discussion in Section 3.3.3). The space smoothing width and time smoothing width are set as 200 m and 10 s, respectively, based on an initial setting suggested by [59] and a quick validation. Other parameters adopt the settings of [59].

- Spatiotemporal hankel low-rank tensor completion (STH-LRTC) [47]: It transforms the original speed matrix into a tensor using spatial and temporal delay embedding. Then, the approach estimates the traffic state matrix by conducting inverse Hankelization on the delay-embedding tensor imputed by a low-rank model. The key parameters include the embedding lengths τ_s and τ_t. We adopt the same hyper-parameter settings $\tau_s = 40$ and $\tau_t = 30$ as the authors. But we do find the method produces poor results in certain cases with extremely low CV penetration rates. Therefore, we increase the τ_s and τ_t with case-specific tuning, as noted in Table 3.5.

- Gaussian process regression with standard ARD kernels (GP-ARD): It extends the basic GP by allowing the kernel function to have a separate length scale parameter for each input dimension, which enables the model to automatically determine the importance of each input variable in predicting the output variable. The hyper-parameters are learned from data using the VSGP approach.

We use Matérn kernel [165] as the basic kernel function for all GP models. We set the number of inducing points $m = \min(0.02n, 500)$, and the initial locations of inducing points are randomly distributed on the grid. As introduced in Section 3.2.4, the hyper-parameters of GP-rotated can be learned from the observed data, which could be time-consuming for a large dataset. However, one may not need to repeatedly learn the hyper-parameters for the same highway segment in reality. Therefore, we also test the performance of the proposed GP using pre-trained hyper-parameters, referred to as "P-GP-rotated". Please note that we do not include comparisons with deep-learning-based models as

many of them depend on external training datasets and are not available as open-source.

It's worth noting that the training data (obtained from CVs) and test data (obtained from all vehicles) for a cell with CV trajectories may differ since the speed may be calculated from different numbers of vehicles in the training and test data. TSE values are only used for the cells without any CV trajectories. For cells with observed trajectories, we directly use the speed from the training data, because we found that observed values on these cells are closer to the test data than the estimated value, no matter what TSE method is used. This can be attributed to the utilization of high-quality datasets. Finally, we use the root mean squared error (RMSE) and mean absolute error (MAE) as shown in the following to evaluate the performance of different TSE models:

$$\text{RMSE} = \sqrt{\frac{\sum_l \sum_s \sum_t (y^l(s,t) - \hat{y}^l(s,t))^2}{STL}}, \tag{3.15}$$

$$\text{MAE} = \frac{\sum_l \sum_s \sum_t |y^l(s,t) - \hat{y}^l(s,t)|}{STL}. \tag{3.16}$$

3.3.3 TSE from vehicle trajectories

We begin by visually examining the TSE performance of different methods under a 5% CV penetration rate using the NGSIM dataset. Fig. 3.2 displays the results. Fig. 3.2 (a) shows the ground truth traffic speed map of all trajectories, exhibiting complex traffic dynamics evolution with shockwaves, making it a suitable dataset for experimentation. Fig. 3.2 (b) displays one of the randomly selected 5% training datasets from ten independent experiments.

By comparing Fig. 3.2 (e) and (f), we can observe that the proposed GP-rotated captures the directional traffic speed correlations that traditional GP-ARD cannot model. When comparing the ASM in Fig. 3.2 (c) with the proposed GP-rotated, we can find they both capture the congestion propagation in the traffic wave because they both use the idea of anisotropic kernels. However, the congestion speed estimated by the ASM is generally lower than the ground truth speed, which is caused by the "smoothing" operation in the ASM. The STH-LRTC in Fig. 3.2 (d) also captures the congestion propagation in
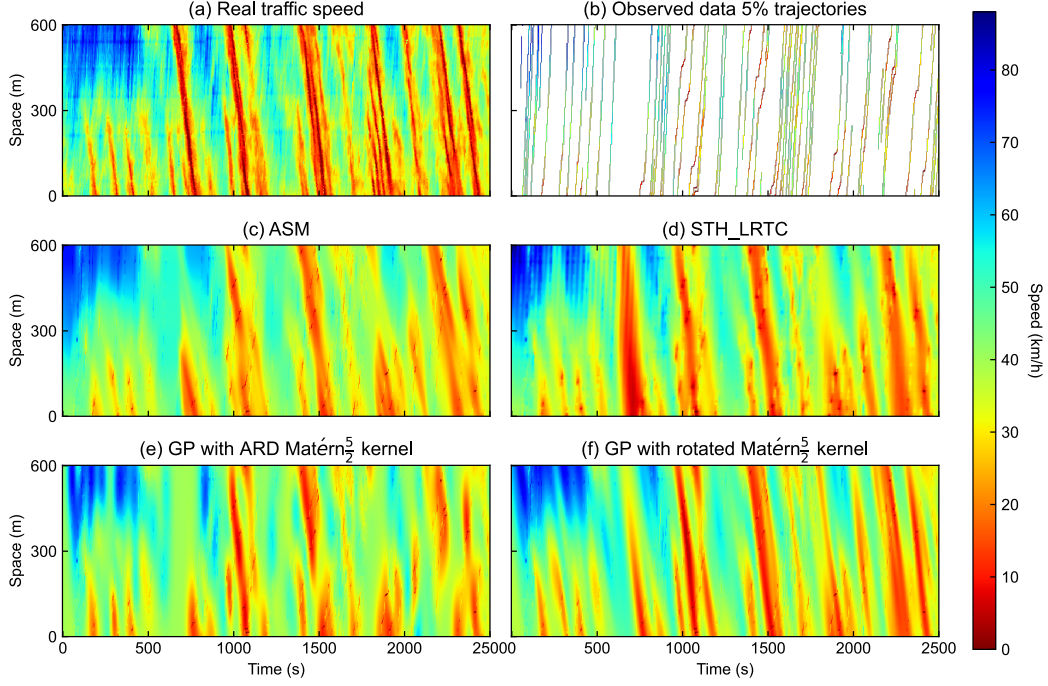
Figure 3.2: A TSE experiment on the NGSIM dataset with 5% CVs penetration rate. The observed trajectories are superimposed on the TSE results. (a) The traffic speed of the full dataset. (b) The traffic speed of observed trajectories. (c) The traffic speed estimated by the ASM method. (d) The traffic speed estimated by the STH-LRTC method. (e) The traffic speed estimated by the GP with ARD Matérn$\frac{5}{2}$ kernel. (f) The traffic speed estimated by the GP with the proposed rotated Matérn$\frac{5}{2}$ kernel.

the traffic wave, but it performs poorly when there is a long period without CV trajectories (e.g., 550s-750s).

Next, we perform more extensive experiments to quantify the performance of the proposed method and the baselines under different penetration rates (percentage of trajectories). For each penetration rate (5%, 10%, 20%, 30%, 40%, and 50%), we repeat the experiments ten times with randomly selected vehicle trajectories from the complete dataset as the training set (see Section 3.3.1). The experiments were conducted on the NGSIM and HighD datasets. Table 3.1 and Table 3.2 display the average MAE (m/s) and RMSE (m/s) with standard deviation for each method under various penetration rates and datasets.

Table 3.1: TSE accuracy for the NGSIM dataset under different penetration rates: mean (std).

Method	ASM		STH-LRTC		GP-ARD		GP-rotated		P-GP-rotated	
Rate	MAE	RMSE	MAE	RMSE	MAE	RMSE	MAE	RMSE	MAE	RMSE
0.05	5.11 (0.32)	7.04 (0.54)	5.51 (1.36)	7.94 (2.38)	6.02 (0.36)	8.62 (0.56)	**4.85 (0.31)**	6.74 (0.56)	4.97 (0.29)	**6.74 (0.47)**
0.10	4.09 (0.15)	5.72 (0.26)	4.19 (1.39)	7.43 (5.62)	4.35 (0.30)	6.42 (0.58)	3.82 (0.22)	5.44 (0.47)	**3.79 (0.13)**	**5.19 (0.22)**
0.20	3.28 (0.10)	4.82 (0.14)	3.01 (1.26)	6.16 (7.14)	3.07 (0.14)	4.61 (0.26)	**2.81 (0.10)**	**4.10 (0.19)**	2.98 (0.08)	4.28 (0.12)
0.30	2.73 (0.06)	4.26 (0.09)	**2.09 (0.05)**	**3.17 (0.12)**	2.43 (0.06)	3.77 (0.11)	2.27 (0.05)	3.43 (0.10)	2.48 (0.05)	3.75 (0.08)
0.40	2.29 (0.06)	3.83 (0.09)	**1.75 (0.05)**	**2.81 (0.12)**	2.03 (0.06)	3.35 (0.11)	1.92 (0.05)	3.08 (0.09)	2.09 (0.05)	3.37 (0.09)
0.50	1.87 (0.05)	3.41 (0.09)	**1.43 (0.04)**	**2.46 (0.11)**	1.67 (0.04)	2.96 (0.10)	1.58 (0.04)	2.71 (0.09)	1.71 (0.04)	2.98 (0.07)

Table 3.2: TSE accuracy for the HighD dataset under different penetration rates: mean (std).

Method	ASM		STH-LRTC		GP-ARD		GP-rotated		P-GP-rotated	
Rate	MAE	RMSE	MAE	RMSE	MAE	RMSE	MAE	RMSE	MAE	RMSE
0.05	4.44 (0.31)	**6.03 (0.50)**	55.9 (29.3)	121.5 (51.1)	5.18 (1.59)	7.19 (2.04)	4.48 (0.50)	6.27 (0.94)	**4.43 (0.27)**	6.06 (0.43)
0.10	3.32 (0.14)	4.67 (0.22)	3.19 (0.10)	4.49 (0.21)	3.22 (0.17)	4.55 (0.28)	**3.18 (0.16)**	**4.45 (0.25)**	3.55 (0.18)	5.00 (0.30)
0.20	2.55 (0.08)	3.79 (0.11)	**2.15 (0.11)**	**3.12 (0.18)**	2.23 (0.09)	3.26 (0.15)	2.23 (0.09)	3.25 (0.13)	2.43 (0.07)	3.52 (0.11)
0.30	2.08 (0.03)	3.30 (0.05)	**1.65 (0.04)**	**2.49 (0.06)**	1.71 (0.05)	2.62 (0.10)	1.71 (0.05)	2.61 (0.10)	1.89 (0.05)	2.90 (0.09)
0.40	1.68 (0.04)	2.85 (0.07)	**1.31 (0.04)**	**2.07 (0.07)**	1.36 (0.04)	2.14 (0.09)	1.35 (0.03)	2.14 (0.08)	1.49 (0.03)	2.39 (0.06)
0.50	1.37 (0.05)	2.49 (0.10)	**1.05 (0.03)**	**1.75 (0.07)**	1.09 (0.03)	1.80 (0.07)	1.09 (0.03)	1.80 (0.06)	1.19 (0.03)	2.03 (0.05)

Table 3.1 and Table 3.2 illustrate that the performance of the STH-LRTC method is the best when the proportion of observed trajectories (penetration rate) is over 30%. This is because the GP-based methods cannot capture the fine-grained texture in traffic flow, which is shown in Section 3.3.6. However, for the cases with sparse observations (CV penetration from 5% to around 20%), our proposed GP-rotated performs the best on both NGSIM and HighD datasets. As the CV penetration rate decreases, the STH-LRTC may fail due to a large block of missing information, which can be observed in the HighD data under the 5% rate. The corresponding MAE and RMSE values can be as high as 55.9 m/s and 121.5 m/s, respectively. The STH-LRTC may be unstable under low penetration rates, with high standard deviation in MAE and RMSE values. In contrast, our proposed GP method provides a very robust estimation, regardless of the percentage of probe vehicles. In the early stages of a mixed traffic environment with a low CV penetration rate, such as 5% to 20%, our proposed method is a suitable choice.

Our proposed method consistently outperforms the ASM benchmark. An advantage of ASM is that it considers the traffic propagation of both congestion and free flow. Therefore, ASM could produce a more natural traffic flow pattern, as demonstrated in the high-speed region (top left corner) of Fig. 3.2 (c). However, the ASM is not as good as the GP-rotated in estimating small shockwaves during the first 500 seconds (bottom left corner). The proposed GP-rotated outperforms ASM in most cases (except for the highD dataset with 5% penetration rate). The gaps between ASM and GP-rotated increase with a larger CV penetration rate.

We also compare the GP-ARD and GP-rotated methods using the Matérn$\frac{5}{2}$ kernel in Tables 3.1 and 3.2. Our results show that the GP-rotated method consistently outperforms the GP-ARD method in terms of average MAE and RMSE, regardless of whether we use the pre-trained parameters or not. This can be attributed to the fact that the ARD kernel is isotropic, meaning it uses distance to measure covariance. However, traffic waves are anisotropic and propagate in spatiotemporal directions. Although GP-ARD can apply different

length scales to different dimensions, it still fails to capture the directional covariance of traffic waves. On the other hand, our proposed anisotropic GP-rotated method with a directional hyper-parameter α accurately models the directional covariance of traffic waves. Furthermore, we observed that the numerical differences in MAE and RMSE between GP-ARD and GP-rotated decrease with an increase in the observation rate. This is because, with more observed trajectories, the GP-ARD method can utilize more information to overcome the directional limitation based on length scale adjustments.

We observe that the P-GP-rotated method can also achieve satisfactory TSE results and even outperform the GP-rotated in some low-penetration scenarios, possibly due to the overfitting of GP-rotated when the number of observed trajectories is small. However, as the CV penetration rate increases, the performance of P-GP-rotated is not as good as GP-rotated, likely because the inducing point locations in P-GP-rotated are not optimized.

The GP-rotated kernel hyperparameters, α, represent the angle between the traffic wave and the spatial direction, and values learned from the data are around $\alpha = 0.108 = 6.20°$ for the NGSIM dataset and $\alpha = 0.160 = 9.16°$ for the HighD dataset. After unit conversion with the size of cells, our estimation shows that the congestion propagation speed is approximately -19.87 km/h and -17.86 km/h for the NGSIM and HighD datasets, respectively, which is faster than the -15 km/h value used in [59].

To ensure a fair comparison between ASM and GP-rotated, we set the congestion propagation speed of ASM in this study using the value derived by α. Additionally, we assess the RMSE of TSE using ASM with various congestion propagation speeds, as depicted in Fig. 3.3. We observe that the speed estimated by GP-rotated (-19.87 km/h) is close to the optimal value (around -19 km/h) with minimum RMSE evaluated on the full NGSIM data (illustrated by the blue curve with dot marks). It's important to note that during the training phase, only 5% of trajectories are observed. Consequently, while the best congestion propagation speed of ASM on the training set hovers around -17 km/h, it may not yield optimal performance for the full data. The

insights from Fig. 3.3 indicate that GP-rotated offers a promising approach for estimating congestion propagation speed from sparse vehicle trajectories.
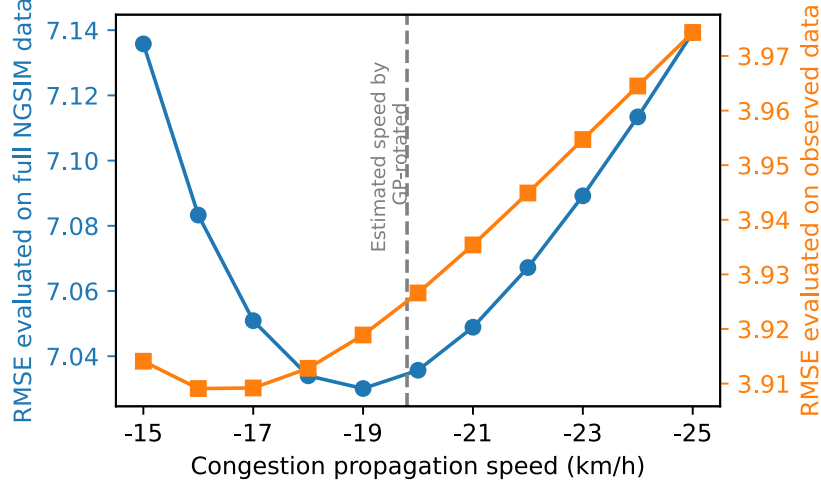
Figure 3.3: When observing 5% trajectories, the RMSE error of ASM when using different congestion propagation speed in the NGSIM dataset.

3.3.4 TSE from loop detectors

The proposed TSE method can also be used when traffic flow information is obtained from loop detectors. Loop detectors are commonly deployed at select road segments to gather specific traffic data, including vehicle count and density. Subsequently, these data points are leveraged to conduct traffic analysis. The installation of loop detectors is often sparse because of the high cost. Therefore, it is critical to utilize these sparse observations from loop detectors to perform TSE to reconstruct the complete traffic conditions on the whole road.

Our experiment commences by conducting TSE exclusively with loop detector data. For the NGSIM dataset, three virtual detectors are positioned at distances of 30 meters, 300 meters, and 570 meters from the starting point, as is shown in Fig. 3.4 (b). For the HighD dataset, the locations of the three detectors are 40 meters, 200 meters, and 360 meters from the starting point. Only the traffic speed at the location of the loop detectors can be observed.

Fig. 3.4 showcases the TSE results of the NGSIM dataset. Fig. 3.4 (a)
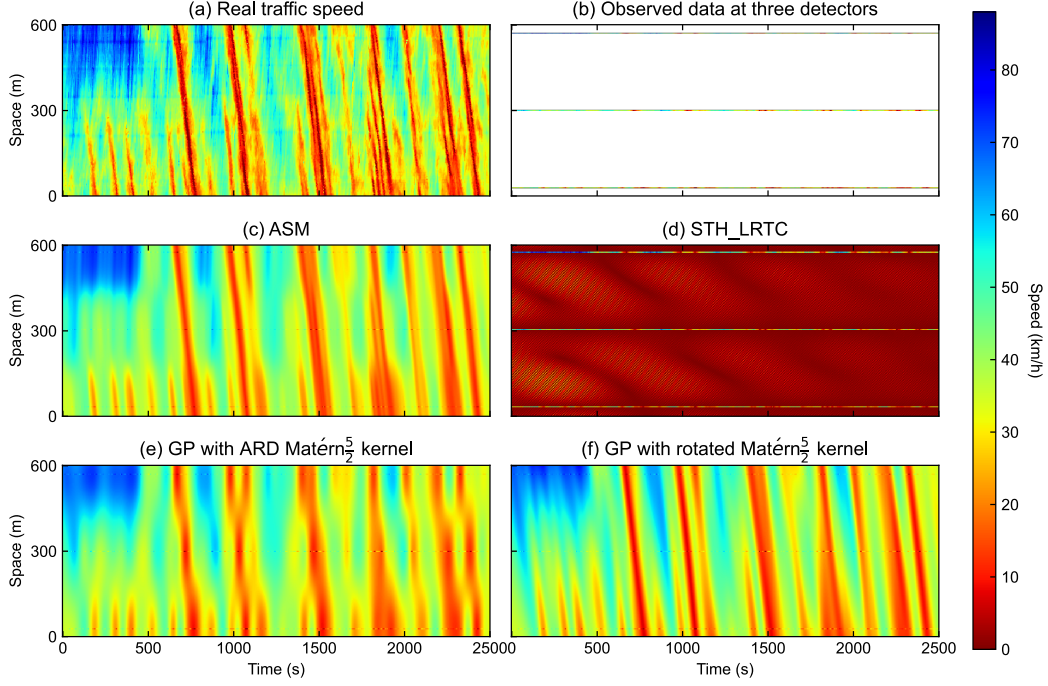
Figure 3.4: A TSE experiment on the NGSIM dataset with observation at three detectors.

presents the ground truth traffic speed map for the entire road segment. Fig. 3.4 (b) portrays the observed traffic states at the three specific locations where loop detectors are installed. Notably, STH-LRTC fails in this case because of blocks of missing rows in the matrix. Upon closer examination of Fig. 3.4 (c) and (f), both ASM and GP-rotated produce an accurate reconstruction of traffic speed, and the success of these methods is largely attributed to the accurate estimation of the congestion propagation speed. By comparing Fig. 3.4 (e) and (f), it is strikingly evident that our proposed GP-rotated method accurately captures congestion propagation and directional traffic wave correlations. This starkly contrasts with the traditional GP-ARD model, which fails to achieve the same level of precision in these aspects.

Table 3.3 presents the MAE and RMSE values measured in m/s for each method applied to the two study areas. These findings align with the performance trends depicted in Fig. 3.4. The proposed GP-rotated method outperforms the others when dealing with limited data obtained from specific

Table 3.3: TSE accuracy with observations at three detectors.

Dataset	NGSIM		HighD	
Method	MAE	RMSE	MAE	RMSE
ASM	4.45	5.78	3.05	4.10
STH-LRTC	34.90	38.22	29.15	34.14
GP-ARD	5.16	6.80	3.05	4.11
GP-rotated	**4.36**	**5.59**	**2.96**	**4.01**

loop detectors. For instance, when comparing the STH-LRTC method with GP-rotated, the former yields an MAE of 34.90 m/s and an RMSE of 38.22 m/s on the NGSIM dataset, whereas our proposed method achieves a significantly lower MSE of 4.36 m/s. This marked difference in performance is attributed to the incapacity of STH-LRTC to function effectively under such conditions. In comparing the GP-ARD and GP-rotated models, the latter demonstrates superior accuracy over the traditional GP model, with gaps in MAE (m/s) and RMSE (m/s) ranging from 0.1 to 1.2 m/s. Although the absolute gaps do not seem vast, the relative difference cannot be ignored. It is vividly shown in Fig. 3.4. The ASM's accuracy surpasses that of GP-ARD but slightly lags behind GP-rotated. While it is possible to further enhance ASM performance by fine-tuning other parameters, such as the smoothing widths and the free-congested transition speed, this process is heavily dependent on prior knowledge; given that detectors offer only limited information to verify these parameters, achieving significant improvements for ASM is challenging.

3.3.5 TSE at a bottleneck

We further validate the performance of our proposed method using simulated traffic data in a bottleneck scenario to ensure its effectiveness in broader contexts. The simulation was executed in SUMO with the Intelligent Driver Model [IDM, 126] chosen as the car-following model. The total road length spans 1 km, with a speed limit of 100 km/h for the initial 750 m, followed by a bottleneck segment of 250 m with a speed limit reduced to 20 km/h. Vehicle

arrivals follow a Poisson process with an expected rate of 720 veh/h. Additionally, we introduced two peak periods with vehicle demand set at 2160 veh/h and 1800 veh/h during the time intervals 800–1000 seconds and 2000–2200 seconds, respectively, to induce shockwaves. The simulation duration spans 3600 seconds, and we only focus on the midsection excluding the warm-up and end times. Average speeds are calculated using a 5-second × 5-meter grid, and the resulting speed profile is illustrated in Fig. 3.5 (a). We test the TSE performance using detector data, CV trajectories, or both data sources. The four detectors are located at 100 m, 400 m, 770 m, and 900 m, respectively. We randomly select the trajectories of 5% vehicles for TSE. The location of detectors and trajectories are shown by white dots/lines in Fig. 3.5. We set $\tau_s = \tau_t = 50$ for STH-LRTC. For ASM, the propagation speed of congestion is set as -10 km /h by measuring from the graph; the space smoothing width and time smoothing width are set as 100 m and 50 s, respectively.

By comparing the estimation results in Fig. 3.5 with Fig. 3.2, we observe that reconstructing the traffic state at a bottleneck presents greater challenges. This is attributed to how congestion not only propagates backward but also forward as it returns to a free-flow state. Similar findings are discussed in Section 3.3 of the work by [59]; the detector data alone is not sufficient for accurately estimating the margins of shockwaves. Using more observations and a fusion of different data sources are required to obtain a good TSE for this complex scenario. Additionally, we note that the estimated rotation angle in GP-rotated no longer aligns with the backward propagation speed of congestion in this bottleneck example (the estimated angle corresponds to a speed ranging from -15 km/h to - 25 km/h, while the real value is around -10 km/h). This discrepancy arises from congestion propagation not being the predominant pattern in this scenario. Despite lacking a clear physical interpretation, GP-rotated achieves the best TSE performance in this experiment, as shown in Table 3.4, showing the versatility of GP-rotated for TSE across diverse scenarios.
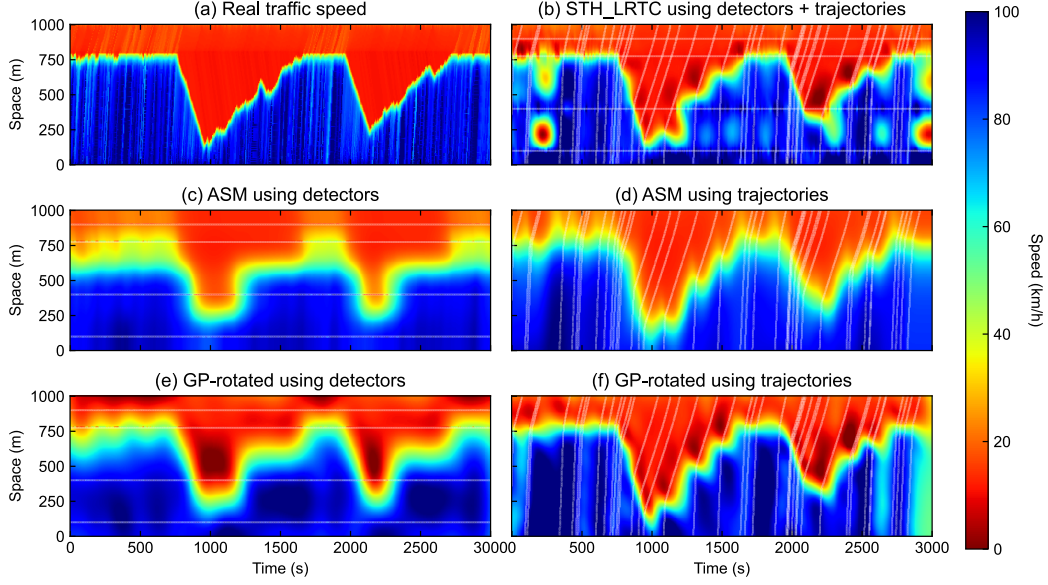
Figure 3.5: A TSE experiment on a simulated bottleneck. Locations of trajectories and detectors are shown in white lines. (a) The traffic speed of full simulated data. (b) The traffic speed of observed trajectories. (c) The traffic speed estimated by the ASM method. (d) The traffic speed estimated by the STH-LRTC method. (e) The traffic speed estimated by the GP with ARD Matérn$\frac{5}{2}$ kernel. (f) The traffic speed estimated by the GP with the proposed rotated Matérn$\frac{5}{2}$ kernel.

Table 3.4: TSE accuracy for a simulated bottleneck with different data sources.

Data source	Detectors		Trajectories		Detectors + trajectories	
Method	RMSE	MAE	RMSE	MAE	RMSE	MAE
ASM	16.27	11.04	13.09	9.40	11.95	8.27
STH-LRTC	54.97	42.05	22.27	12.51	15.07	8.25
GP-ARD	19.34	13.83	16.80	11.46	12.51	8.99
GP-rotated	**13.40**	**9.55**	**12.67**	**8.45**	**9.75**	**6.27**

3.3.6 Uncertainty quantification

Our research incorporates uncertainty quantification as a crucial aspect to enable reliable and accurate predictions while acknowledging the inherent variability and unpredictability of the system under investigation, which is a lacking feature in existing methods. The GP framework provides a natural way to quantify uncertainty through the predictive covariance matrix, as shown in Eq. (3.13). We can use the diagonal elements of the covariance matrix (i.e., variance) to quantify the uncertainty of the TSE at each cell. The comparison between the TSE residuals and the uncertainty is presented in Fig. 3.6, which provides a comprehensive understanding of the uncertainties associated with our findings.

The uncertainties (shown by three standard deviations) of the TSE using GP-rotated and the observed trajectories are demonstrated in Fig. 3.6 (c). First, we can find that the uncertainties are larger for regions with no CV trajectories, such as time ranges of 600 s to 700 s and 1800 s to 1900 s. It is notable that the uncertainty is anisotropic, propagating along the traffic wave, highlighting the need for an approach that can accurately capture this behavior. By comparing Fig. 3.6 (b) and (c), we can find that the predictive uncertainties are, in general, consistent with the absolute residuals, meaning the predicted variance of GP-rotated is a reliable indicator for uncertainty quantification.

Finally, if we look at Fig. 3.6 (a), we can find that there are still spatiotemporal correlations in the residuals, meaning that there is still space for improvement in the TSE estimation. For example, we can use the addition of multiple GP kernels, one for the congestion propagation and the other for the free-flow traffic, to capture the complex traffic dynamics. We have actually tried to use multiple GP kernels in our research, but the results do not improve. We believe that this is because the propagation of free flow speed is not as apparent as the congestion propagation, which does not provide enough information to improve the TSE estimation. But the correlations in the residuals still indicate that a more capable kernel design is needed to capture the
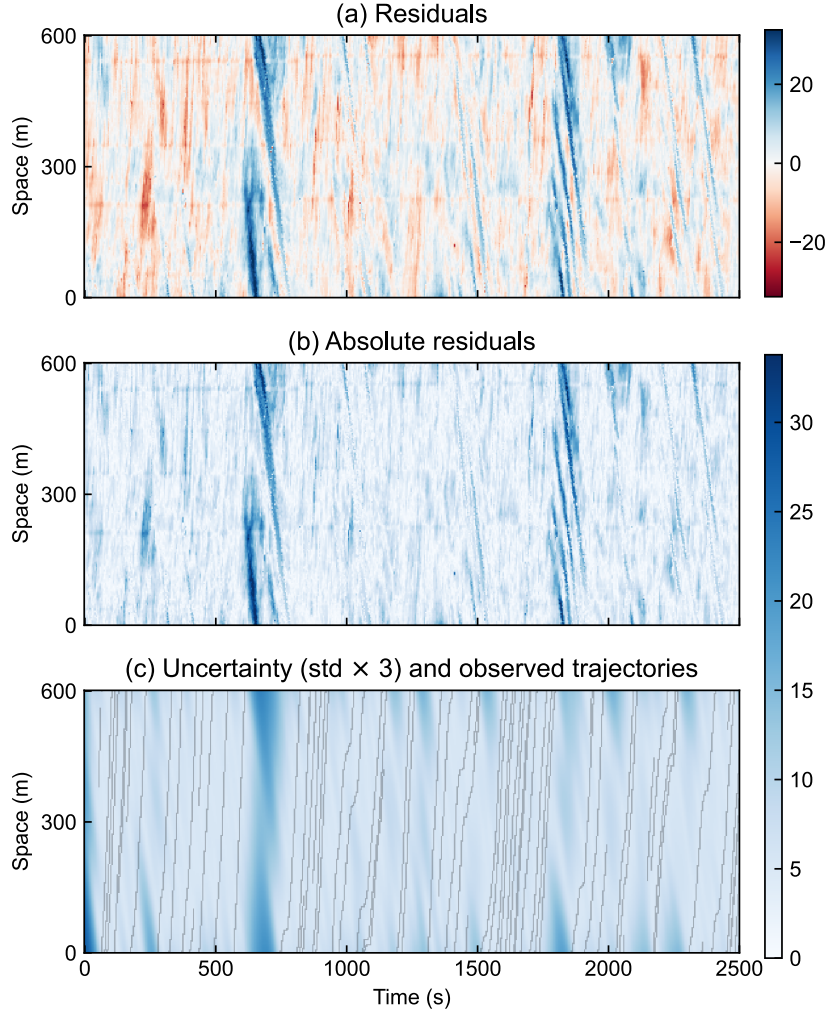
Figure 3.6: The uncertainty quantification of the GP-rotated estimation method on the NGSIM dataset with 5% observed trajectories. (a) The residuals of the estimation. (b) The absolute residuals of the estimation. (c) The uncertainty and 5% observed trajectories.

complex traffic dynamics.

In conclusion, our research emphasizes the importance of using an approach that can accurately capture the behavior of traffic waves in TSE. The GP-rotated method we propose is crucial in accounting for uncertainty propagation and allows us to provide reliable and accurate predictions. Through our approach, we can evaluate the validity of our model while also providing a measure of confidence in our predictions.

3.3.7 Computational time

In Table 3.5, we present the running time taken by four different methods, namely ASM, STH-LRTC, GP-rotated, and Pre-trained GP-rotated (P-GP-rotated), on both NGSIM and HighD datasets. Among these methods, the P-GP-rotated approach stands out for its significantly shorter computational time. This is because the P-GP-rotated method uses fixed kernel hyperparameters and random inducing points without any learning process. It is worth noting that ASM and STH-LRTC also use fixed parameters without a parameter estimation stage, which makes it appropriate to compare them with P-GP-rotated rather than GP-rotated.

Table 3.5: Computational time in seconds, mean (std).

		NGSIM		
Rate	ASM	STH-LRTC	GP-rotated	P-GP-rotated
0.05	7.40 (0.57)	908.21 (38.61)^a	27.30 (2.92)	**3.84 (0.27)**
0.1	14.18 (0.43)	850.90 (19.61)^a	77.54 (4.68)	**9.25 (0.42)**
0.2	26.77 (0.92)	206.72 (1.85)	153.07 (3.67)	**13.43 (1.68)**
0.3	38.38 (1.38)	199.99 (1.77)	204.61 (2.71)	**13.97 (0.19)**
0.4	48.15 (3.98)	196.09 (2.66)	245.37 (3.76)	**14.94 (0.16)**
0.5	54.21 (2.83)	191.46 (1.93)	280.01 (5.28)	**15.85 (0.26)**
		HighD		
Rate	ASM	STH-LRTC	GP-rotated	P-GP-rotated
0.05	0.46 (0.03)	67.61 (3.38)	11.97 (1.89)	**0.35 (0.05)**
0.1	0.87 (0.04)	823.65 (10.74)^b	12.54 (0.29)	**0.42 (0.05)**
0.2	1.67 (0.07)	54.29 (1.39)	19.86 (0.40)	**0.83 (0.16)**
0.3	2.30 (0.05)	51.46 (1.06)	29.78 (0.66)	**1.25 (0.15)**
0.4	2.84 (0.08)	49.50 (0.89)	40.46 (0.86)	**1.63 (0.21)**
0.5	3.22 (0.09)	48.14 (0.82)	50.93 (1.49)	**2.27 (0.21)**

^{a} Delay-embedding lengths $\tau_s = 50$, $\tau_t = 50$.
^{b} Delay-embedding lengths $\tau_s = 60$, $\tau_t = 50$.

We can see the running time in the highD dataset is faster than the NGSIM dataset. This is because the highD dataset has a smaller grid size. The computational time of STH-LRTC is considerably higher compared to other methods. For instance, on HighD data, it takes approximately 20 to 60 times

longer than the P-GP-rotated method and 15 to 30 times longer than ASM computation. Moreover, the computational efficiency of STH-LRTC drops significantly with a lower the penetration rate. This is mainly due to the increase in the spatiotemporal delay embedding lengths (τ_s and τ_t), which impacts the computation time substantially. As a result, the computational cost of STH-LRTC becomes extremely high under such scenarios. However, it is essential to note that this trend might not always hold, and a slight change in the parameters of the delay embedding in STH-LRTC could alter the trend.

We observe that the computational time of ASM, GP-rotated, and P-GP-rotated methods increases as the penetration rate increases. This is understandable as more data needs to be processed, leading to higher computation costs due to the increased traffic information. It's worth highlighting that both ASM and GP-based methods can benefit from using a locality approximation that excludes distant points in the filters/covariance matrices to speed up the computation [e.g., 178]. Besides, our testing only employs a naive implementation of ASM. Faster implementations of ASM exist, leveraging efficient matrix operations and the Fast Fourier Transform (FFT) [60], which can reduce computation time by two orders of magnitude. Considering these, while P-GP-rotated demonstrates satisfactory computational efficiency, ASM can be significantly faster with proper implementations.

3.3.8 TSE on multiple lanes

Most previous works have focused on modeling the TSE of each lane independently without considering the correlations and interactions between neighboring lanes. This section demonstrates the multi-output GP introduced in Section 3.2.5 that enhances the TSE by learning the correlations of traffic states on multiple lanes. Specifically, we use the trajectories from all lanes as the input features to the multi-output GP model and predict the traffic state for each lane as a separate output dimension. By sharing the same covariance structure across all output dimensions, the multi-output GP model can capture the correlations and dependencies between the traffic states on different

lanes, bringing more accurate and robust predictions.

The correlation between traffic speed profiles on different lanes of a highway segment is evident from Fig. 3.7 (a). The ground truth traffic speed profiles for Lane 1 and Lane 2 demonstrate that these two lanes are correlated, with both lanes experiencing congestion during the first 200 seconds and the last 100 seconds of the observed period. From 250 s to 350 s, the traffic speeds on both lanes are high. However, when we have only 5% of trajectory data for each lane, accurately and simultaneously estimating the traffic state on these two lanes becomes challenging.
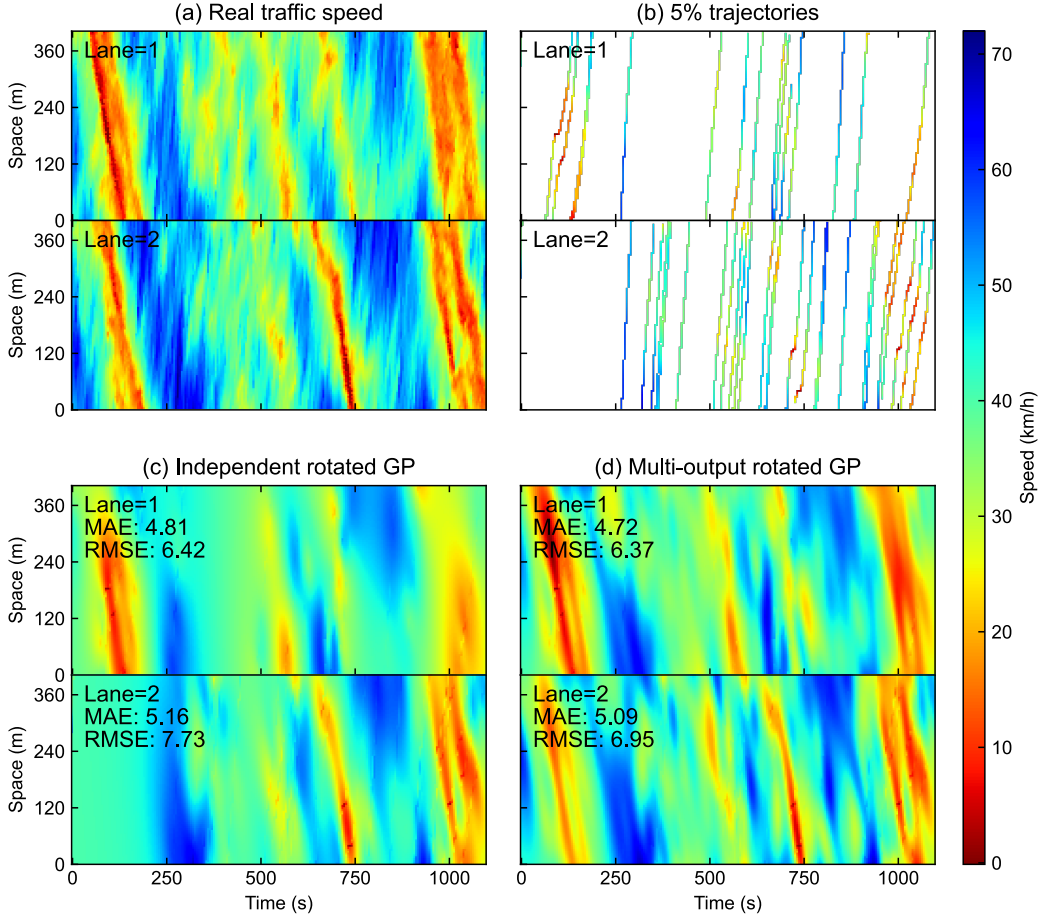
Figure 3.7: The TSE on multiple lanes on the HighD dataset. TSE errors are marked on the top-left corner. (a) The traffic speed profile of the full dataset. (b) The traffic speed profile of the 5% observed trajectories. (c) The traffic state is estimated by the independent rotated GP method. (d) The traffic state is estimated by the multi-rotated GP method.

In Fig. 3.7 (b), it can be observed that either Lane 1 or Lane 2 has a gap without any observations, lasting from 260 s to 490 s on lane 1 and from 0 to 250 s on lane 2, respectively. When using the independent GP-rotated method to perform TSE, the resulting traffic state profiles are shown in Fig. 3.7 (c). It is evident from the figure that the speed map of Lane 1 does not contain much traffic information during the time period between 250 s and 500 s, while the speed map of Lane 2 loses most of the traffic information between 0 and 250 seconds. These results demonstrate that performing independent TSE in each lane cannot achieve high estimation accuracy.

Despite the long periods of missing observations in either Lane 1 or Lane 2, we can observe that the trajectories from the other lane can compensate for the missing period, which is the main idea behind using a multi-output GP to output TSE in multiple lanes. Fig. 3.7 (d) shows that the multi-output GP performs better than the independent GP method. Specifically, during the period between 0 s and 250 s, the multi-output GP can reconstruct the shockwave of Lane 2 using the information from Lane 1, whereas the independent rotated GP fails to rebuild this shockwave. As shown in the top-left corner of Fig. 3.7 (c) and (d), the MAE and RMSE error of multi-output rotated GP is significantly smaller than independent rotated GP.

3.4   Conclusion and Discussions

This study presents a novel approach for traffic speed estimation using Gaussian process regression with a rotated kernel parametrization. The rotated kernel is designed to model anisotropic traffic flow, allowing for capturing the directional dependence of traffic wave propagation. The proposed method is a generalization of the ARD kernel function and can be applied to other kernel functions like Matérn and rational quadratic kernels. To validate the effectiveness of the proposed method, we conduct experiments on two real-world datasets from the NGSIM and HighD programs, as well as a simulated dataset for a traffic bottleneck scenario. The findings from comprehensive experiments

underscore the capability of the GP-rotated TSE method across varying CV penetration rates and detector types. Notably, our approach achieves state-of-the-art accuracy in scenarios with sparse CV penetration rates. Moreover, GP-rotated offers a promising approach for estimating congestion propagation speed from sparse vehicle trajectories. The outputs of GP-rotated also provide statistical uncertainty quantification, which is crucial for data-driven TSE models, especially under limited training data. We also extend GP-rotated to capture the speed correlations of multiple lanes, significantly improving the TSE accuracy for multiple lanes with sparse observations. Overall, the proposed method is a promising approach for traffic speed estimation, offering improved performance and the ability to capture directional traffic flow patterns.

While the proposed method shows promising results in traffic speed estimation, there are some limitations and potential future research directions. First, the current model is only tested on the traffic speed estimation problem, and it may be possible to estimate speed, density, and other traffic state variables simultaneously using multi-output Gaussian process regression. Second, future research can extend the model to assess the traffic wave by incorporating additional information, such as traffic signals and road geometry, to make the model suitable for more scenarios. Third, the proposed method is evaluated on real-world trajectory datasets that simulate the trajectory data obtained from connected vehicles. To further validate the effectiveness of the proposed method, it is suggested to test on commercial CV datasets.

Chapter 4

Adaptive Midblock Crossing Control for a Traffic-efficient Arterial via Signal Optimization

4.1 Introduction

Midblock crossings are special crosswalks placed between intersections for pedestrians and cyclists to cross the road. Midblock crossings provide convenient locations for pedestrians to access destinations (such as bus stops and building entrances) without detouring. In practice, a midblock crossing is usually set when the distance between the two intersections exceeds four hundred meters [179]–[181]. In addition, it is common to see safety facilities, such as a pedestrian island, warning signages or signal control, at midblock crossings.

For signalized midblock crossings, a pushbutton is often installed to offer a dedicated pedestrian phase after pedestrians push the button. The Forest City Electronic Company in the UK invented the very early version of the pushbutton system called Forest City System [106]. Subsequently, many variants of the pushbutton control system developed, such as pedestrian light-controlled (Pelican), pedestrian user-friendly intelligent (Puffin) and high intensity activated crosswalk (HAWK), sometimes called pedestrian hybrid beacon (PHB) [107], [109], [182]. These variants are similar in the control logic and have only small differences caused by regional preferences/manuals. The pushbutton signal control enhances pedestrians' safety and has little impact on the traffic flow

when pedestrian crossing demand is low. However, the pushbutton-type mid-block crossing is highly inefficient when the vehicle or pedestrian demand is high because every crossing request brings a considerable interruption to the traffic flow [111]. Significantly, the impact of an on-demand pedestrian phase could propagate to upstream or downstream intersections and break the green waves of the arterial [119]. Therefore, many midblock crossings with push-buttons installed use predetermined signal plans (i.e., fixed phase and timing control), and the pushbutton only works in specific time periods [183]. Because the fixed signal plans are unresponsive to pushbutton activation and may constitute a long wait for pedestrians [184], pedestrians may ignore the signal control once they believe pushbuttons are just "placebo buttons" [185]. Subsequently, this can increase the accident risk [184], [186].

To summarize, pushbutton control is only efficient for low-demand conditions. Fixed phase and timing control is more suitable for high-demand scenarios, and the mixed "placebo button" approach often causes safety concerns. No existing midblock control method addresses the efficiency and the safety problem simultaneously. Therefore, we propose an adaptive midblock crossing control (AMCC) method to bring together the benefits of both while addressing the drawbacks of each. AMCC is a pushbutton-based control, but the pedestrian wait time (PWT, the time interval between the button pressed and the pedestrian phase) is optimized to minimize the interruption to vehicles' leaving at the downstream intersection. A threshold restricts the maximum PWT to prioritize the pedestrian phase. We consider a midblock crossing and two adjacent intersections as an integrated system and develop two types of AMCC—AMCC-band and AMCC-vehicle—based on the available information from transportation facilities. When only the signal control plans of adjacent intersections are known, the optimal PWT is obtained by minimizing the overlap between the pedestrian phase and downstream green bands (AMCC-band). When vehicles' locations are also available (e.g., obtained from V2I communication, CVs, or advanced sensors), the optimal PWT is obtained by minimizing the number of vehicles projected to be impeded by the pedestrian

67

phase (AMCC-vehicle). In the experiment, we test AMCC in an open source simulation platform - SUMO with a two-intersection traffic network. Results show that using AMCC at a midblock crossing consistently reduces vehicle delay under a wide range of traffic conditions compared to Fixed or Pelican. Meanwhile, pedestrian delay using AMCC is slightly longer than Pelican but notably shorter than Fixed. We also find that using additional vehicle location information in AMCC further reduces PWT. Based on our comprehensive sensitivity analyses, we conclude that AMCC is an efficient midblock crossing control method suitable for most traffic conditions. We summarize the advantages of AMCC as follows:

- AMCC is a pushbutton-based midblock crossing control that minimizes the interruption to the traffic flow;

- AMCC can be applied to synchronized and unsynchronized arterial with existing signal control plans at adjacent intersections unchanged;

- In most traffic conditions, AMCC has shorter vehicle delay than Fixed and Pelican and has shorter pedestrian delay than Fixed;

- AMCC avoids the safety concern of mixing the fixed phase and timing control and the pushbutton control.

4.2 Methodology

This section proposes the AMCC method. To begin, we introduce the problem and basic notations. Next, we present the two types of AMCCs, depending on whether the real-time vehicle location information is available. Finally, we summarize the control logic.

4.2.1 Problem description

This paper considers a road segment with one midblock crossing between two signalized intersections, as illustrated in the left part of Fig. 4.1. The midblock

68

crossing is equipped with a pushbutton control system that provides a dedicated pedestrian phase after a pushbutton activation. We assume the signal control schemes of intersections 1 and 2 are predetermined. Our goal is to design an adaptive pushbutton control method at the midblock crossing that is friendly to both pedestrians and vehicles. We focus on the vehicle travel time of the *target road segment* between intersections 1 and 2.

We denote l_1 and l_2 respectively as the distance between the stop lines at the midblock crossing and intersections 1 and 2 downstream in either direction, as shown in Fig. 4.1. We assume that l_1 and l_2 are not so long so that the control at the midblock crossing affects downstream intersections; a distance of fewer than 800 meters is preferred according to MUTCD [110]. The desired speed of the road segment is v. Without loss of generality, intersections 1 and 2 can have different cycle lengths and are not necessarily synchronized. Because our midblock crossing control is adaptive to real-time traffic conditions, we assume we can access the real-time signal status and control scheme of intersections 1 and 2. In fact, this step can be hard-coded into the program if the signal control schemes of the two adjacent intersections are predetermined.

The total length of a pedestrian phase is r (including all potential leading and rear clearance phases). We consider r as a fixed value with no extension period. After each pushbutton activation, the proposed algorithm seeks the location of the pedestrian phase within an acceptable interval to minimize the impact on the traffic flow. Graphically speaking, the decision variable is the w in Fig. 4.1, representing the pedestrian wait time between a pushbutton activation and the subsequent pedestrian phase. We hereby name our method AMCC and introduce AMCC-band and AMCC-vehicle as follows, depending on whether the system can access the real-time vehicle location information (e.g., obtained by surveillance cameras, V2I communication, or CVs).

4.2.2 AMCC-band

To begin, we analyze how the midblock crossing affects travel time on the target road segment. A vehicle's travel time between intersections 1 and 2 is
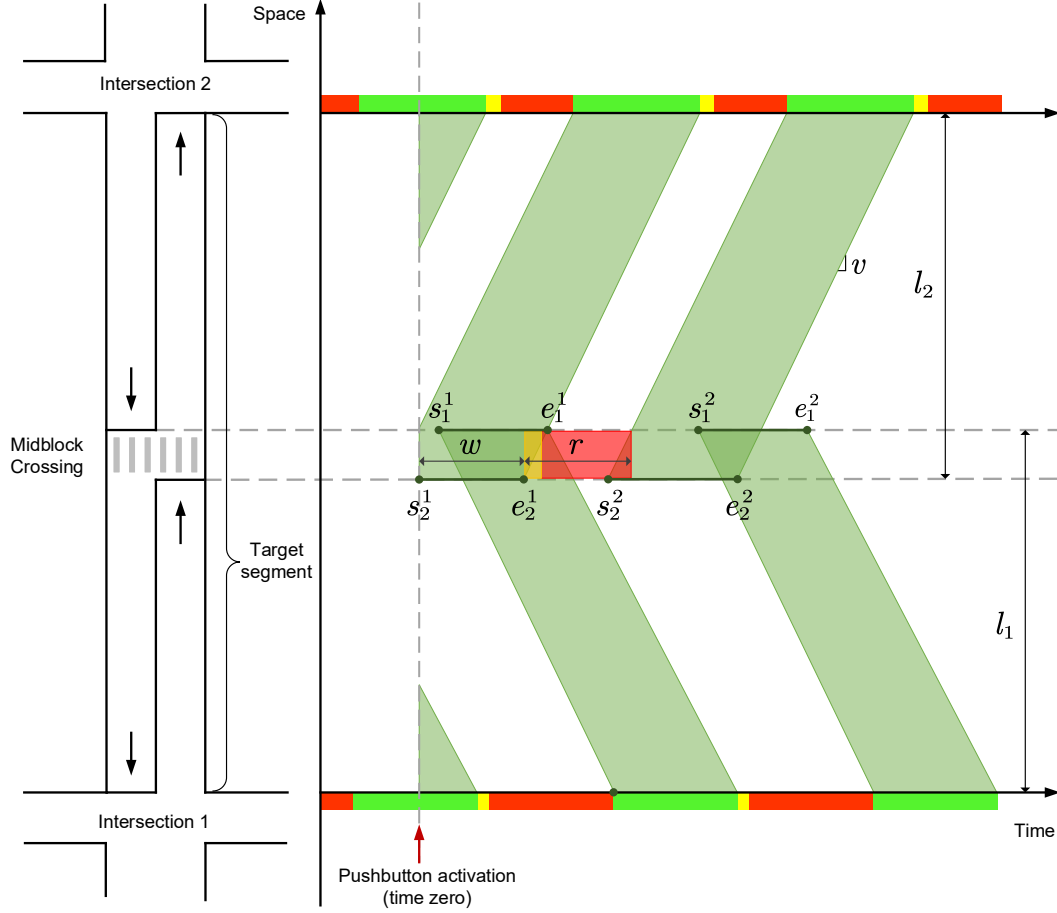
Figure 4.1: An illustration of the adaptive midblock crossing control (AMCC), solving the best pedestrian wait time (PWT) w given real-time traffic information (e.g., the signal status of intersections 1 and 2 or vehicles' location).

determined by the time when the vehicle leaves the downstream intersection in its driving direction. For ease of description, we refer to the time when a vehicle passes through the stop line at the downstream intersection as its *exit time*. Vehicles' exit time can be affected by the pedestrian phase at the midblock crossing, particularly for vehicles that could have encountered a green light at the downstream intersection but had to stop at the midblock crossing. This section uses the green band to evaluate the effect of the pedestrian phase at the midblock crossing on vehicles' exit time.

Similar to many arterial coordination methods [83], [84], [86], [88]–[91], [187], we backtrack the vehicle's green phase of the downstream intersections to the midblock crossing using the desired vehicle speed v and distances l_1 and

l_2, as shown by the green band of Fig. 4.1. Doing so allows us to know whether a pedestrian phase at the midblock crossing overlaps with a downstream green band. A vehicle should encounter a green light at the downstream intersection if it is within a downstream green band. An overlap between the pedestrian phase and a downstream green band impedes vehicles from passing through the target segment and, therefore, should be avoided. AMCC-band aims to minimize the overlap between the pedestrian phase and flow-weighted downstream green bands.

We regard a pushbutton activation as time zero. After a pushbutton activation, we denote s_i^j to be the j -th backtracked green-start time of intersection i at the mid-block crossing, and e_i^j to be the j -th backtracked green-end time of intersection i at the mid-block crossing, as shown in Fig. 4.1. Note we only consider the green bands after time zero; thus, a negative green-start time is set to zero when required (e.g., the $s_2^1{=}0$ in Fig. 4.1). As shown in Fig. 4.1, the overlapping period o_i^j between a green band $\left[s_i^j, e_i^j\right]$ and the pedestrian phase $[w, w + r]$ is:

$$o_i^j = \max\left(0, \min\left(e_i^j, w + r\right) - \max\left(s_i^j, w\right)\right).\qquad(4.1)$$

Next, AMCC-band determines the best PWT w by the following optimization problem:

$$\begin{aligned}
\min_w & \sum_{i=1}^{2}\sum_{j=1}^{2} q_i o_i^j + \lambda w \\
\text{s.t. } & w_{\min} \leq w \leq w_{\max},
\end{aligned}\qquad(4.2)$$

where q_i is the average flow rate for the traffic traveling towards intersection i, λ is a non-negative weight factor, w_{min} and w_{max} are respectively the lower and upper bounds for the pedestrian wait time. Note Eq. 4.2 only considers the first two green bands after time zero because the length of the pedestrian wait time w should not be excessively long. The objective function in Eq. 4.2 contains two terms. The first term minimizes the total overlapping period between the pedestrian phase and flow-weighted green bands. The second term punishes an excessively long pedestrian wait time. Based on a study by Van Houten et al. [186], we set $w_{max} = 35$ seconds, a short value that is acceptable to most pedestrians. The minimum pedestrian wait time w_{min}

relates to whether the minimal vehicle green time is reached, to be discussed in Section 4.2.4. Because the optimization problem has only one decision variable w (an integer in practice), it can be solved efficiently by single variable minimization algorithms (e.g., Brent's method [188]) or even an enumeration method.

To clarify, AMCC-band has no restriction to the signal control method of intersections 1 and 2, although it uses the concept of "green band". In fact, various signal control methods, such as fixed phase and timing, coordinate and adaptive, can be used in intersections 1 and 2 as long as the signal status can be accessed in real-time. By adjusting the pedestrian wait time w, AMCC-band maximizes the green band between the midblock crossing and the downstream intersection to shorten vehicles' exit time. Our method keeps the original signal control methods of intersections 1 and 2, which is convenient when adding a new midblock crossing to existing infrastructure.

4.2.3   AMCC-vehicle

With the help of V2X communication and advanced sensors, it is possible to improve AMCC with real-time vehicle location and route information. The idea of AMCC-vehicle is to minimize the estimated number of affected vehicles. AMCC-vehicle is a more accurate control method that requires a higher level of infrastructure.

After a pushbutton activation, the first step in AMCC-vehicle is to forecast when vehicles will reach the midblock crossing assuming no pedestrian phase. We use intersection 1 in Fig. 4.2 to illustrate the forecast method applied in this paper (the same for intersection 2). For vehicles already passed the stop line (i.e., vehicles 4, 5, and 6), their travel time to the midblock crossing is estimated according to the remaining distance to the midblock crossing divided by the desired speed. For vehicles still in upstream approaches (i.e., vehicles 1, 2, and 3), we use a random forest [189]

$$\hat{y}_i = \mathcal{F}\left(\mathbf{x}_i\right) \tag{4.3}$$

to do the forecasting, where $\mathcal{F}$ is the random forest model, $\mathbf{x}_i$ is the feature vector for vehicle i, and $\hat{y}_i$ is the estimated travel time for vehicle i from the current position to 100 meters ahead of the midblock crossing. As illustrated in Fig. 4.2, features in $\mathbf{x}_i$ include the lane of vehicle i, the distance to the stop bar, the time in a signal cycle, the number of leading vehicles before the stop bar and the current speed of vehicle i. Because the forecasting model $\mathcal{F}$ is trained using historical observations, the target data $\hat{y}_i$ is collected from 100 meters ahead of the midblock crossing to avoid the impact of pedestrian phases; the travel time on the rest of the 100-meter road will be added to the final estimated travel time. Note that we use the random forest in this paper to illustrate the effect of AMCC-vehicle, although any accurate forecast model can be used in its place in practice.
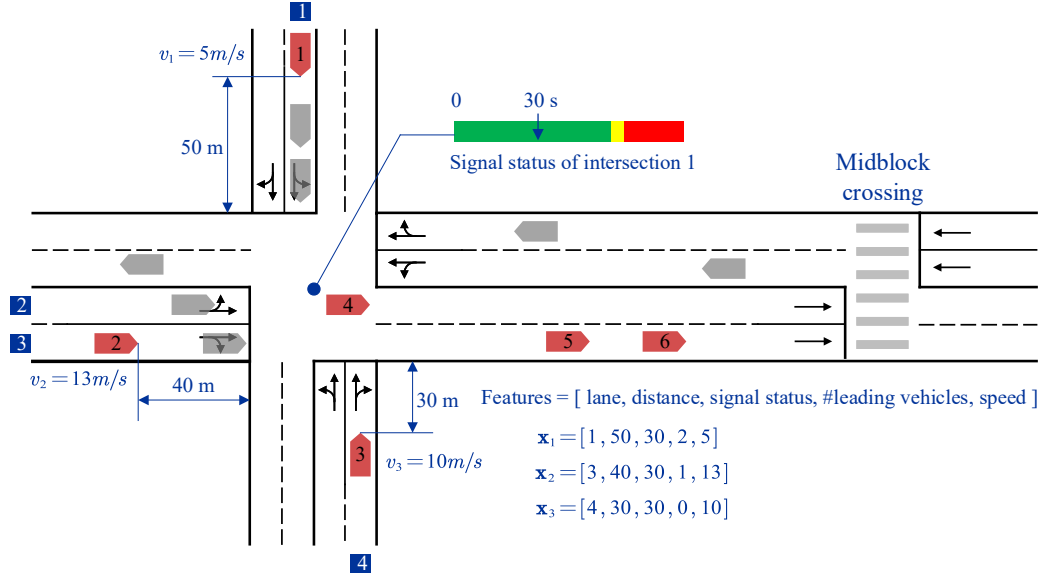
Figure 4.2: An illustration of vehicle location at a pushbutton activation. Only numbered red vehicles will pass the midblock crossing. For vehicles already passed the stop line (i.e., vehicles 4, 5, and 6), their travel time to the midblock crossing is estimated by the remaining distance divided by the desired speed. For vehicles in upstream approaches (i.e., vehicles 1, 2, and 3), we input features into a random forest to forecast the travel time from their current locations to 100 meters before the midblock crossing.

Next, we denote $q_i(t)$ as the number of vehicles that will reach the stop line of the midblock crossing at the t-th second after the time zero for the

direction with downstream intersection i. We can directly obtain $q_i(t)$ from the estimated travel time of the previous step. The optimization function of AMCC-vehicle is thus to minimize the number of vehicles that are in a downstream green band and projected to be impeded by the pedestrian phase

$$\min_{w} \sum_{i=1}^{2} \sum_{j=1}^{2} \sum_{t=\max\left(s_i^j, w\right)}^{\min\left(e_i^j, w+r\right)} q_i(t) + \lambda w, \qquad (4.4)$$

where $\max\left(s_i^j, w\right)$ and $\min\left(e_i^j, w+r\right)$ are the start and end times respectively of the overlap interval between the j-th green band of downstream intersection i and pedestrian phase. When $\max\left(s_i^j, w\right) \geq \min\left(e_i^j, w+r\right)$, the pedestrian phase does not overlap with the downstream green band, and the summation becomes zero. Note the constraint of Eq. 4.2 also applies to Eq. 4.4. The best pedestrian wait time w of Eq. 4.4 can be solved by the same method as Eq. 4.2.

4.2.4 Control logic

AMCC-band or AMCC-vehicle is integrated into a control framework that ensures a minimum vehicle green time at the midblock crossing, as is shown in Fig. 4.3.

Let g_v be the green time for vehicles after the last pedestrian phase at the midblock crossing. The g_v between every two pedestrian phases should be long enough to empty the queueing vehicles at the midblock crossing. Therefore, we set a minimum vehicle green time $g_{v,\min}$ to control the interval between two pedestrian phases. Note that $g_{v,\min}$ should be a value smaller than the maximum pedestrian wait time w_{max}. The minimum pedestrian wait time w_{min} is determined by the control logic of Fig. 4.3.

4.3 Experiments

In this section, we describe our testing of AMCC in a SUMO simulation. We begin with a description of experimental settings and evaluation metrics. Next, we compare the efficiency of AMCC with Fixed and Pelican controls. Finally,
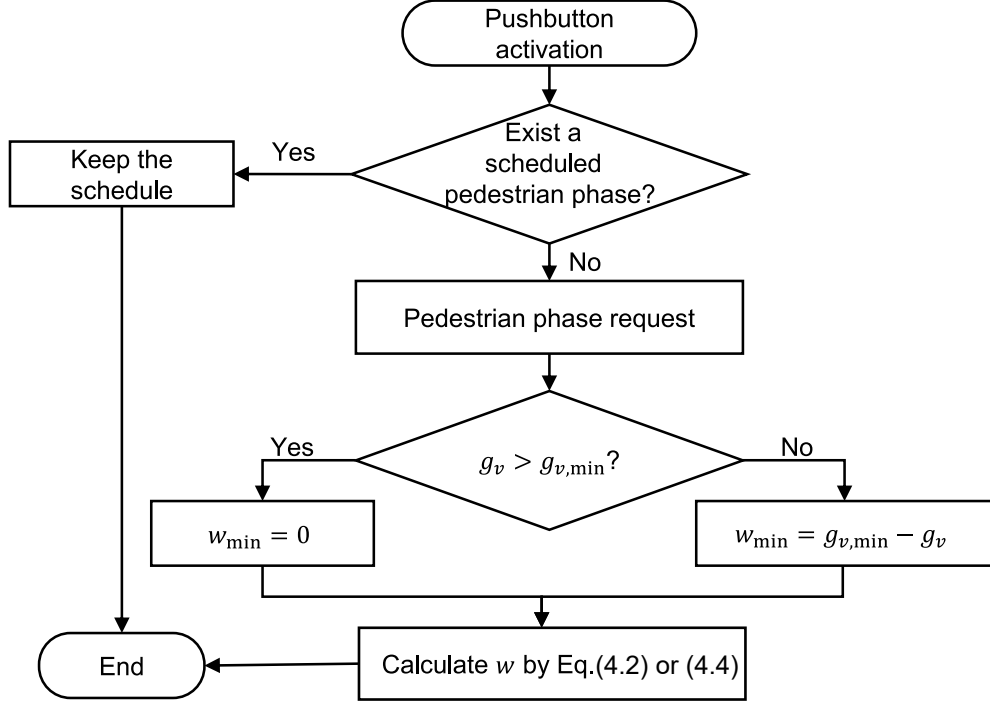
Figure 4.3: The flowchart of calculating w after each pushbutton activation.

we outline our sensitivity analyses to these midblock control methods under various pedestrian and vehicle demands.

4.3.1 Experimental setup

We constructed the network and conducted the simulation in SUMO. The control models and analyses were implemented in Python. The interaction between SUMO and Python was realized by the application programming interface (API). We used a two-intersection network and the detailed network layout can be found in Fig. 4.4. There were two lanes in each direction and the distance between the center of the two intersections was 700 meters. The midblock crossing was in the middle point. We used the default car-following model in SUMO with the desired speed (free-flow speed) of 50 km/h (13.89 m/s).

The vehicle demand was generated based on a predefined origin-destination matrix mimicking medium-sized traffic flow initially, shown in Table 4.1. The representations of numbers are shown in the network layout in Fig. 4.4. The
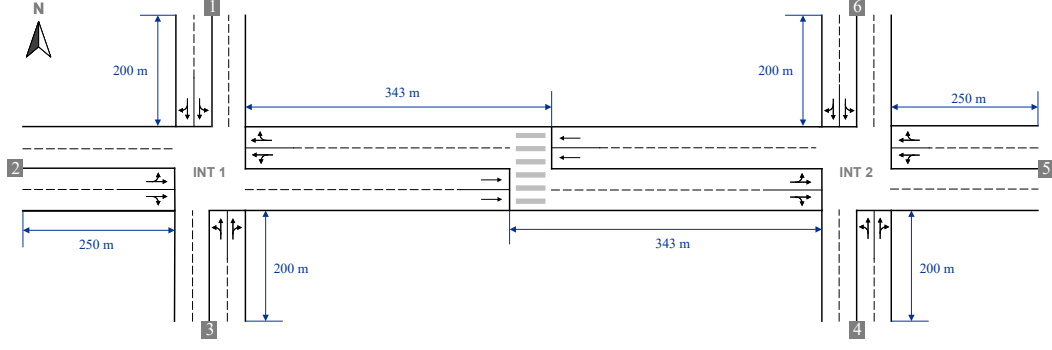
Figure 4.4: The network layout in the SUMO simulation.

flow rates of the two directions were not symmetric. The flow rate from inter-
section 1 to intersection 2 on the target segment was 1296 vehicles per hour
(vph) and 864 in the other direction. The crossing demand at the midblock
crossing was set to 40 pedestrians per hour (pph).

Table 4.1: Initial setting of vehicle origin-destination demand.

OD	1	2	3	4	5	6	O
1	0	72	72	72	72	0	288
2	72	0	72	72	432	72	720
3	72	72	0	0	72	72	288
4	36	36	0	0	36	72	180
5	36	360	36	36	0	36	504
6	0	36	36	72	36	0	180
D	216	576	216	252	648	252	2160

The traffic signalization of intersections 1 and 2 was determined by Web-
ster's method independently; details of the signal phase and timing plans are
listed in Fig. 4.5 and Table 4.2. The cycle lengths were 80 seconds and 70 sec-
onds for intersections 1 and 2, respectively. Note the two intersections were
not coordinated. Although AMCC also works for coordinated arterials, the
"optimal allocation" of pedestrian phases at the midblock was constant in dif-
ferent cycles once given a particular coordination plan. Therefore, we designed
two uncoordinated intersections to test AMCC as a more general case with
increased variability.

The critical step of AMCC is adding a dynamic PWT w to the front of
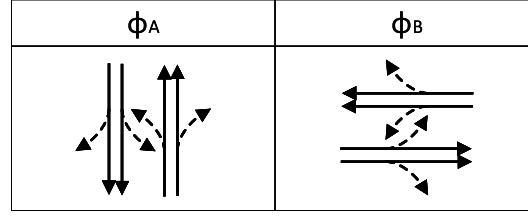
(a) Phase diagram of intersection 1 and 2
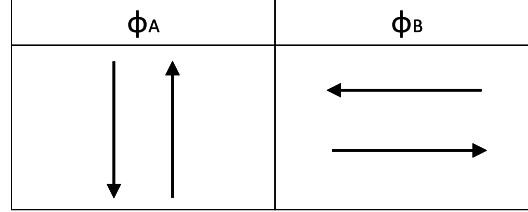
(b) Phase diagram of the midblock crossing

Figure 4.5: Signal phase diagrams for the arterial. (a) Signal phase plan of intersection 1 and 2. (b) Signal phase plan of the midblock crossing.

Table 4.2: Initial signal timing and offset settings in the arterial.

	Cycle length	Phase A	Phase B	Offset
Intersection 1	80	31+4 s	41+4 s	0
Intersection 2	70	21+4 s	41+4 s	0*
Mid-block crossing	80	20+5 s	50+5 s	55

* At the initial (0th second) of each simulation.
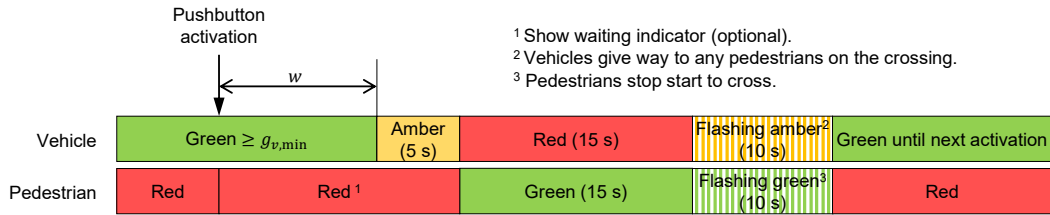
Figure 4.6: The signal phase and timing plan of AMCC.

a pedestrian phase to protect the smooth running of traffic. We can apply this step to any pushbutton control methods, and the effect of using AMCC is similar to these methods. In our experiment, we chose the widely used Pelican control as the baseline model. And the signal control plan of AMCC is shown in Fig. 4.6. The phase duration was set according to road width to provide sufficient crossing time. When $w = 0$, AMCC is equivalent to Pelican. In total, we tested and compared the following four midblock crossing control methods in the experiment:

- **Fixed**: The cycle length was fixed at 80 seconds; the pedestrian phase was 20 seconds with additional 5 seconds of amber time. To maximize the efficiency, the fixed vehicle green phase was coordinated with intersection 1 (see details in Fig. 4.5 and Table 4.2).

- **Pelican**: A standard pushbutton control method. The signal setting was the same as Fig. 4.6, with the PWT at zero (i.e., $w = 0$). The minimum vehicle green time $g_{v,\min}$ was 15 seconds.

- **AMCC-band**: The signal setting is outlined in Fig. 4.6, where w was determined by the method described above. We set the $\lambda = 0$, and the maximum PWT $w_{\max}$ was configured at 35 seconds, a reasonable value according to [186] (a larger value may significantly increase the probability of pedestrian violations). The minimum vehicle green time $g_{v,\min}$ was 15 seconds.

- **AMCC-vehicle**: Similar to the AMCC-band, but w was determined by the method described in Section 4.2.3. The random forest forecast model was pre-trained using the data from an additional 7200-second simulation. We implemented the model via the scikit-learn Python package [190] and used the default model setting. The random forest model was only trained once and was used in all the experiments with AMCC-vehicle control.

4.3.2 Evaluation metrics

The length of each simulation was 7200 seconds. We performed 20 simulations with different initial random seeds for each experimental setting, and we compared the final results by the mean and standard deviation of the 20 simulations. Specifically, we evaluated the performance of different midblock control methods by the following metrics:

- **Average vehicle travel time**: The average travel time of vehicles on the target road segment.

- **Average vehicle delay**: It is the average of all vehicles' delays on the segment. The vehicle delay is calculated by subtracting the expected travel time from the actual travel time.

- **Average vehicle stops**: The average number of vehicles' stops on the target segment.

- **Average pedestrian delay**: It is the average of all pedestrians' delays. A pedestrian's delay is calculated by subtracting the expected travel time from the actual travel time.

- **Average person delay**: We regard one vehicle as 1.7 persons based on the average vehicle occupancy factors suggested by FHWA [191]. So it is the average delay of the total equivalent person (pedestrians and people on target segment vehicles).

A lower average vehicle travel time, delay, stops indicate the traffic moves more smoothly with higher speed, and the green wave on the arterial is less disrupted. A lower average pedestrian delay means pedestrians wait for less time. Moreover, a lower average person indicates better performance for a control method for the whole system.

4.3.3 Traffic efficiency comparisons

This section investigates the performance of AMCC and baseline models. Table 4.3 outlines the results when the midblock crossing was under the control of

Fixed, Pelican, AMCC-band, and AMCC-vehicle. We can observe the AMCC outperformed both Fixed and Pelican when considering vehicle efficiency. The better performance can be attributed to the dynamic PWT when considering the coordination between the midblock crossing and the downstream intersection.

Table 4.3: Performances (mean (std)) of the four pushbutton control methods.

Midblock crossing control method	Average vehicle travel time (s)	Average vehicle delay (s)	Average vehicle stops (#)	Average pedestrian delay (s)	Average person delay (s)
Fixed	71.96 (0.79)	18.96 (0.79)	1.17 (0.05)	29.21 (2.38)	19.12 (0.78)
Pelican	70.51 (0.88)	17.51 (0.88)	1.09 (0.05)	**11.32 (1.21)**	17.41 (0.87)
AMCC-band	68.82 (0.74)	15.82 (0.74)	1.01 (0.04)	26.71 (2.05)	15.99 (0.73)
AMCC-vehicle	**68.70 (0.82)**	**15.70 (0.82)**	**1.01 (0.04)**	21.18 (2.05)	**15.79 (0.80)**

Compared with Fixed and Pelican, two types of AMCC reduce the average vehicle travel time/average vehicle delay by 2 to 3 seconds, indicating an improvement to the vehicle's travel on the target segment. Meanwhile, the average number of stops for AMCC is around 8 to 13 percent lower than the Fixed and Pelican, effectively reducing emissions and risk of rear-end collision. The pedestrian delay for AMCC is higher than Pelican, but it is considerably lower than the Fixed control. Note that the maximum PWT in our algorithm is 35 seconds, an acceptable value for pedestrians, according to [186]. Furthermore, although the two types of AMCC have similar performances for vehicles, AMCC-vehicle is more accommodating to pedestrians as it further reduces the average pedestrian delay by 20.7 percent, from 26.71 seconds to 21.18 seconds. Most importantly, the proposed two types of AMCC have the lowest average person delay, indicating the whole road users (i.e., passengers in vehicles and pedestrians) can benefit from using AMCCs at the midblock crossing.

Moreover, we selected one group of data to illustrate the cumulative distribution functions (CDFs) of vehicle travel time on the target segment. Fig. 4.7(a) shows vehicles going from intersection 1 to intersection 2 (west to east) through the target segment, and Fig. 4.7(b) shows the case for the opposite direction. Overall, the AMCC performed better than both Fixed and Pelican in both directions. Furthermore, they are much better at reducing the total delays from
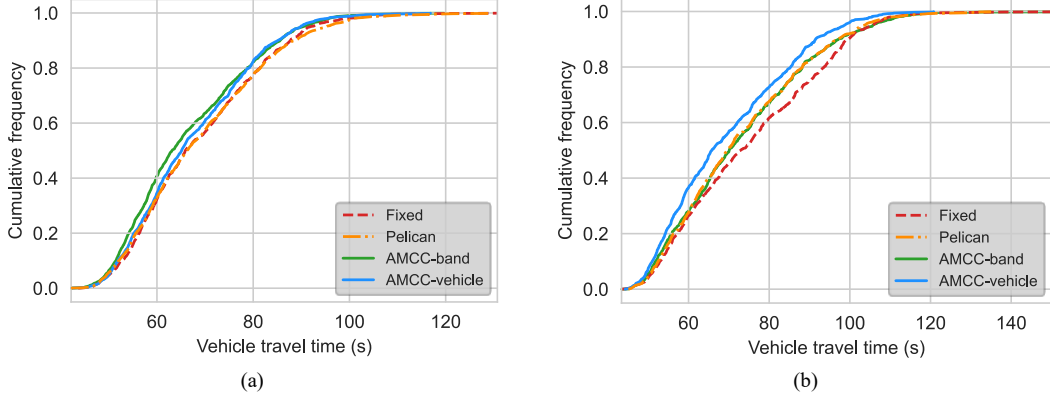
Figure 4.7: Travel time cumulative distribution functions of vehicles along the target segment: (a) west to east, (b) east to west.

the west to the east because the AMCC-band method favors the direction with higher traffic volume and gives optimization priority.

The trajectory plot is an effective tool to visualize vehicles' movement along the arterial and the control effect. There were three pushbutton activations (shown by black cross marks) during the 325-second period. Fig. 4.8 shows the trajectories along the target segment from intersection 1 to intersection 2 (west to east). The direction from west to east has a more significant flow rate and is assigned a greater weight in the objective functions (Eq. 4.2 and Eq. 4.4). We thus focus on west to east to explain the advantages/effects of AMCC.

We can see the Pelican control switched to a pedestrian phase immediately after each pushbutton activation. However, there is a possibility of significant interruption to the traffic flow. For example, we can see that the immediate Pelican control pedestrian phase blocked vehicles from passing through the downstream intersection in the third pushbutton activation of Fig. 4.8. As a result, these blocked vehicles encountered red phases twice (one in the midblock crossing and the other in intersection 2, as shown by the arrows in Fig. 4.8), causing considerable delay. By contrast, AMCC-band and AMCC-vehicle optimized the PWT minimizing the impact on road traffic. The best example of AMCC-band's effects is the third pushbutton activation in Fig. 4.8. There, we can see AMCC-band extended the vehicle phase at the midblock

81

crossing to release vehicles that could pass downstream intersection 2 without stopping, thus avoiding the "twice-red-phases" problem of Pelican. However, a shortcoming of AMCC-band is unnecessary waiting time for pedestrians. As shown in the first pushbutton activation of Fig. 4.8, there was a long period of unused time (no vehicle passing) in the PWT of AMCC-band. This shortcoming of AMCC-band can be solved in AMCC-vehicle with the help of real-time vehicle location information. For the first pushbutton activation, AMCC-vehicle extended the vehicle phase for a short period and immediately switched to the pedestrian phase when there was no oncoming vehicle. In summary, the trajectory plot shows that AMCC methods significantly reduce vehicle delay compared to Pelican, and the AMCC-vehicle further avoids the unnecessary PWT in the AMCC-band.

The effect of AMCCs is less evident in the direction of Fig. 4.9 because of the relatively lower flow rate. Nevertheless, the queueing length in the downstream intersection (intersection 1) is notably shorter for the two AMCC methods than Pelican. In summary, the two trajectory plots show that AMCC methods significantly reduce vehicle delay compared to Pelican, and the AMCC-vehicle further avoids the unnecessary PWT in the AMCC-band.

4.3.4 Sensitivity analysis to pedestrian demands

This section examines the sensitivity of Fixed, Pelican, AMCC-band, and AMCC-vehicle control algorithms to the pedestrian demand. Fourteen levels of pedestrian demand are tested: 5 to 200 pph with an increment of 15 pph. For each method and each demand level, we performed 20 simulation runs. The results for average vehicle delay, average pedestrian delay, and average person delay for each level of pedestrian demand are outlined in Fig. 4.10 and the error bars are the standard deviations of 20 simulations. We can see AMCC-band and AMCC-vehicle are strikingly similar in terms of impact on vehicles. The two types of AMCC performed better than Pelican and Fixed because the AMCC resulted in shorter average vehicle and average person delays under all pedestrian demand levels when compared to Pelican and Fixed.
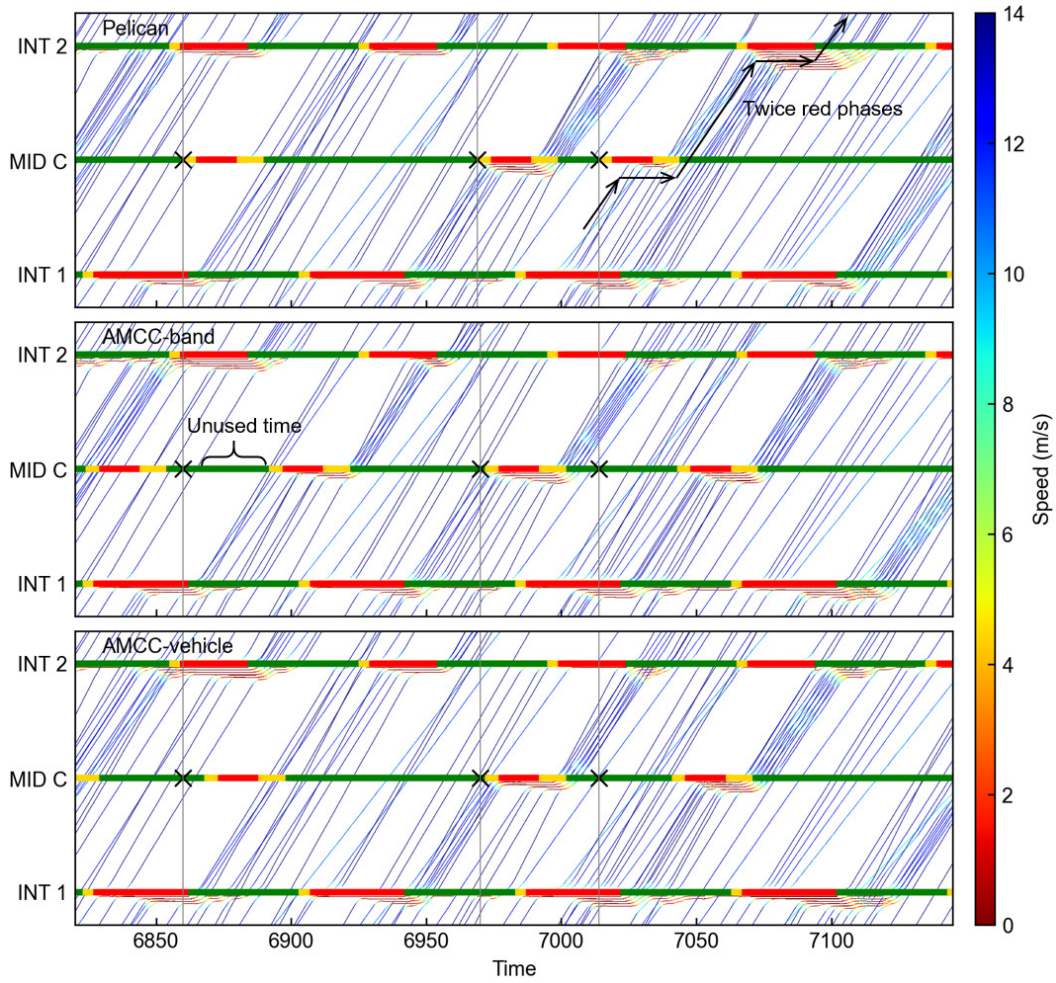
Figure 4.8: Vehicle trajectories from intersection 1 to 2 (west to east) in a selected period. Pelican, AMCC-band, or AMCC-vehicle control the mid-block crossing. Cross marks represent pushbutton activations. Pelican control switches to a pedestrian phase immediately after each pushbutton activation, which causes significant impacts to traffic (e.g., the two successive red phases). AMCC-band reduces the effect on vehicles but may cause unnecessary PWT (e.g., the unused time). AMCC-vehicle avoids the problems in Pelican and AMCC-band.
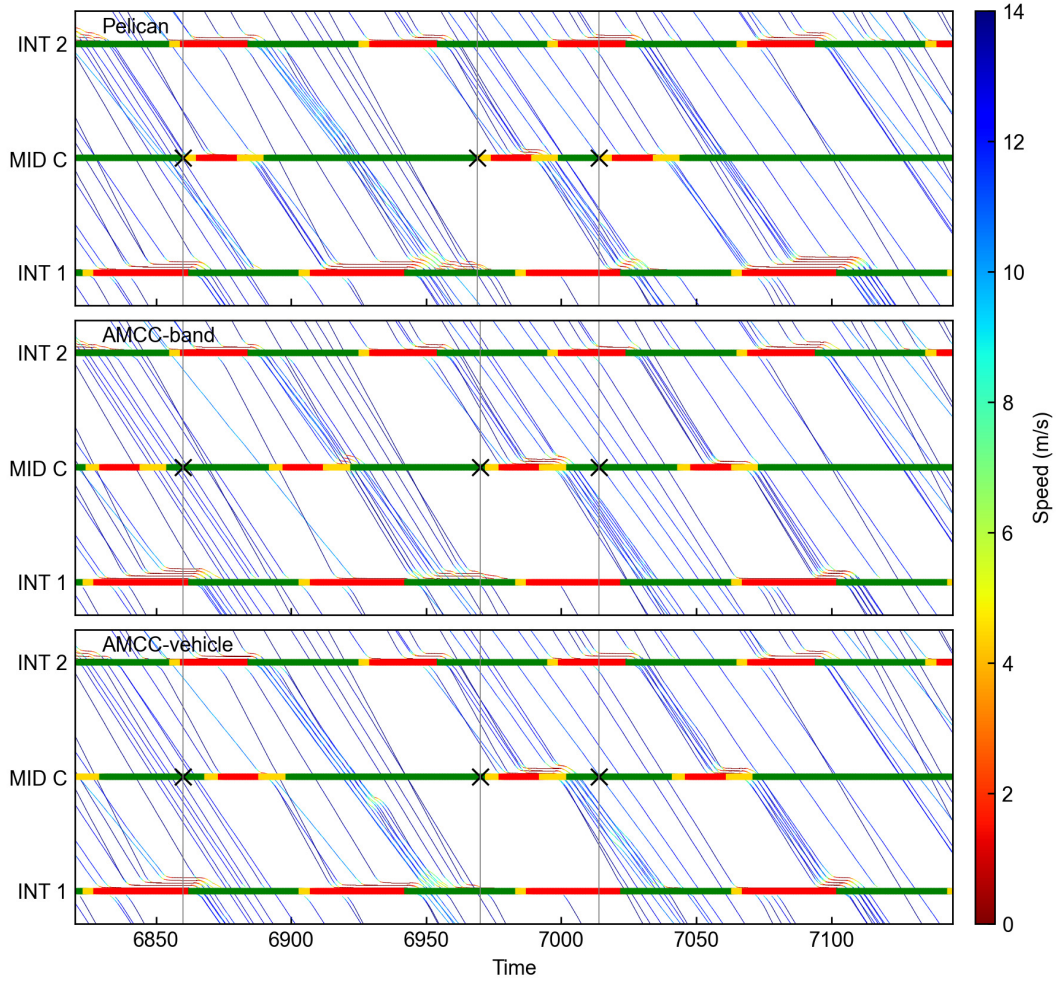
Figure 4.9: Vehicle trajectories from intersection 2 to 1 (east to west) in a selected period. Pelican, AMCC-band, or AMCC-vehicle control the midblock crossing. Cross marks represent pushbutton activations. The queueing length in the downstream intersection (intersection 1) is notably shorter for the two AMCC methods than Pelican.

84

The pedestrian delay under Fixed and Pelican was relatively steady, with only slight fluctuations in a wide range of pedestrian demand testing. The AMCC consistently produced significantly fewer pedestrian delays than the Fixed and more than Pelican. Moreover, the average pedestrian delay was much less than that using AMCC-band when utilizing AMCC-vehicle. Overall, our proposed AMCC method possesses a wide adaptation range for pedestrian demand.

Figure 4.10: The average vehicle, pedestrian, and person delay of four midblock crossing control algorithms under different pedestrian demands. The error bars are the standard deviations of 20 simulations.

When looking at Fig. 4.10(a), we note that the average vehicle delay under Fixed was relatively stable at around 19 seconds (with a slight fluctuation) because the cycle length and phase split determined the average vehicle delay to some extent. However, when Pelican and AMCC controlled the midblock crossing, the average vehicle delay grew with increased pedestrian demand. Moreover, in Fig. 4.10(a), we observe that the vehicle delay caused by AMCC was always smaller than that caused by Pelican or Fixed, regardless of the pedestrian demand level, which indicates the AMCC method performs the best regarding vehicle efficiency. Although in the case of extra-low pedestrian demand, such as 5 pph, vehicle delay under AMCCs was similar to that under Pelican. The advantage of AMCC over Pelican was magnified with increased pedestrian demand, further reducing average vehicle delay. Moreover, it is noticeable that when the pedestrian flow reaches a certain level, such as 200 pph, the average vehicle delay caused by the AMCC approached the result of Fixed. However, 200 pph means a pedestrian comes every 18 seconds, which would be a rare occurrence for a midblock crossing. Therefore, we would not

continue to test higher pedestrian demand.

It is worth noting that when the pedestrian demand was lower than approximately 60 pph, Pelican can achieve a better effect than Fixed in causing shorter vehicle and pedestrian delays. Therefore, for low pedestrian demand, Pelican is preferred for the midblock crossing control in real-world engineering cases. Our AMCC resulted in greater pedestrian delay below the pedestrian demand level of 60 pph but a shorter vehicle delay than Pelican. However, the PWT caused by AMCC-vehicle was around 20 seconds (indicated in Fig. 4.10(b)), which is acceptable. By contrast, Fixed had advantages over Pelican when the pedestrian demand was more than 60 pph since the average vehicle delay was lower than that of Pelican, indicated in Fig. 4.10(a). Thus, engineers would apply Fixed to the midblock crossing in real-world engineering cases. However, the vehicle delay caused by AMCC was always shorter than that caused by Fixed when pedestrian demand was over 60 pph. What is more, the pedestrian delay caused by AMCC was always less than that caused by Fixed. Therefore, the AMCC can reduce vehicle and pedestrian delays simultaneously compared with Fixed when pedestrian demand is over 60 pph; the AMCC can have a wide range of adaptions to various pedestrian demands.

Besides, the average pedestrian delay caused by AMCC-band decreases due to the aggregation effects of more pedestrians with a rise in pedestrian demand, as is evident in Fig. 4.10(b). Pedestrians that triggered the pushbutton at different time points can be allowed to cross after the same optimized PWT; this effect is more subtle when the pedestrian volume is relatively low. It is worth mentioning that when AMCC-vehicle was applied to the midblock crossing, the average pedestrian delay was significantly smaller than that under the AMCC-band, improving the pedestrian-friendly effect.

4.3.5 Sensitivity analysis to vehicle demands

After examining the sensitivity to the pedestrian demand, we further tested the control effect of Fixed, Pelican, and the two types of AMCC under different vehicle demands given a fixed pedestrian demand (40 pph). Because the

objective functions of AMCC considered the traffic flow of two directions, we were particularly interested in the control effect of AMCC when the flow rates of the two directions were imbalanced. To do so, we multiplied the vehicle demand of the west-to-east (WE) direction (intersection 1 to 2) by a factor ranging from 0.5 to 1.5 at a 0.1 interval while keeping the vehicle demand of the other direction unchanged. At the ratio of 0.66, the vehicle demands of the two directions were more or less balanced. When the ratios were below 0.66, the number of vehicles going from intersection 2 to 1 (east to west, EW) was greater than from intersection 1 to 2 (WE). On the other hand, when the ratios were above 0.66, the traffic volume from intersection 2 to intersection 1 was less than that from intersection 1 to intersection 2.

Based on the above setting, Fig. 4.11(a)-(c) shows the performance of the four control methods under different vehicle demand ratios. As expected, the vehicle delays under all the control models grew with increased vehicle demand. However, the advantages of AMCC compared with Fixed and Pelican were consistent under different vehicle demand ratios, which corroborates the effect of AMCC in reducing vehicle (and person) delay. As seen in Fig. 4.11(b), the average pedestrian delay was relatively stable under different vehicle demands. Pelican resulted in the lowest average pedestrian delay, followed by AMCC-vehicle and AMCC-band; Fixed still had the highest pedestrian delay.
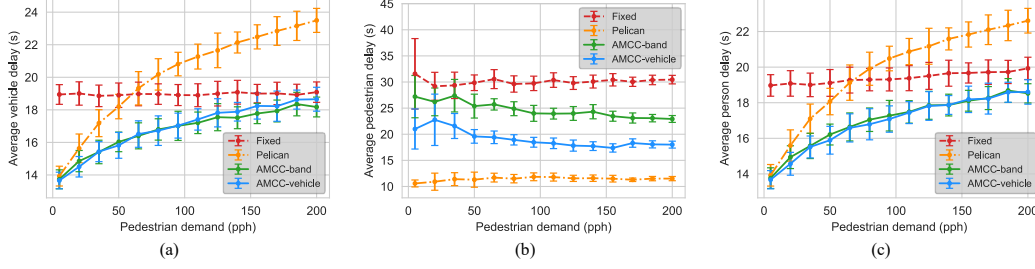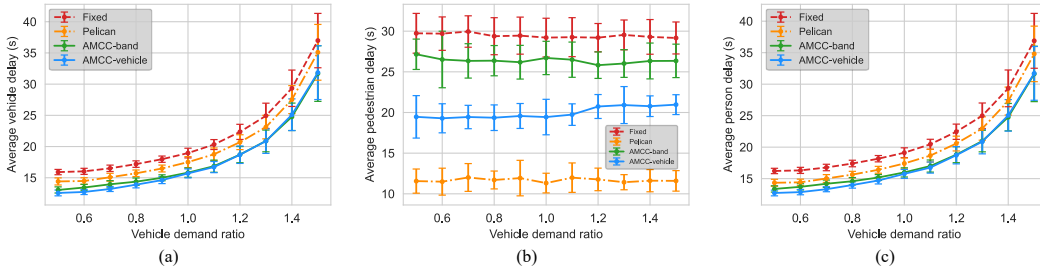

Figure 4.11: The average vehicle, pedestrian, and person delay of four midblock crossing control algorithms under different vehicle demands. The error bars are the standard deviations of 20 simulations.

Next, we went one step further to investigate the impact of imbalanced vehicle demands, as shown in Fig. 4.12. Interestingly, although the overall average vehicle delay was similar for AMCC-band and AMCC-vehicle, the
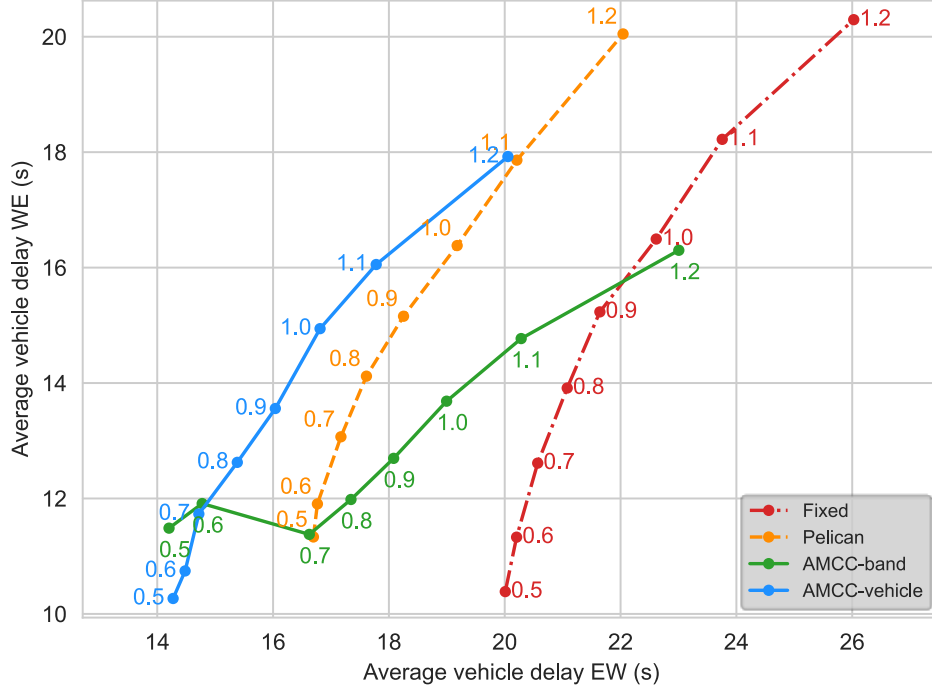
Figure 4.12: The average vehicle delays of each direction for the control methods (numbers along markers indicate different vehicle demand ratios of west-to-east direction).

average vehicle delays of the two AMCC methods were different in each direction. In Fig. 4.12, the curve of AMCC-band is different from the other three methods—it is the only non-monotonic curve. There is a clear abnormal shift from a vehicle demand ratio 0.6 to 0.7, and the average vehicle delay suddenly drops for WE but increases for EW. This is because EW is the primary direction (i.e., the direction with a greater flow rate) when the ratio is 0.6 or less, while WE becomes the primary direction when the ratio is 0.7 and above. The AMCC-band always favors the direction with the greater flow rate caused by its objective function in Eq. 4.2. Favoring the primary direction may not impact the overall vehicle delay, but it may cause inequitable control [192]. In contrast, AMCC-vehicle—a control with similar average vehicle delay but low average pedestrian delay—is a more equitable control method because it optimizes the PWT based on real-time vehicle information and no flow rate term exists in its objective function Eq. 4.4.

Aside from equitability, we can see the data points of the two types of

AMCC are almost always on the left lower side of the other two control methods under each demand ratio. This indicates the improvement for vehicles' travel under AMCC was two-directional, which accords with our objective functions (Eq. 4.2 and Eq. 4.4). Overall, the above results show that the AMCC method can be applied to imbalanced vehicle demand in two directions. Therefore, vehicle delay can be effectively controlled using the proposed AMCC method.

4.4   Conclusion and Discussions

This research proposes two types of adaptive pushbutton traffic signal control methods (AMCC-band and AMCC-vehicle) for pedestrian midblock crossings. These two kinds of AMCC methods optimize PWT after each pushbutton activation to ensure vehicles can leave the downstream intersection without too much additional delay. On the premise of meeting pedestrian crossing requirements, the proposed method can improve signal coordination between the midblock crossing and the downstream intersection. We tested the performance of the two kinds of AMCC control methods in SUMO simulations with extensive sensitivity analyses. Results showed that the two AMCC controls reduce vehicle delay when compared to Fixed and Pelican controls. AMCC' pedestrian delay is greater than that of Pelican while much smaller than that of Fixed. When comparing AMCC-band and AMCC-vehicle, AMCC-vehicle is superior for smaller pedestrian delay and more equitable for two-direction vehicle delay. Nevertheless, AMCC-band is simpler and perhaps a more feasible approach under current transportation infrastructure. Overall, the two AMCC methods are very flexible and can be applied unchanged to synchronized and unsynchronized arterial with existing signal control plans at adjacent intersections. Most importantly, AMCC can be applied to a broader range of traffic conditions, continuously offering relatively low vehicle and pedestrian delay, thereby complementing existing midblock control methods.

Finally, we propose several directions for future research. First, it is com-

mon to see pedestrian islands and two-stage midblock crossings on wide roads. Therefore, a practical problem is how to extend AMCC to multi-stage midblock crossings. In addition, incorporating extension periods (similar to Puffin and PA) in pedestrian phases for AMCC is also worth investigating. Second, the location of a midblock crossing is critical when coordinating with the traffic signals of adjacent intersections. Therefore, the location choice problem could be integrated into a midblock control method. Lastly, we tested our approach on a simulation framework; a field study is highly recommended to learn the real-world feedback and further improve the algorithm. In particular, acquiring feedback from pedestrians and drivers is necessary when applying a new control method.

Chapter 5

CAV Trajectory Control at a Mixed-traffic Intersection: a Deep Reinforcement Learning Approach

5.1 Introduction

With increasing concerns regarding urban congestion, environmental impacts, and human safety, there is a growing demand for innovative solutions to enhance traffic efficiency, reduce vehicle emissions, and improve traveling safety. In recent years, the rapid advancement of CAV technologies has emerged as an up-and-coming solution, garnering significant attention. CV technology facilitates real-time communication not only between V2V but also between V2I, while AV technology enables precise control of vehicle trajectories. The integration of these technologies enables advanced trajectory planning for CAVs and presents opportunities for innovative approaches to enhance traffic operations. Furthermore, as highlighted by [5], it is projected that CVs or AVs may not fully dominate the traffic stream until the 2040s to 2050s. This forecast suggests an extended period of coexistence among conventional HDVs, CVs, CAVs, and other road users like pedestrians, leading to a mixed traffic environment. Therefore, it becomes imperative to address the complexity of trajectory control in such mixed traffic scenarios, accommodating HDVs, CAVs, and pedestrians. This approach is essential for fostering efficient and

sustainable traffic management.

CAV trajectory control can be broadly categorized into two primary objectives: enhancing traffic efficiency or reducing emissions. Most studies in this field emphasize the optimal control-based approach. Initially, in fully CAV environments, significant research has focused on optimizing CAV trajectory at intersections and exploring joint optimization of CAV trajectory and traffic signal timing [155]. This effort aims to facilitate CAV passage on green lights or enable preemptive speed adjustments to avoid unnecessary stops. Meanwhile, to reduce vehicle emissions, CAV trajectory planning is integrated into the development of eco-driving systems. These systems optimize speed harmonization based on predictions of preceding vehicles and signal timing. Examples include eco-cooperative adaptive cruise control (Eco-CACC) [193] and optimal eco-driving control utilizing CAV communication with traffic signals. Subsequently, considerable research has been dedicated to CAV trajectory control in mixed-traffic environments involving both CAVs and HDVs. For instance, [194] explored cooperative signal timing and trajectory optimization strategies to enhance traffic efficiency. Additionally, eco-driving optimization models have been developed to improve energy efficiency at signalized intersections in mixed traffic scenarios [195]. Although much of the aforementioned research focuses on mixed traffic, the majority of studies are centered around signalized intersections. Few studies are addressing CAV trajectory control at unsignalized intersections, such as those employing reservation-based methods [196] or dynamic controllers utilizing RL policy [197]. Furthermore, beyond the mixed traffic of CAVs and HDVs, there are studies examining CAV control at signal-free intersections when CAVs share the road with pedestrians, as seen in [198].

To sum up, firstly, it's important to note that the research discussed above is primarily conducted in fully CAV environments and focused on signalized intersections. The evidence presented highlights a notable gap in the literature regarding mixed traffic scenarios that comprehensively integrate all road users, including CAVs, HDVs, and pedestrians. Secondly, while much research

focuses on enhancing traffic efficiency or reducing vehicle emissions, there is a tendency to overlook the critical aspect of safety improvement. Lastly, a key limitation in these studies is the assumption that all CAVs possess complete awareness of other vehicles and can make global decisions. However, the presence of CAVs from various manufacturers can pose challenges to information sharing. Moreover, many researchers tend to propose system-optimal controls based on the aforementioned assumptions. Nonetheless, it's essential to recognize that optimal control methods may encounter computational challenges as traffic demand increases. Instead, there should be a greater emphasis on individual user considerations, with each vehicle making driving decisions based on its own best interests.

To address the above research gap, we propose an RL-based trajectory control algorithm for CAVs in a mixed-traffic intersection. We aim to examine CAVs' capabilities in enhancing traffic efficiency, reducing emissions, improving safety, and how these capabilities are influenced by different CAV penetration rates. The acceleration of the CAV is optimized through the deep deterministic policy gradient (DDPG) [199] algorithm to maximize a reward function that considers safety, energy efficiency, and traffic efficiency. By verifying the proposed algorithm in SUMO, we found that the proposed CAV control method significantly improves traffic efficiency and reduces fuel consumption, with a notable reduction in vehicle-vehicle and vehicle-pedestrian conflicts. To summarize, our major contributions include:

- We propose an RL-based trajectory control algorithm for CAVs in the mixed traffic scenario.

- We consider multiple control objectives that include enhancing traffic efficiency, safety, and reducing emission.

- We evaluate the control performances under different CAV penetration rates to verify the CAV benefits.

5.2 Problem Formulation

5.2.1 Reinforcement learning

RL has demonstrated remarkable success across a spectrum of domains. A notable achievement thus far resides in its application to gameplay [200] and signal control [201], showcasing a program with this approach capable of completing tasks with certain expertise. RL stands out as a strong technique within the realm of CAV, offering substantial potential to support safety measures in self-driving operations. Furthermore, RL represents a flexible approach, facilitating rapid decision-making and real-time responses. Rooted in the dynamic interplay between an agent (vehicle) and its surrounding (traffic environment), RL entails the agent undertaking diverse actions and receiving corresponding rewards for each action. RL operates as a model-free algorithm, ignoring the need for detailed probabilistic modeling of the environment. This attribute empowers RL to adapt to unfamiliar and previously unobserved scenarios through trial-and-error learning, making it particularly well-suited for autonomous driving applications.

RL is an interdisciplinary area of machine learning and optimal control that serves as a methodology for teaching intelligent agents control strategies in dynamic environments through iterative experimentation as described by Sutton and Barto [202]. These agents engage with the environment by executing actions and leveraging ensuing feedback (comprising rewards and subsequent states) to reinforce behaviors conducive to achieving desired objectives. RL usually states the learning problem in the form of a Markov decision process (MDP). At each step t, the agent observes a state S_t in the environment, chooses an action a_t, gets a reward r_{t+1}, and the environment transitions to the next state S_{t+1}. An MDP comprises multiple terms $(\mathcal{S}, \mathcal{A}, \mathcal{P}, \mathcal{R})$ with the following conditions:

- 1) $\mathcal{S}$ is a finite set of all possible states ($s \in \mathcal{S}$).

- 2) $\mathcal{A}$ is a set of actions that an agent can perform ($a \in \mathcal{A}$).

- 3) $\mathcal{P} : \mathcal{S} \times \mathcal{A} \times \mathcal{S} \rightarrow [0,1]$ is the state transition that provides the probability that an agent in the state will arrive in another state after acting.

- 4) $\mathcal{R} : \mathcal{S} \times \mathcal{A} \times \mathcal{S} \rightarrow \mathbb{R}$ is the immediate scalar reward which the agent will receive when it executes an action in a state and arrives to a new state.

The probability of taking action a_t in the state s_t at a discrete time step t is called policy π. The primary objective of an agent is to determine a policy $\pi : S \rightarrow A$, and the probability can be expressed as follows:

$$\pi\left(a_t \mid s_t\right) = P\left[A = a_t \mid S = s_t\right].\tag{5.1}$$

Many RL algorithms, such as Q-learning, establish and refine a value function $Q(s,a) : \mathcal{S} \times \mathcal{A} \rightarrow \mathbb{R}$, where these values directly signify the potential returns achievable from various states by taking different actions. Upon discovering the optimal value function Q^*, determining the optimal policy π^* for the agent becomes straightforward:

$$\pi^*(s) = \arg\max_a Q^*(s,a).\tag{5.2}$$

The RL process entails two primary stages: 1) The agent tries to explore its environment by taking random actions; 2) The agent exploits prior knowledge by taking advantage of the exploration phase and follows an optimal policy π_* to achieve the best action by maximizing the cumulative future discounted reward or return:

$$R_t = r_t + \gamma r_{t+1} + \gamma^2 r_{t+2} + \ldots + \gamma^T r_{t+T} = \sum_{k=0}^{T} \gamma^k r_{t+k},\tag{5.3}$$

where $\gamma \in [0,1]$ represents the discount factor that penalizes future rewards, r_t is the reward at time t, and T represents the end time of the episode.

5.2.2 Deep deterministic policy gradient

In general, RL algorithms can be categorized into two main classes based on whether the agent learns a model of the environment: model-free RL and

model-based RL. In model-based RL, the agent utilizes a model of the environment to make decisions, which can be either learned from data (e.g., Model-Based Value Expansion (MBVE) [203]) or a given model (e.g., AlphaZero [204]). Alternatively, model-free RL exclusively relies on trial-and-error learning, eschewing explicit modeling of the environment, and can also be regarded as deep reinforcement learning (DRL). Within the realm of model-free RL, we can further classify techniques into two main categories: (i) Q-learning, characterized by discrete algorithms exemplified by Deep Q-Networks (DQN) [205]; and (ii) policy optimization, comprising continuous algorithms. This category includes the stochastic policy approach (e.g., Asynchronous Advantage Actor-Critic (A2C/A3C) [206]) as well as the deterministic technique (e.g., Deep Deterministic Policy Gradient (DDPG) [199]).

As to CAV driving, action spaces manifest as continuous variables. For instance, steering angles can range from -90° to 90°, while acceleration spans from zero to a certain high value. Traditional value-based methods struggle with such continuous action spaces, often resulting in poor performance. Consequently, our project employs policy-based methods to navigate these challenges. Simultaneously, random exploration poses significant risks in autonomous driving, potentially leading to unforeseen outcomes and terrible consequences. To mitigate this, we've used the DDPG algorithm in our research. DDPG offers a deterministic approach to action selection and stochasticity for a more reliable decision-making process. DDPG stands out by combining the strengths of deterministic policy gradient algorithms, actor-critics, and deep Q-networks. This combination empowers our system to solve the complexities of CAV driving with enhanced stability and performance.

In this research, we employ DDPG which combines actor-critics and DQN based on the Deterministic Policy Gradient (DPG) algorithm. As to DPG, a stochastic policy can be defined as:

$$\pi_\theta = P[a|s;\theta]. \tag{5.4}$$

Then the corresponding gradient is:

$$\nabla_\theta J\left(\pi_\theta\right) = E_{s\sim p^\pi, a\sim\pi_\theta}\left[\nabla_\theta \log \pi_\theta(a|s)Q^\pi(s,a)\right].\qquad(5.5)$$

To explore the environment effectively, the DPG algorithm employs off-policy learning, drawing inspiration from actor-critic algorithms. In this setup, DPG consists of two key components: an actor, responsible for learning the policy, and a critic, tasked with estimating the Q-value function. The actor generates actions based on the current state of the environment, while the critic evaluates these actions, providing feedback for improvement. Assuming the function parameters for the critic and actor are denoted by μ and θ respectively, the gradient for the deterministic policy is then formulated as follows:

$$\nabla_\theta J\left(\mu_\theta\right) = E_{s\sim p^\mu}\left[\nabla_\theta\mu_\theta(s)\nabla_a Q^\mu(s,a) \mid a = \mu_\theta(s)\right].\qquad(5.6)$$

For exploration of stochastic policy β and off-deterministic policy $\mu_\theta(s)$, we can derive the off-policy policy gradient:

$$\nabla_\theta J_\beta\left(\mu_\theta\right) = E_{s\sim p^\beta}\left[\nabla_\theta\mu_\theta(s)\nabla_a Q^\mu(s,a) \mid a = \mu_\theta(s)\right].\qquad(5.7)$$

The DDPG algorithm closely resembles the DPG algorithm, with one notable distinction: it utilizes DQN function approximators for both the actor and critic. For the actor and critic networks, the parameters w and θ are updated respectively according to:

$$\theta' = \tau\theta + (1-\tau)\theta',\qquad(5.8)$$

$$w' = \tau w + (1-\tau)w',\qquad(5.9)$$

where τ is the target update rate. This allows for effective learning in large state and action spaces in an online manner. The DDPG algorithm incorporates the use of target networks, whereby separate copies of both the actor and critic networks are created. These target networks serve the purpose of providing target values during training. The weights of these target networks are updated at fixed intervals.

5.2.3 Proposed architecture

This study addresses the challenge of efficiently, safely, and energy-effectively controlling CAVs as they navigate through a signal-free intersection scenario. We consider various road participants, including CAVs, HDVs, and pedestrians, in a mixed-traffic condition. Real-world driving is a complex task that contains multiple modules such as sensing and control. Here, as we focus on examining the potential of RL-based trajectory control for CAVs in mixed traffic environments, we simplify the problem to only control the acceleration of CAVs and assume that the CAVs have perfect sensing and communication capabilities. The whole proposed architecture is illustrated in Fig. 5.1.
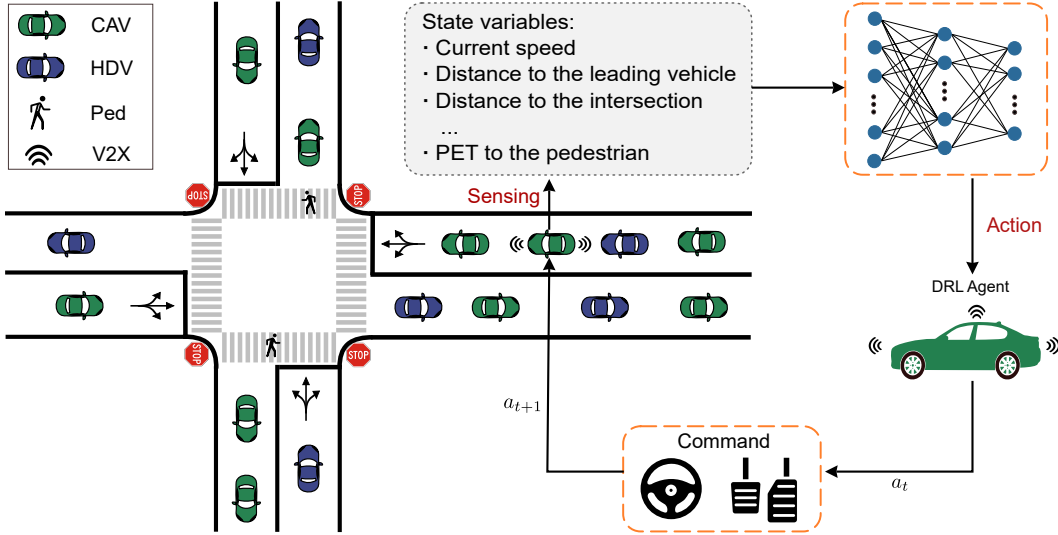
Figure 5.1: The illustration of the proposed model for the CAV control.

Following the default setting in the SUMO environment, the action space at each step for each CAV is in the range of $[-4.5, 2.6]$ m/s^2 for acceleration. Other details of the RL-based CAV trajectory control are elaborated as follows.

State variables:

We assume each CAV can observe the state variables listed in Table 5.1 for making actions. All state variables with float values are normalized to a comparable scale before being fed into the neural network, while one-hot encoding is used as binary variables. The state variables are fed into the actor-network

to generate the acceleration action for the CAV.

In contrast to conventional car-following models that only focus on the leading vehicles, we use a richer set of state variables in our RL-based CAV trajectory control. For instance, we use the distance to both the leading vehicle and the following vehicle; this enables the algorithm to stabilize the traffic flow and reduce stop-and-go waves. Moreover, we consider the distance to the intersection and information regarding whether vehicle conflicts exist at the junction, allowing the CAV to adjust its speed in advance to avoid potential conflicts. The distance to the nearest pedestrian with conflict and the expected Pedestrian Encounter Time (PET)[207] are included to take preemptive actions to enhance pedestrian safety, where PET is defined as the time interval between the moment when a road user (e.g., a pedestrian) leaves the area of conflict and the moment when another road user (e.g., a vehicle) enters that same space. These state variables are designed to provide comprehensive information to the CAV, enabling it to make informed decisions in various traffic scenarios.

Reward function:

As we aim to enhance traffic efficiency, safety, and energy efficiency, we design a reward function that considers these objectives. The reward function is formulated as follows:

$$\mathcal{R} = \sum_{i,t} \left(w_v * v_{i,t} - w_{\text{fuel}} \times f_{i,t} - w_{\text{safe}} \times S_{i,t}^v - w_{\text{safe}} \times S_{i,t}^p \right), \qquad (5.10)$$

where $v_{i,t}$ is the velocity (m/s) of vehicle i at the t-th simulation step, $f_{i,t}$ is the fuel consumption (mg) of vehicle i at the t-th simulation step, S^v is a safety penalty factor to avoid vehicle-vehicle collisions, S^p is a safety penalty factor to avoid vehicle-pedestrian collisions. w_v, w_{fuel}, and w_{safe} are the weights for velocity, fuel consumption, and safety, respectively. The reward function encourages CAVs to maintain high speeds, reduce fuel consumption, and avoid conflicts with other vehicles and pedestrians. The weights are adjusted to balance the trade-offs between these objectives, as well as to normalize units

Table 5.1: State variables for the RL-based CAV trajectory control.

Description	Type
Cumulative delay	Float
Current acceleration	Float
Current speed	Float
Distance to the leading vehicle	Float
Distance to the following vehicle	Float
The distance to the intersection	Float
The direction of the vehicle	One-hot encoding to differentiate going straight, turning left, or turning right.
The location of the vehicle	One-hot encoding to differentiate the incoming approach, the junction, and the outgoing approach.
Whether a vehicle conflict at the junction will exist if the current speed is maintained	Bool
The distance to the nearest pedestrian with conflict	Float
The expected PET to the nearest pedestrian with conflict	Float

into a similar magnitude.

We use the Time-To-Collision (TTC) [207] as a surrogate measure to design the vehicle-vehicle safety penalty factor. TTC represents the shortest estimated time until potential collision is observed during a conflict between two vehicles. According to the literature [208]–[210], we consider 1.5 s and 3 s as the critical and cautionary TTC thresholds, respectively. The vehicle-vehicle safety penalty factor S^v is a piecewise function that calculates the penalty based on the TTC value:

$$S^{v1} = \begin{cases} 1000 & \text{if} \quad \text{TTC} \leq 0.2 \\ 100 & \text{if} \quad 0 < \text{TTC} \leq 1.5 \\ 10 \times \frac{3-\text{TTC}}{1.5} & \text{if} \quad 1.5 < \text{TTC} \leq 3 \\ 0 & \text{if} \quad \text{TTC} > 3 \end{cases} \tag{5.11}$$

$$S^{v2} = \begin{cases} 100 & \text{if} \quad \text{GAP} \leq 2.5 \\ 0 & \text{if} \quad \text{GAP} > 2.5 \end{cases} \tag{5.12}$$

$$S^v = \max(S^{v1}, S^{v2}) \tag{5.13}$$

where GAP is the bumper-to-bumper distance to the front vehicle.

The calculation of vehicle-pedestrian safety penalty factor is similar to the vehicle-vehicle safety penalty factor. The pedestrian safety penalty factor S^p is a piecewise function that calculates the penalty based on the PET value:

$$S^{p1} = \begin{cases} 1000 & \text{if} \quad \text{PET} \leq 0.5 \\ 100 & \text{if} \quad \text{PET} \leq 1.5 \\ 10 \times \frac{3-\text{PET}}{1.5} & \text{if} \quad 1.5 < \text{PET} \leq 3 \\ 0 & \text{if} \quad \text{PET} > 3 \end{cases} \tag{5.14}$$

$$S^{p2} = \begin{cases} 100 & \text{if} \quad \text{Distance} \leq 1.5 \\ 0 & \text{if} \quad \text{Distance} > 1.5 \end{cases} \tag{5.15}$$

$$S^p = \max(S^{p1}, S^{p2}) \tag{5.16}$$

where Distance is the distance from the vehicle's bumper to the pedestrian.

Note that it is possible to include other factors, such as the comfort of the passengers, the smoothness of the acceleration, and the jerk of the vehicle, into the reward function. However, we focus on the traffic efficiency, safety, and energy efficiency, thus other factors are preserved for other more specific research.

5.3 Experimental Setup

We set up an intersection scenario in the SUMO simulation environment to evaluate the RL-based CAV trajectory control algorithm. The intersection consists of four approaches: northbound, southbound, eastbound, and westbound. Our simulation environment includes 200 meters upstream from the intersection. Each approach has an incoming lane and an outgoing two lanes, and the speed limit is set to 50 km/h.

We set the following demand as a base experimental setup: we set the same vehicle demand of 324 vehicles per hour (vph) for all approaches, with a total of 1296 vph at the intersection. The vehicles arrive following a Poisson distribution; the proportion of left-turn, straight, and right-turn vehicles is 2:5:2. In addition, this research assumes that all vehicles are standard passenger cars, and thus does not account for the potential variation in NO_x emissions that could arise from different vehicle types, or fleet management practices. There are pedestrian crossings at approaching lanes of the intersection, and

the pedestrian demand is set to 36 pedestrians per hour for each of the four crossings.

The control group (CAV penetration rate of 0%) consists of only HDVs; the intersection runs in a first come, first served (FCFS) manner for the control group. While the experimental group includes both CAVs and HDVs, we set the CAV penetration rate from 10%, 25%, 50%, 75%, and 100% to evaluate the performance of the RL-based CAV trajectory control algorithm under different CAV penetration rates.

We set $w_v = 100$, $w_{\text{fuel}} = 20$, and $w_{\text{safe}} = 1$ to balance the trade-offs between velocity, fuel consumption, and safety. The learning rate for the actor-network is set to 0.0001, and the learning rate for the critic network is set to 0.001. The model is trained by the Adam [211] optimizer for 500 episodes with the first 20 episodes as a warm-up using the default SUMO control to initialize the replay buffer. Each episode is a simulation run of 3600 seconds with a random seed and a random CAV penetration rate from 10%, 25%, 50%, 75%, and 100%. This is because we aim for the proposed RL framework to result in a general control model. After training, a single-actor model is applied to all CAVs regardless of the CAV penetration rate. The actor and the critic models are neural networks consisting of two fully connected layers with 32 units and ReLU activation functions. The output of the actor model is normalized into [-4.5, 2.6] m/s^2 to represent the acceleration action, and an adjustment step is taken to ensure vehicle speeds are non-negative. The target update rate τ is set to 0.005, the discount factor γ is set to 0.99, and the exploration noise is 0.1.

5.4 Results and Analyses

In this section, we performed 10 simulations with different initial random seeds for each experimental setting, each simulation lasted 3600 seconds, and we compared the final results by the mean and standard deviation of the 10 simulations.

5.4.1 Travel performance

Table 5.2 presents a comprehensive analysis of various traffic performance metrics as influenced by different rates of CAV penetration, ranging from 0% to 100%. The table lists the mean values and standard deviations for several performance indicators: delay per vehicle (in seconds), number of stops per vehicle, fuel consumption (in kilograms), carbon dioxide emissions (CO_2 in kilograms), and nitrogen oxides emissions (NO_x in grams).

There is a clear trend of decreasing delay times as CAV penetration increases. At 0% CAV penetration rate, the average delay is 22.73 seconds per vehicle, which significantly drops to 12.34 seconds per vehicle at 100% penetration rate. This suggests that CAVs can effectively reduce the traffic congestion and decrease the travel time.

Similarly, the number of stops per vehicle decreases as CAV penetration increases. At 0% CAV penetration, the average number of stops is 1.53 per vehicle, which decreases to 1.12 stops per vehicle at 100% penetration. This indicates that CAVs can optimize traffic flow and reduce the frequency of stops, contributing to smoother traffic operations.

Fuel consumption and emissions also exhibit a decreasing trend with increasing CAV penetration rates. At 0% CAV penetration, the average fuel consumption is 63.34 kg, which decreases to 59.11 kg at 100% penetration. Similarly, CO_2 emissions decreased from 199.46 kg to 185.33 kg, and NO_x emissions decreased from 82.57 g to 73.83 g, which demonstrates the potential environmental benefits of fully implementing CAV technologies, contributing to cleaner air by reducing vehicle emissions. These results suggest that CAV controlling can enhance energy efficiency and reduce environmental impacts.

Moreover, we find that the benefits of using CAVs increase as the CAV penetration rate increases. For example, Table 5.2 shows that there are no significant differences between the control group (0% CAV penetration rate) and the 10% CAV penetration rate group in terms of delay, stops, fuel consumption, CO_2 emissions, and NO_x emissions. However, the benefits of using CAVs become more apparent as the CAV penetration rate increases. Overall, the

data from Table 5.2 strongly suggests that increased CAV penetration corre-lates with improvements in several key traffic performance metrics, including reduced delays, fewer stops, lower fuel consumption, and decreased emissions.

Table 5.2: Performance (mean(std)) under different CAV penetration rates.

CAV Rate	Delay (s/veh)	Stops/veh	Fuel (kg)	CO_2 (kg)	NO_x (g)
0%	22.73 (0.9)	1.53 (0.04)	63.34 (1.2)	199.46 (4.7)	82.57 (1.9)
10%	22.67 (1.0)	1.54 (0.04)	63.52 (1.3)	199.16 (5.0)	82.42 (2.2)
25%	20.23 (0.9)	1.41 (0.03)	62.57 (1.2)	196.18 (4.7)	80.67 (2.0)
50%	17.04 (1.0)	1.37 (0.04)	60.57 (1.3)	189.89 (4.8)	77.22 (2.1)
75%	14.51 (0.9)	1.25 (0.03)	60.36 (1.3)	189.23 (4.5)	76.19 (2.0)
100%	12.34 (0.8)	1.12 (0.03)	59.11 (1.1)	185.33 (4.4)	73.83 (1.9)

Fig. 5.2 comprises two heat maps, representing the velocity profiles of ve-hicles at an intersection under two different CAV penetration rates: 0% and 100% CAV penetration rates, respectively. Each map is plotted on a Cartesian coordinate system where the x-axis and y-axis represent the spatial dimensions of the intersection in meters, and the color scale means vehicle speed in meters per second.

Fig. 5.2 (a) shows the velocity distribution at 0% CAV penetration rate. We can see that the incoming lanes have a longer queue of vehicles compared to the outgoing lanes, which is typical of traditional traffic patterns. Fig. 5.2 (b) illustrates the velocity distribution at 100% CAV penetration rate. In con-trast to Fig. 5.2 (a), the heat map exhibits a more uniform color distribution, particularly around the intersection zone. This indicates a more consistent vehicle speed, suggesting that CAVs maintain steadier speeds even as they navigate through the intersection.

By comparing Fig. 5.2 (a) with Fig. 5.2 (b), we can observe that the queue length is significantly reduced at 100% CAV penetration rate. This suggests that CAVs can effectively optimize traffic flow and reduce congestion at in-tersections, leading to smoother traffic operations and improved travel times. Essentially, the improvement of CAV stems from the elimination of human factors, such as variance in driving behaviors and longer reaction times, which can contribute to traffic congestion and delays.

Overall, the figure illustrates how vehicle velocity distribution at an intersection can be significantly influenced by CAV integration levels, with full CAV penetration facilitating a smoother and more consistent traffic flow. This has broad implications for improving urban transport efficiency, enhancing safety, and reducing environmental impacts.
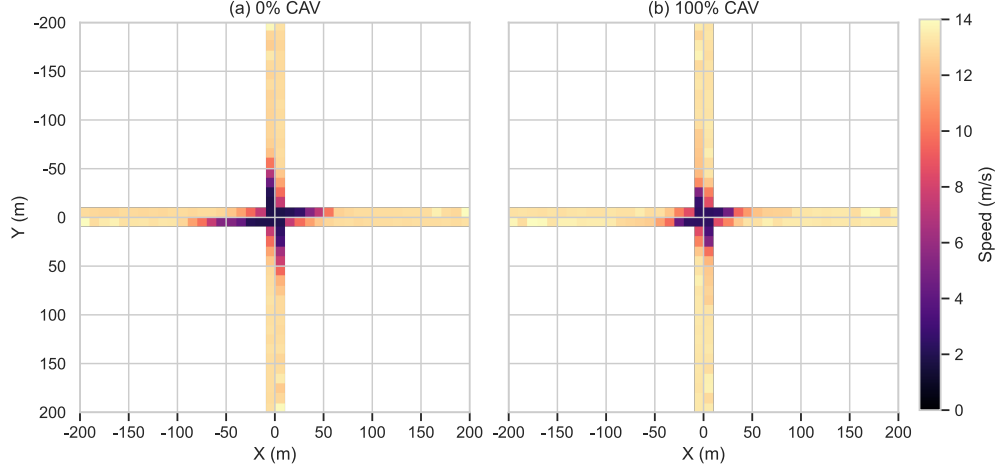
Figure 5.2: The vehicle velocity distribution at the intersection.

5.4.2 Safety evaluation

In our study, we employ surrogate safety measures to comprehensively quantify safety outcomes for both vehicles and pedestrians within the traffic system. For vehicles, we utilize TTC as a primary metric to assess safety performance in different scenarios, including rear-end conflicts and crossing conflicts at intersections. This metric is particularly useful in evaluating how effectively CAV technologies can mitigate the risk of collisions under various traffic conditions. For pedestrian safety, we use the PET to evaluate the risk and severity of crossing conflicts. A lower PET value indicates a higher potential risk of conflict, making it a critical indicator of the effectiveness of pedestrian safety measures implemented with CAV technologies.

The provided Fig. 5.3 consists of two charts, labeled (a) and (b), which illustrate the number of vehicle-vehicle conflicts under varying CAV penetra-

tion rates. The x-axis of the figure displays CAV penetration rates from 0% to 100% in increments of 10%, while the y-axis indicates the number of conflicts. Each figure is further distinguished by different TTC thresholds: less than 1.5 seconds for Fig. 5.3 (a) and less than 3.0 seconds for chart Fig. 5.3 (b).
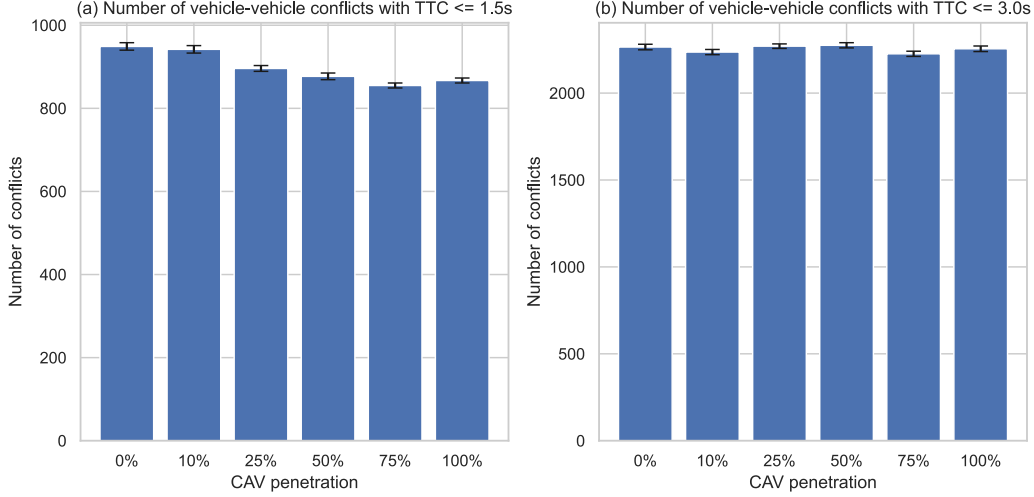
Figure 5.3: The number of vehicle-vehicle conflicts under different CAV penetration rates.

Fig. 5.3 (a) reveals that there is a decreasing trend in the number of conflicts with increasing CAV penetration rates, indicating that using CAV and the RL-based control significantly reduced the vehicle-vehicle conflicts when using the TTC threshold of 1.5 seconds. However, Fig. 5.3 (b) shows the conflict numbers consistently hovering between 1900 and 2000 when using the TTC threshold of 3 seconds, suggesting that the CAV penetration rate does not significantly affect the number of conflicts under this threshold. This indicates that CAVs can effectively reduce vehicle-vehicle conflicts in critical situations where the TTC threshold is less than 1.5 seconds, while the benefits are less pronounced when the threshold is set to 3 seconds.

The provided Fig. 5.4 (a) and (b) detail the number of vehicle-pedestrian conflicts at various CAV penetration rates, categorized by different PET thresholds. In Fig. 5.4 (a), which considers conflicts with a PET of less than or equal to 1.5 seconds, there is a visible trend of decreasing conflicts as CAV penetration increases, starting from approximately 115 conflicts at 0% penetration

and gradually reducing to around 85 conflicts at 100% penetration. This suggests that higher CAV penetration rates may enhance pedestrian safety at this critical threshold.

Fig. 5.4 (b), observing the number of conflicts where PET is less than or equal to 3.0 seconds, exhibits a more constant pattern across different penetration rates. The conflicts range narrowly from about 300 at 0% CAV penetration rate to approximately 270 at 100% penetration rate. The slight decline in conflicts as CAV penetration increases, although modest, supports the notion that CAV integration could marginally improve pedestrian safety even under less stringent conditions.

Overall, Fig. 5.4 illustrates a downward trend in vehicle-pedestrian conflicts as CAV penetration rates increase, indicating the potential safety benefits of autonomous vehicles in urban traffic environments. The findings from these observations can contribute to discussions on transportation safety policy and the role of autonomous technology in enhancing benefits for pedestrians.
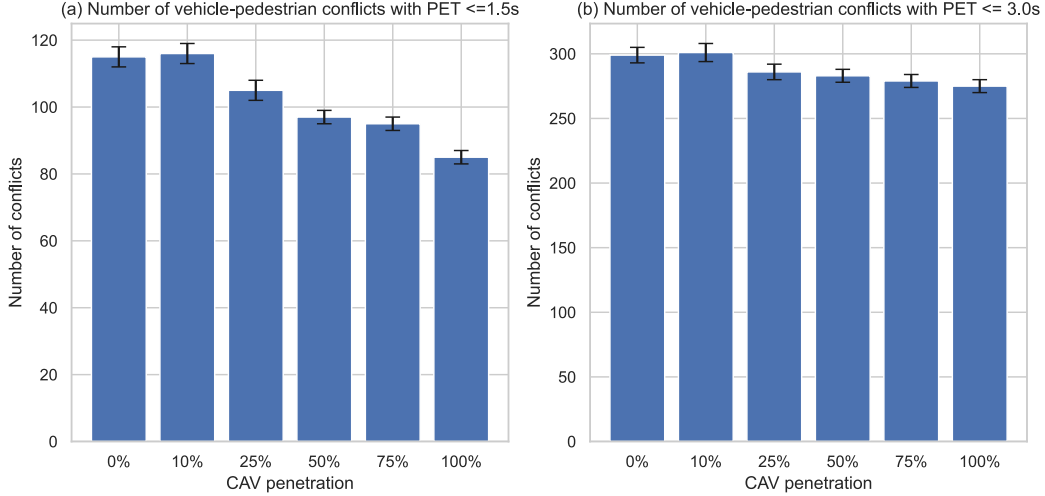
Figure 5.4: The number of vehicle-pedestrian conflicts under different CAV penetration rates.

5.4.3 Sensitivity analysis

To further investigate the impact of CAV at different traffic demand levels, we conducted a sensitivity analysis by varying the vehicle demand ratio from 0.25

to 1.5 times the base demand. The CAV penetration rate is set to 0%, 50% and 100% for this sensitivity analysis. The results regarding the intersection efficiency and surrogate safety measures are shown in Fig. 5.5 and Fig. 5.6, respectively.

From Fig. 5.5 (a), we can see that the average vehicle delay increases as the vehicle demand ratio increases. However, CAVs can effectively mitigate the delays, as we can see that the delay is lower when there is a higher CAV penetration rate. For Fig. 5.6 (b), we can find that the control group (0% CAV penetration rate) reaches the maximum throughput at the vehicle demand ratio of 1.25 and 1.5, while the number of vehicles per hour continues to increase at these demand ratios with a CAV penetration rate of 50% and 100%. This indicates that CAVs can optimize traffic flow and reduce congestion, leading to reduced delays for vehicles.
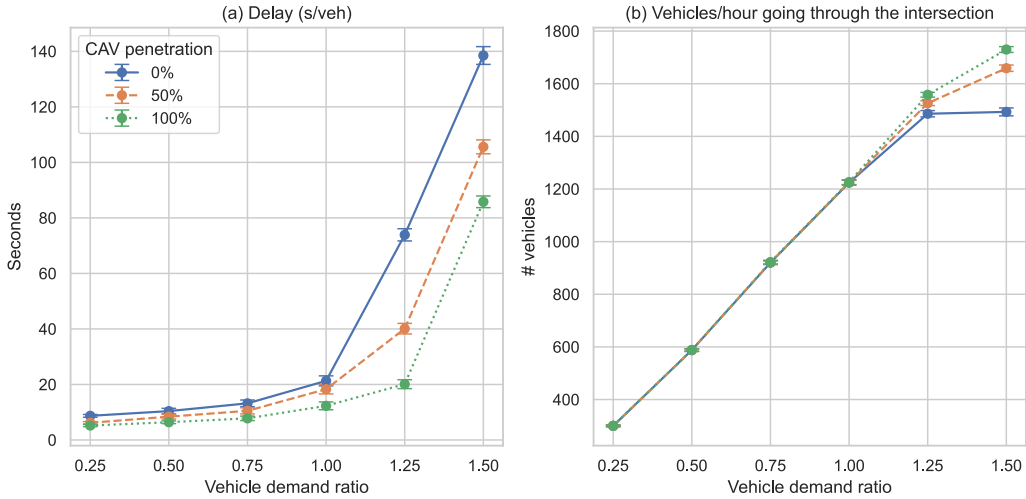
Figure 5.5: Intersection efficiencies regarding different vehicle demand ratios.

Fig. 5.6 (a) and (b) illustrate the surrogate safety measures regarding different vehicle demand ratios, where we use 1.5 seconds as the threshold for both the vehicle-vehicle TTC and vehicle-pedestrian PET conflicts. As shown in Fig. 5.6 (a), the number of vehicle-vehicle conflicts increases with the vehicle demand ratio. The conflicts remain comparable across various CAV penetration rates until the demand ratio reaches 1.25. Beyond this point, at a demand

ratio of 1.5, it is evident that CAVs significantly reduce vehicle-vehicle conflicts. This is because the 1.5 demand ratio exceeds the maximum throughput of the control group, exacerbating the stop-and-go waves and increasing the number of conflicts, whereas the use of CAVs can eliminate the start-up delay, and thus greatly mitigate the conflicts. A similar trend is observed for vehicle-pedestrian conflicts in Fig. 5.6 (b), where CAV usage significantly decreases conflicts, particularly at a demand ratio of 1.5.
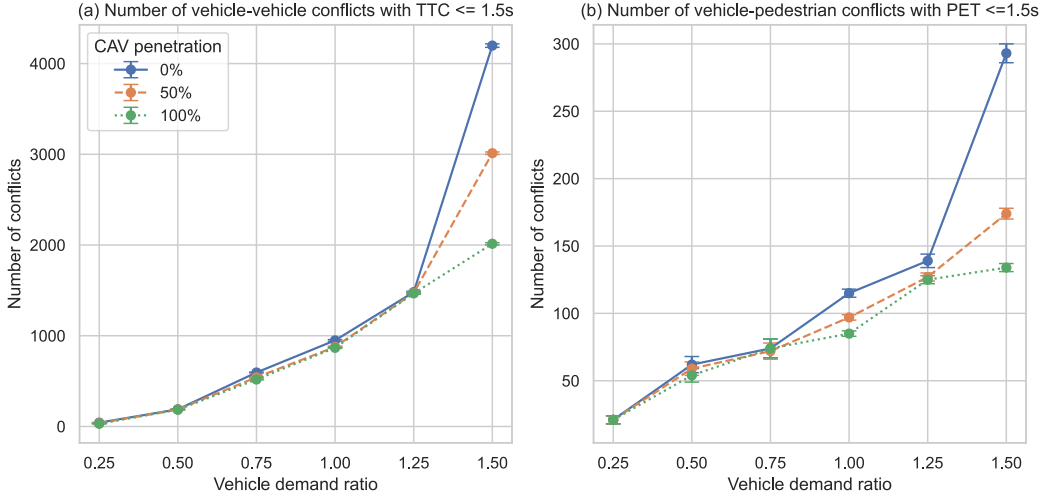
Figure 5.6: Surrogate safety measures regarding different vehicle demand ratios.

Overall, we find through the sensitivity analysis that, although the RL-based CAV trajectory control brings some benefits in the low-demand scenario, the benefits of using CAVs become more apparent as the vehicle demand ratio increases, particularly in the case when the traditional intersection control has reached its maximum throughput.

5.5 Conclusion and Discussions

This study explores how CAVs can enhance traffic efficiency, reduce emissions, and improve safety using an RL-based trajectory control algorithm for CAVs at mixed-traffic intersections. Utilizing the deep deterministic policy gradient algorithm, the CAVs' acceleration is optimized to maximize a reward function

that balances safety, energy efficiency, and traffic efficiency. Empirical validation through SUMO simulations under various CAV penetration rates demonstrates that our CAV control approach notably enhances traffic efficiency and reduces fuel consumption while significantly mitigating both vehicle-vehicle and vehicle-pedestrian conflicts.

While our study provides valuable insights into the potential benefits of CAVs in mixed-traffic environments, several limitations and future research directions should be considered. First, our study assumes perfect sensing and communication capabilities for CAVs, which may not reflect real-world conditions. Future research should consider the impact of sensor noise, communication delays, and other uncertainties on CAV control performance. Second, our study focuses on a single unsignalized intersection scenario, and future research should explore the scalability and generalizability of our CAV control approach to more complex urban traffic networks. Third, our study does not consider the impact of human-driven vehicles on CAV performance, and future research should investigate the interactions between CAVs and human-driven vehicles in mixed-traffic environments. Moreover, our experiment is conducted in a simulated environment, meaning the learning outcomes are based on simulation data, and real-world performance may differ. Therefore, further validation through field tests is necessary to confirm the effectiveness of our CAV control approach in real-world traffic scenarios. Additionally, emissions are sensitive to factors such as vehicle types, fleet composition, and fuel sources, which warrant further real-world testing and analysis to assess the environmental impacts of CAVs accurately.

Chapter 6

Final Conclusion and Future Work

6.1 Summary of Results

With the development of vehicle technology and communication technology, CAV has huge potential to transform the transportation system. However, the deployment of a fully CAV environment faces many challenges, and so it is important to first address the era of mixed autonomy of different road participants like CAVs, HDVs, and pedestrians. There are also urgent requirements to solve traffic-related problems like safety, congestion, energy consumption and environment. This dissertation is devoted to solving traffic management problems in the mixed autonomy environment, including sensing from sparse CAV data, traffic signal control, and trajectory planning for CAVs to provide a safe, efficient and sustainable transportation system.

Chapter 3 firstly attempts to solve the problem of sensing and accurately predicting the full traffic state from sparse CV data in mixed traffic. A novel GP method is introduced to address this challenge. Employing a kernel rotation re-parametrization technique, a conventional isotropic GP kernel transforms into an anisotropic variant, enhancing the modeling of traffic wave propagation within flow data. This innovative approach enables the effective estimation of traffic states using sparse sensing data acquired from fixed sensors, probe vehicles, and CVs, while also offering robust statistical uncertainty quantification, thereby improving reliability. Furthermore, the extension to a

multi-output GP facilitates simultaneous estimation of traffic states across multiple lanes. Experimental results demonstrate its superiority over benchmark methods in terms of accuracy, efficiency, and robustness. Notably applicable to various segments of freeways, highways, or arterials, this methodology significantly contributes to the realm of mixed-traffic systems, like HDVs mixed with CVs. The contributions of this study bear substantial implications for real-time and cost-efficient traffic monitoring, particularly within the context of near-term mixed-traffic scenarios.

Chapter 4 then focuses on a traffic signal control problem in the mixed traffic environment. It especially pays attention to a prevalent real-world scenario: an arterial road with a midblock crossing between two intersections with mixed traffic involving HDVs, CVs, and pedestrians. In such settings, the conventional pushbutton control for midblock crossings often leads to substantial traffic disruptions due to frequent pedestrian crossing requests. The study introduces two adaptive midblock crossing control methods (AMCC-band and AMCC-vehicle). The AMCC-band method utilizes data from adjacent intersections, including SPaT, while the AMCC-vehicle method leverages real-time vehicle location information, particularly from CVs. These methods, compared with baseline models, prioritize pedestrian safety while enhancing signal coordination between midblock crossings and downstream intersections. This optimization effectively reduces both vehicle and pedestrian delays. This study contributes to adaptive and efficient traffic signal control in mixed traffic and expands the application scope of traditional pushbutton control methods, shedding light on the design of a more efficient mixed-traffic system that caters to the diverse needs of vehicles and pedestrians.

Chapter 5 shifts the focus to addressing the trajectory planning challenge for CAVs navigating signal-free intersections in a mix of HDVs, CAVs, and pedestrians. The chapter presents a pioneering trajectory planning framework that merges a deep reinforcement learning algorithm with a multi-agent control strategy. Leveraging the DDPG algorithm, the DRL method empowers CAVs to learn optimal control policies within the complexities of mixed traffic

scenarios. The acceleration of the CAV is optimized through the DDPG algorithm to maximize a reward function that considers safety, energy efficiency, and traffic efficiency. Through evaluation of simulated mixed traffic in SUMO, the proposed framework showcases notable improvements in traffic efficiency, reduction in vehicle emissions, and enhancement of traffic safety. This study contributes significantly to the advancement of intelligent CAVs while offering a promising efficient, safe, and sustainable solution to the trajectory planning puzzle within mixed-traffic environments.

6.2 Limitations and Future Work

In addition to the specific limitations summarized in each chapter, there are some general limitations and future directions for the dissertation. As to Chapter 3 and Chapter 4, the assumed scenario of mixed traffic covers only CVs, HDVs, and pedestrians. The controllability of AVs has not been utilized in the two studies. Only the connectivity and controllability of CAVs in Chapter 5 have been utilized. However, to leverage the full potential of CAVs, the controllability of AVs and the connectivity of CVs should be both considered and used. Second, the methods proposed in Chapter 4 and Chapter 5 are tested in simulation software due to the limitation of field test conditions and the complexity of implementing experiments in reality. However, it is important to implement it in the real world to validate the results and make a difference in the transportation system. To pave the way for more robust future research and innovations, specific directions for future work are proposed based on some specific limitations:

Effective data collection and sensing are vital for the success of our GP-based TSE methods. The quality and quantity of data directly impact how well our methods perform. In our research, we examined three datasets to test how well our methods could adapt to different situations. Looking ahead, as the penetration rate of CVs increases, we need to explore more advanced sensors and data collection techniques to gather richer datasets. For instance,

we could incorporate trajectories obtained from video data to enhance the accuracy and depth of our analysis.

To improve signal optimization, the adaptive midblock crossing control methods are tailored for a specific scenario. To make them more widely applicable, we should expand these methods to cover broader scenarios in the future. As the mixed autonomy specifically covers HDVs, CVs, and pedestrians, gathering input from pedestrians and drivers is essential when implementing a new control method in future work. Additionally, it's crucial to test these methods in real-world settings to assess their effectiveness. While we conducted simulations to validate our approach, conducting field studies is strongly advised to gather real-world feedback and enhance the algorithm further.

For CAV trajectory planning, we tackled a complex scenario involving CAVs, HDVs, and pedestrians—a scenario that has received limited attention in research. Our proposed DRL-based model aims to enhance CAV navigation through intersections, leading to improved traffic efficiency, reduced emissions, and enhanced safety. However, we evaluated the proposed trajectory planning framework solely in a simulated environment. Moving forward, it is imperative to validate the framework's performance in real-world scenarios. Despite the scarcity of research in this area, expanding the framework to encompass even more intricate scenarios is essential for comprehensive evaluation. In addition to exploring learning-based algorithms, considering alternative control algorithms could provide additional ground-truth data for training purposes.

Finally, the dissertation has made significant contributions to the field of mixed traffic management. The proposed methods have shown promising results in enhancing safety, traffic efficiency, and sustainability. However, there is still much work to be done to address the limitations and further improve the proposed methods. By exploring new techniques and validating proposed models in field tests, we can continue to advance the mixed-traffic systems, even within a fully CAV environment. Meanwhile, it is necessary to consider ongoing technology transformations like AI and human interactions, along with ethical considerations, to ensure seamless adaptation to future transportation.

References

[1] H. Company, *How many cars are there in the world in 2024?* Accessed March 04, 2024, Hedges Company, 2024. [Online]. Available: https://hedgescompany.com/blog/2021/06/how-many-cars-are-there-in-the-world/.

[2] B. Pishue, *2022 inrix global traffic scorecard*, Accessed March 04, 2024, INRIX, 2024. [Online]. Available: https://inrix.com/scorecard/.

[3] EPA, *Fast facts: U.s.transportation sector greenhouse gas emissions 1990 –2021*, Accessed March 04, 2024, EPA Offce of Transportation and Air Quality, 2023. [Online]. Available: https://www.epa.gov/system/files/documents/2023-06/420f23016.pdf.

[4] B. N. Silva, M. Khan, and K. Han, "Towards sustainable smart cities: A review of trends, architectures, components, and open challenges in smart cities," *Sustainable cities and society*, vol. 38, pp. 697–713, 2018.

[5] T. Litman, "Autonomous vehicle implementation predictions," 2017.

[6] F. Zheng, C. Liu, X. Liu, S. E. Jabari, and L. Lu, "Analyzing the impact of automated vehicles on uncertainty and stability of the mixed traffic flow," *Transportation research part C: emerging technologies*, vol. 112, pp. 203–219, 2020.

[7] C. Wu, *Learning and Optimization for Mixed Autonomy Systems: A Mobility Context*. University of California, Berkeley, 2018.

[8] Y. Guo, "Connected and automated traffic control at signalized intersections under mixed-autonomy environments," Ph.D. dissertation, University of Cincinnati, 2020.

[9] J. Li, C. Yu, Z. Shen, Z. Su, and W. Ma, "A survey on urban traffic control under mixed traffic environment with connected automated vehicles," *Transportation research part C: emerging technologies*, vol. 154, p. 104 258, 2023.

[10] F. Wu, Z. Cheng, H. Chen, Z. Qiu, and L. Sun, "Traffic state estimation from vehicle trajectories with anisotropic gaussian processes," *Transportation Research Part C: Emerging Technologies*, vol. 163, p. 104 646, 2024, ISSN: 0968-090X. DOI: https://doi.org/10.1016/j.trc.2024.104646. [Online]. Available: https://www.sciencedirect.com/science/article/pii/S0968090X24001670.

[11] F. Wu, H. Chen, K. Hou, Z. Cheng, and T. Z. Qiu, "Adaptive push-button control for signalized pedestrian midblock crossings," *Journal of transportation engineering, Part A: Systems*, vol. 148, no. 4, p. 04 022 011, 2022.

[12] J. B. Kenney, "Dedicated short-range communications (dsrc) standards in the united states," *Proceedings of the IEEE*, vol. 99, no. 7, pp. 1162–1182, 2011.

[13] F. C. Commission *et al.*, "Dedicated short range communications (dsrc) service," *Washington, DC http://wireless. fcc. gov/services/index. htm*, 2019.

[14] D. Jiang and L. Delgrossi, "Ieee 802.11 p: Towards an international standard for wireless access in vehicular environments," in *VTC Spring 2008-IEEE Vehicular Technology Conference*, IEEE, 2008, pp. 2036–2040.

[15] S. Chen, J. Hu, Y. Shi, *et al.*, "Vehicle-to-everything (v2x) services supported by lte-based systems and 5g," *IEEE Communications Standards Magazine*, vol. 1, no. 2, pp. 70–76, 2017.

[16] C. R. Storck and F. Duarte-Figueiredo, "A survey of 5g technology evolution, standards, and infrastructure associated with vehicle-to-everything communications by internet of vehicles," *IEEE access*, vol. 8, pp. 117 593–117 614, 2020.

[17] S. International, "Taxonomy and definitions for terms related to driving automation systems for on-road motor vehicles," *SAE Int.*, vol. 4970, no. 724, pp. 1–5, 2018.

[18] M. M. Rana and K. Hossain, "Connected and autonomous vehicles and infrastructures: A literature review," *International Journal of Pavement Research and Technology*, vol. 16, no. 2, pp. 264–284, 2023.

[19] S. E. Shladover, "Connected and automated vehicle systems: Introduction and overview," *Journal of Intelligent Transportation Systems*, vol. 22, no. 3, pp. 190–200, 2018.

[20] T. Seo, A. M. Bayen, T. Kusakabe, and Y. Asakura, "Traffic state estimation on highway: A comprehensive survey," *Annual reviews in control*, vol. 43, pp. 128–151, 2017.

[21] M. J. Lighthill and G. B. Whitham, "On kinematic waves ii. a theory of traffic flow on long crowded roads," *Proceedings of the Royal Society of London. Series A. Mathematical and Physical Sciences*, vol. 229, no. 1178, pp. 317–345, 1955.

[22] P. I. Richards, "Shock waves on the highway," *Operations research*, vol. 4, no. 1, pp. 42–51, 1956.

[23] H. J. Payne, "Model of freeway traffic and control," *Mathematical Model of Public System*, pp. 51–61, 1971.

[24] G. B. Whitham, *Linear and nonlinear waves*. John Wiley & Sons, 2011.

[25] A. Aw and M. Rascle, "Resurrection of" second order" models of traffic flow," *SIAM journal on applied mathematics*, vol. 60, no. 3, pp. 916–938, 2000.

[26] H. M. Zhang, "A non-equilibrium traffic model devoid of gas-like behavior," *Transportation Research Part B: Methodological*, vol. 36, no. 3, pp. 275–290, 2002.

[27] S. C. Vishnoi, S. A. Nugroho, A. F. Taha, and C. G. Claudel, "Traffic state estimation for connected vehicles using the second-order aw-rascle-zhang traffic model," *arXiv preprint arXiv:2209.02848*, 2022.

[28] C. Nanthawichit, T. Nakatsuji, and H. Suzuki, "Application of probe-vehicle data for real-time traffic-state estimation and short-term travel-time prediction on a freeway," *Transportation research record*, vol. 1855, no. 1, pp. 49–59, 2003.

[29] L. Mihaylova, R. Boel, and A. Hegyi, "An unscented kalman filter for freeway traffic estimation," *IFAC Proceedings Volumes*, vol. 39, no. 12, pp. 31–36, 2006.

[30] Y. Wang and M. Papageorgiou, "Real-time freeway traffic state estimation based on extended kalman filter: A general approach," *Transportation Research Part B: Methodological*, vol. 39, no. 2, pp. 141–167, 2005.

[31] D. B. Work, S. Blandin, O.-P. Tossavainen, B. Piccoli, and A. M. Bayen, "A traffic model for velocity data assimilation," *Applied Mathematics Research eXpress*, vol. 2010, no. 1, pp. 1–35, 2010.

[32] C. P. Van Hinsbergen, T. Schreiter, F. S. Zuurbier, J. Van Lint, and H. J. Van Zuylen, "Localized extended kalman filter for scalable real-time traffic state estimation," *IEEE transactions on intelligent transportation systems*, vol. 13, no. 1, pp. 385–394, 2011.

[33] M. A. Makridis and A. Kouvelas, "An adaptive framework for real-time freeway traffic estimation in the presence of cavs," *Transportation Research Part C: Emerging Technologies*, vol. 149, p. 104 066, 2023.

[34] L. Mihaylova, R. Boel, and A. Hegyi, "Freeway traffic estimation within particle filtering framework," *Automatica*, vol. 43, no. 2, pp. 290–300, 2007.

[35] M. Treiber and D. Helbing, "Reconstructing the spatio-temporal traffic dynamics from stationary detector data," *Cooperative Transportation Dynamics*, vol. 1, no. 3, pp. 3–1, 2002.

[36] M. Zhong, P. Lingras, and S. Sharma, "Estimation of missing traffic counts using factor, genetic, neural, and regression techniques," *Transportation Research Part C: Emerging Technologies*, vol. 12, no. 2, pp. 139–166, 2004.

[37] D. Ni and J. D. Leonard, "Markov chain monte carlo multiple imputation using bayesian networks for incomplete intelligent transportation systems data," *Transportation research record*, vol. 1935, no. 1, pp. 57–67, 2005.

[38] W. Yin, P. Murray-Tuite, and H. Rakha, "Imputing erroneous data of single-station loop detectors for nonincident conditions: Comparison between temporal and spatial methods," *Journal of Intelligent Transportation Systems*, vol. 16, no. 3, pp. 159–176, 2012.

[39] S. Tak, S. Woo, and H. Yeo, "Data-driven imputation method for traffic data in sectional units of road links," *IEEE Transactions on Intelligent Transportation Systems*, vol. 17, no. 6, pp. 1762–1771, 2016.

[40] Y. Jia, J. Wu, and Y. Du, "Traffic speed prediction using deep learning method," in *2016 IEEE 19th international conference on intelligent transportation systems (ITSC)*, IEEE, 2016, pp. 1217–1222.

[41] B. T. Thodi, Z. S. Khan, S. E. Jabari, and M. Menéndez, "Incorporating kinematic wave theory into a deep learning method for high-resolution traffic speed estimation," *IEEE Transactions on Intelligent Transportation Systems*, 2022.

[42] F. Rempe, P. Franeck, and K. Bogenberger, "On the estimation of traffic speeds with deep convolutional neural networks given probe data," *Transportation research part C: emerging technologies*, vol. 134, p. 103 448, 2022.

[43] Y. Han and S. Ahn, "Estimation of traffic flow rate with data from connected-automated vehicles using bayesian inference and deep learning," *Frontiers in Future Transportation*, vol. 2, p. 644 988, 2021.

[44] R. Shi, Z. Mo, K. Huang, X. Di, and Q. Du, "A physics-informed deep learning paradigm for traffic state and fundamental diagram estimation," *IEEE Transactions on Intelligent Transportation Systems*, vol. 23, no. 8, pp. 11 688–11 698, 2021.

[45] R. Shi, Z. Mo, and X. Di, "Physics-informed deep learning for traffic state estimation: A hybrid paradigm informed by second-order traffic models," in *Proceedings of the AAAI Conference on Artificial Intelligence*, vol. 35, 2021, pp. 540–547.

[46] D. Xu, C. Wei, P. Peng, Q. Xuan, and H. Guo, "Ge-gan: A novel deep learning framework for road traffic state estimation," *Transportation Research Part C: Emerging Technologies*, vol. 117, p. 102 635, 2020.

[47] X. Wang, Y. Wu, D. Zhuang, and L. Sun, "Low-rank hankel tensor completion for traffic speed estimation," *IEEE Transactions on Intelligent Transportation Systems*, vol. 24, no. 5, pp. 4862–4871, 2023.

[48] L. Li, Y. Li, and Z. Li, "Efficient missing data imputing for traffic flow by considering temporal and spatial dependence," *Transportation research part C: emerging technologies*, vol. 34, pp. 108–120, 2013.

[49] T. Seo, T. Kusakabe, and Y. Asakura, "Traffic state estimation with the advanced probe vehicles using data assimilation," in *2015 IEEE 18th International Conference on Intelligent Transportation Systems*, IEEE, 2015, pp. 824–830.

[50] R. Florin and S. Olariu, "On a variant of the mobile observer method," *IEEE Transactions on Intelligent Transportation Systems*, vol. 18, no. 2, pp. 441–449, 2016.

[51] T. Seo and T. Kusakabe, "Probe vehicle-based traffic state estimation method with spacing information and conservation law," *Transportation Research Part C: Emerging Technologies*, vol. 59, pp. 391–403, 2015.

[52] Y. Yuan, H. Van Lint, F. Van Wageningen-Kessels, and S. Hoogendoorn, "Network-wide traffic state estimation using loop detector and floating car data," *Journal of Intelligent Transportation Systems*, vol. 18, no. 1, pp. 41–50, 2014.

[53] T. Seo, T. Kusakabe, and Y. Asakura, "Estimation of flow and density using probe vehicles with spacing measurement equipment," *Transportation Research Part C: Emerging Technologies*, vol. 53, pp. 134–150, 2015.

[54] V. Kyriacou, Y. Englezou, C. G. Panayiotou, and S. Timotheou, "Bayesian traffic state estimation using extended floating car data," *IEEE Transactions on Intelligent Transportation Systems*, 2022.

[55] M. Usama, R. Ma, J. Hart, and M. Wojcik, "Physics-informed neural networks (pinns)-based traffic state estimation: An application to traffic network," *Algorithms*, vol. 15, no. 12, p. 447, 2022.

[56] R. Chen and M. W. Levin, "Traffic state estimation based on kalman filter technique using connected vehicle v2v basic safety messages," in *2019 IEEE Intelligent Transportation Systems Conference (ITSC)*, IEEE, 2019, pp. 4380–4385.

[57] M. Fountoulakis, N. Bekiaris-Liberis, C. Roncoli, I. Papamichail, and M. Papageorgiou, "Highway traffic state estimation with mixed connected and conventional vehicles: Microscopic simulation-based testing," *Transportation Research Part C: Emerging Technologies*, vol. 78, pp. 13–33, 2017.

[58] N. Bekiaris-Liberis, C. Roncoli, and M. Papageorgiou, "Highway traffic state estimation per lane in the presence of connected vehicles," *Transportation research part B: methodological*, vol. 106, pp. 1–28, 2017.

119

[59] M. Treiber, A. Kesting, and R. E. Wilson, "Reconstructing the traffic state by fusion of heterogeneous data," *Computer-Aided Civil and Infrastructure Engineering*, vol. 26, no. 6, pp. 408–419, 2011.

[60] T. Schreiter, H. van Lint, M. Treiber, and S. Hoogendoorn, "Two fast implementations of the adaptive smoothing method used in highway traffic state estimation," in *13th International IEEE Conference on Intelligent Transportation Systems*, IEEE, 2010, pp. 1202–1208.

[61] C. Yang, B. T. Thodi, and S. E. Jabari, "Generalized adaptive smoothing using matrix completion for traffic state estimation," in *2022 IEEE 25th International Conference on Intelligent Transportation Systems (ITSC)*, IEEE, 2022, pp. 787–792.

[62] C. Yang, A. S. V. Ramana, and S. E. Jabari, "Generalized adaptive smoothing based neural network architecture for traffic state estimation," *IFAC-PapersOnLine*, vol. 56, no. 2, pp. 3483–3490, 2023.

[63] P. Hunt, D. Robertson, R. Bretherton, and M. C. Royle, "The scoot online traffic signal optimisation technique," *Traffic Engineering & Control*, vol. 23, no. 4, 1982.

[64] D. I. Robertson and R. D. Bretherton, "Optimizing networks of traffic signals in real time-the scoot method," *IEEE Transactions on vehicular technology*, vol. 40, no. 1, pp. 11–15, 1991.

[65] J. Luk, "Two traffic-responsive area traffic control methods: Scat and scoot," *Traffic engineering & control*, vol. 25, no. 1, 1984.

[66] D. I. Robertson, "'tansyt'method for area traffic control," *Traffic Engineering & Control*, vol. 8, no. 8, 1969.

[67] P. P. Jovanis and J. A. Gregor, "Coordination of actuated arterial traffic signal systems," *Journal of Transportation Engineering*, vol. 112, no. 4, pp. 416–432, 1986.

[68] E. C.-P. Chang, "Guidelines for actuated controllers in coordinated systems," *Transportation Research Record*, vol. 1554, no. 1, pp. 61–73, 1996.

[69] G. E. Shoup and D. Bullock, "Dynamic offset tuning procedure using travel time data," *Transportation Research Record*, vol. 1683, no. 1, pp. 84–94, 1999.

[70] Y. Yin, M. Li, and A. Skabardonis, "Offline offset refiner for coordinated actuated signal control systems," *Journal of transportation engineering*, vol. 133, no. 7, pp. 423–432, 2007.

[71] H. Hu and H. X. Liu, "Arterial offset optimization using archived high-resolution traffic signal data," *Transportation Research Part C: Emerging Technologies*, vol. 37, pp. 131–144, 2013.

[72] R. Ghaman, D. Gettman, L. Head, and P. B. Mirchandani, "Adaptive control software for distributed systems," in *IEEE 2002 28th Annual Conference of the Industrial Electronics Society. IECON 02*, IEEE, vol. 4, 2002, pp. 3103–3106.

[73] D. Gettman, S. G. Shelby, L. Head, D. M. Bullock, and N. Soyke, "Data-driven algorithms for real-time adaptive tuning of offsets in coordinated traffic signal systems," *Transportation Research Record*, vol. 2035, no. 1, pp. 1–9, 2007.

[74] K. Pandit, D. Ghosal, H. M. Zhang, and C.-N. Chuah, "Adaptive traffic signal control with vehicular ad hoc networks," *IEEE Transactions on Vehicular Technology*, vol. 62, no. 4, pp. 1459–1471, 2013.

[75] C. Priemer and B. Friedrich, "A decentralized adaptive traffic signal control using v2i communication data," in *2009 12th international ieee conference on intelligent transportation systems*, IEEE, 2009, pp. 1–6.

[76] A. H. Chow, R. Sha, and Y. Li, "Adaptive control strategies for urban network traffic via a decentralized approach with user-optimal routing," *IEEE Transactions on Intelligent Transportation Systems*, vol. 21, no. 4, pp. 1697–1704, 2019.

[77] F. Luyanda, D. Gettman, L. Head, S. Shelby, D. Bullock, and P. Mirchandani, "Acs-lite algorithmic architecture: Applying adaptive control system technology to closed-loop traffic signal control systems," *Transportation Research Record*, vol. 1856, no. 1, pp. 175–184, 2003.

[78] Q. He, K. L. Head, and J. Ding, "Pamscod: Platoon-based arterial multi-modal signal control with online data," *Transportation Research Part C: Emerging Technologies*, vol. 20, no. 1, pp. 164–184, 2012.

[79] Y. Feng, K. L. Head, S. Khoshmagham, and M. Zamanipour, "A real-time adaptive signal control in a connected vehicle environment," *Transportation Research Part C: Emerging Technologies*, vol. 55, pp. 460–473, 2015.

[80] B. Beak, K. L. Head, and Y. Feng, "Adaptive coordination based on connected vehicle technology," *Transportation Research Record*, vol. 2619, no. 1, pp. 1–12, 2017.

[81] P. S. Wang, P. T. Li, F. R. Chowdhury, L. Zhang, and X. Zhou, "A mixed integer programming formulation and scalable solution algorithms for traffic control coordination across multiple intersections based on vehicle space-time trajectories," *Transportation research part B: methodological*, vol. 134, pp. 266–304, 2020.

[82] C. M. Day, S. Langdon, A. Stevanovic, *et al.*, "Traffic signal systems research: Past, present, and future trends," *Centennial Papers*, 2019.

[83] J. T. Morgan and J. D. Little, "Synchronizing traffic signals for maximal bandwidth," *Operations Research*, vol. 12, no. 6, pp. 896–912, 1964.

[84] J. D. Little, "The synchronization of traffic signals by mixed-integer linear programming," *Operations Research*, vol. 14, no. 4, pp. 568–594, 1966.

[85] C. J. Messer, R. H. Whitson, C. L. Dudek, and E. J. Romano, "A variable-sequence multiphase progression optimization program," *Highway Research Record*, vol. 445, no. 1973, pp. 24–33, 1973.

[86] J. D. Little, M. D. Kelson, and N. H. Gartner, "Maxband: A versatile program for setting signals on arteries and triangular networks," 1981.

[87] E. C. Chang, S. L. Cohen, C. Liu, N. A. Chaudhary, and C. Messer, "Maxband-86: Program for optimizing left-turn phase sequence in multiarterial closed networks," *Transportation Research Record*, 1988.

[88] N. H. Gartner, S. F. Assman, F. Lasaga, and D. L. Hou, "A multiband approach to arterial traffic signal optimization," *Transportation Research Part B: Methodological*, vol. 25, no. 1, pp. 55–74, 1991.

[89] C. Stamatiadis and N. H. Gartner, "Multiband-96: A program for variable-bandwidth progression optimization of multiarterial traffic networks," *Transportation Research Record*, vol. 1554, no. 1, pp. 9–17, 1996.

[90] C. Zhang, Y. Xie, N. H. Gartner, C. Stamatiadis, and T. Arsava, "Amband: An asymmetrical multi-band model for arterial traffic signal coordination," *Transportation Research Part C: Emerging Technologies*, vol. 58, pp. 515–531, 2015.

[91] J. A. Hillier and R. Rothery, "The synchronization of traffic signals for minimum delay," *Transportation Science*, vol. 1, no. 2, pp. 81–94, 1967.

[92] N. H. Gartner, J. D. Little, and H. Gabbay, "Optimization of traffic signal settings by mixed-integer linear programming: Part i: The network coordination problem," *Transportation Science*, vol. 9, no. 4, pp. 321–343, 1975.

[93] L. D'Acierno, G. De Luca, and M. Gallo, "Minimisation of total delay in two-way coordinated arterials," in *Proceedings of the 19th International Conference on Urban Transport and the Environment, UT 2013*, 2013, pp. 41–51.

[94] D. C. Gazis, "Traffic control, time—space diagrams, and networks," in *Traffic Control*, Springer, 1965, pp. 47–63.

[95] A. Anwar, W. Zeng, and S. M. Arisona, "Time–space diagram revisited," *Transportation Research Record*, vol. 2442, no. 1, pp. 1–7, 2014.

[96] B. Coifman, "Time space diagrams for thirteen shock waves," 1997.

[97] L. Ponlathep, "A simple adaptive signal control algorithm for isolated intersections using time-space diagrams," in *13th International IEEE Conference on Intelligent Transportation Systems*, IEEE, 2010, pp. 273–278.

[98]   J. Zheng, H. X. Liu, S. Misgen, K. Schwartz, B. Green, and M. Anderson, "Use of event-based traffic data in generating time–space diagrams for evaluation of signal coordination," *Transportation Research Record*, vol. 2439, no. 1, pp. 94–104, 2014.

[99]   M. K. Hosseini and A. Talebpour, "Traffic prediction using time-space diagram: A convolutional neural network approach," *Transportation Research Record*, vol. 2673, no. 7, pp. 425–435, 2019.

[100] C. M. Day, R. Haseman, H. Premachandra, *et al.*, "Evaluation of arterial signal coordination: Methodologies for visualizing high-resolution event data and measuring travel time," *Transportation Research Record*, vol. 2192, no. 1, pp. 37–49, 2010.

[101] T. M. Brennan Jr, C. M. Day, J. R. Sturdevant, and D. M. Bullock, "Visual education tools to illustrate coordinated system operation," *Transportation research record*, vol. 2259, no. 1, pp. 59–72, 2011.

[102] Q. Wang and M. Abbas, "Visualizing vehicle arrivals in coordinated arterials using a colored pcd concept," in *2017 IEEE 20th International Conference on Intelligent Transportation Systems (ITSC)*, IEEE, 2017, pp. 1–6.

[103] T. Huang, S. Poddar, C. Aguilar, *et al.*, "Building intelligence in automated traffic signal performance measures with advanced data analytics," *Transportation Research Record*, vol. 2672, no. 18, pp. 154–166, 2018.

[104] B. Beak, K. L. Head, and S. Khosravi, "Quantitative analysis of smooth progression in traffic signal systems," *Journal of Transportation Engineering, Part A: Systems*, vol. 144, no. 3, p. 04017082, 2018.

[105] J. Zheng, H. X. Liu, S. Misgen, and G. Yu, "Performance diagnosis tool for arterial traffic signals," *Transportation research record*, vol. 2356, no. 1, pp. 109–116, 2013.

[106] Forest City, *Push button pedestrian signals*, Accessed June 19, 2021, The Forest City Electric Company, 1931. [Online]. Available: https: //www.roads.org.uk/sites/default/files/articles/pedestrian-crossings/ pdf/forestcity.pdf.

[107] T. Deng, Y. Ni, and K. Li, "Pedestrian crossings at mid-block locations: A comparative study of existing signal operations," in *Transportation Research Board 92nd Annual Meeting*, 2013.

[108] N. S. Kim, S. S. Yoon, and D. Yook, "Performance comparison between pedestrian push-button and pre-timed pedestrian crossings at midblock: A korean case study," *Transportation planning and technology*, vol. 40, no. 6, pp. 706–721, 2017.

[109] *Pedestrian hybrid beacon guide–recommendations and case study*, Accessed June 19, 2021, Federal Highway Administration (FHWA), 2014. [Online]. Available: https://safety.fhwa.dot.gov/ped_bike/tools_solve/fhwasa14014/.

[110] *Manual on uniform traffic control devices (mutcd)-2009 edition*, Accessed June 19, 2021, Federal Highway Administration, 2009. [Online]. Available: https://mutcd.fhwa.dot.gov/pdfs/2009/pdf_index.htm.

[111] R. P. Godavarthy, "Effectiveness of a pedestrian hybrid beacon at midblock pedestrian crossings in decreasing unnecessary delay to drivers and a comparison to other systems," Ph.D. dissertation, Kansas State University, 2010.

[112] G. Lu and D. A. Noyce, "Pedestrian crosswalks at midblock locations: Fuzzy logic solution to existing signal operations," *Transportation research record*, vol. 2140, no. 1, pp. 63–78, 2009.

[113] W. Ma, X. Yang, W. Pu, and Y. Liu, "Signal timing optimization models for two-stage midblock pedestrian crossing," *Transportation research record*, vol. 2198, no. 1, pp. 133–144, 2010.

[114] Z. Yang, B. Wang, X. Yan, J. Ma, and W. Tang, "Improving pedestrian hybrid beacon crosswalk by using upstream detection strategy," *Journal of Advanced Transportation*, vol. 2019, 2019.

[115] D. A. Noyce and B. L. Bentzen, "Determination of pedestrian pushbutton activation duration at typical signalized intersections," *Transportation research record*, vol. 1939, no. 1, pp. 63–68, 2005.

[116] J.-D. Schmöcker, S. Ahuja, and M. G. Bell, "Multi-objective signal control of urban junctions–framework and a london case study," *Transportation Research Part C: Emerging Technologies*, vol. 16, no. 4, pp. 454–470, 2008.

[117] A. M. Roshandeh, H. S. Levinson, Z. Li, H. Patel, and B. Zhou, "New methodology for intersection signal timing optimization to simultaneously minimize vehicle and pedestrian delays," *Journal of Transportation Engineering*, vol. 140, no. 5, p. 04 014 009, 2014.

[118] X. Liang, S. I. Guler, and V. V. Gayah, "Traffic signal control optimization in a connected vehicle environment considering pedestrians," *Transportation Research Record*, vol. 2674, no. 10, pp. 499–511, 2020.

[119] N. Teketi and S. S. Pulugurtha, "Effect of pedestrian hybrid beacon signal on operational performance measures at the mid-block location and adjacent signalized intersection," in *Transportation Research*, Springer, 2020, pp. 99–111.

[120] W. Ma and X. Yang, "Signal coordination models for midblock pedestrian crossing and adjacent intersections," in *2009 Second International Conference on Intelligent Computation Technology and Automation*, IEEE, vol. 2, 2009, pp. 193–196.

[121] C. Zheng, G. Ma, J. Wu, X. Zhang, and X. Zhang, "A signal coordination control based on traversing empty between mid-block street crossing and intersection," *Discrete Dynamics in Nature and Society*, vol. 2012, 2012.

[122] C. Yu, W. Ma, H. K. Lo, and X. Yang, "Optimization of mid-block pedestrian crossing network with discrete demands," *Transportation research part B: methodological*, vol. 73, pp. 103–121, 2015.

[123] D. C. Gazis, R. Herman, and R. B. Potts, "Car-following theory of steady-state traffic flow," *Operations research*, vol. 7, no. 4, pp. 499–505, 1959.

[124] G. F. Newell, "Nonlinear effects in the dynamics of car following," *Operations research*, vol. 9, no. 2, pp. 209–229, 1961.

[125] P. G. Gipps, "A behavioural car-following model for computer simulation," *Transportation research part B: methodological*, vol. 15, no. 2, pp. 105–111, 1981.

[126] M. Treiber, A. Hennecke, and D. Helbing, "Congested traffic states in empirical observations and microscopic simulations," *Physical review E*, vol. 62, no. 2, p. 1805, 2000.

[127] K. Katsaros, R. Kernchen, M. Dianati, and D. Rieck, "Performance study of a green light optimized speed advisory (glosa) application using an integrated cooperative its simulation platform," in *2011 7th International Wireless Communications and Mobile Computing Conference*, IEEE, 2011, pp. 918–923.

[128] S. Stebbins, M. Hickman, J. Kim, and H. L. Vu, "Characterising green light optimal speed advisory trajectories for platoon-based optimisation," *Transportation Research Part C: Emerging Technologies*, vol. 82, pp. 43–62, 2017.

[129] M. A. S. Kamal, M. Mukai, J. Murata, and T. Kawabe, "Model predictive control of vehicles on urban roads for improved fuel economy," *IEEE Transactions on control systems technology*, vol. 21, no. 3, pp. 831–841, 2012.

[130] H. Yang and W.-L. Jin, "A control theoretic formulation of green driving strategies based on inter-vehicle communications," *Transportation Research Part C: Emerging Technologies*, vol. 41, pp. 48–60, 2014.

[131] X.-Y. Lu, J. K. Hedrick, and M. Drew, "Acc/cacc-control design, stability and robust performance," in *Proceedings of the 2002 American Control Conference (IEEE Cat. No. CH37301)*, IEEE, vol. 6, 2002, pp. 4327–4332.

[132] K. C. Dey, L. Yan, X. Wang, *et al.*, "A review of communication, driver characteristics, and controls aspects of cooperative adaptive cruise control (cacc)," *IEEE Transactions on Intelligent Transportation Systems*, vol. 17, no. 2, pp. 491–509, 2015.

[133] K. J. Malakorn and B. Park, "Assessment of mobility, energy, and environment impacts of intellidrive-based cooperative adaptive cruise control and intelligent traffic signal control," in *Proceedings of the 2010 IEEE International Symposium on Sustainable Systems and Technology*, IEEE, 2010, pp. 1–6.

[134] X. He, H. X. Liu, and X. Liu, "Optimal vehicle speed trajectory on a signalized arterial with consideration of queue," *Transportation Research Part C: Emerging Technologies*, vol. 61, pp. 106–120, 2015.

[135] H. Yao, J. Cui, X. Li, Y. Wang, and S. An, "A trajectory smoothing method at signalized intersection based on individualized variable speed limits with location optimization," *Transportation Research Part D: Transport and Environment*, vol. 62, pp. 456–473, 2018.

[136] C. Yu, Y. Feng, H. X. Liu, W. Ma, and X. Yang, "Integrated optimization of traffic signals and vehicle trajectories at isolated urban intersections," *Transportation research part B: methodological*, vol. 112, pp. 89–112, 2018.

[137] Y. Feng, C. Yu, and H. X. Liu, "Spatiotemporal intersection control in a connected and automated vehicle environment," *Transportation Research Part C: Emerging Technologies*, vol. 89, pp. 364–383, 2018.

[138] H. Liu, C. E. Flores, J. Spring, S. E. Shladover, and X.-Y. Lu, "Field assessment of intersection performance enhanced by traffic signal optimization and vehicle trajectory planning," *IEEE Transactions on Intelligent Transportation Systems*, vol. 23, no. 8, pp. 11 549–11 561, 2021.

[139] K. Dresner and P. Stone, "A multiagent approach to autonomous intersection management," *Journal of artificial intelligence research*, vol. 31, pp. 591–656, 2008.

[140] M. Hausknecht, T.-C. Au, and P. Stone, "Autonomous intersection management: Multi-intersection optimization," in *2011 IEEE/RSJ International Conference on Intelligent Robots and Systems*, IEEE, 2011, pp. 4581–4586.

[141] Z. Li, M. V. Chitturi, D. Zheng, A. R. Bill, and D. A. Noyce, "Modeling reservation-based autonomous intersection control in vissim," *Transportation research record*, vol. 2381, no. 1, pp. 81–90, 2013.

[142] M. Choi, A. Rubenecia, and H. H. Choi, "Reservation-based autonomous intersection management considering vehicle failures in the intersection," in *2020 International Conference on Information Networking (ICOIN)*, IEEE, 2020, pp. 654–659.

[143] S. A. Fayazi and A. Vahidi, "Mixed-integer linear programming for optimal scheduling of autonomous vehicle intersection crossing," *IEEE Transactions on Intelligent Vehicles*, vol. 3, no. 3, pp. 287–299, 2018.

[144] Z. Li, Q. Wu, H. Yu, *et al.*, "Temporal-spatial dimension extension-based intersection control formulation for connected and autonomous vehicle systems," *Transportation Research Part C: Emerging Technologies*, vol. 104, pp. 234–248, 2019.

[145] A. Mirheli, M. Tajalli, L. Hajibabai, and A. Hajbabaie, "A consensus-based distributed trajectory control in a signal-free intersection," *Transportation research part C: emerging technologies*, vol. 100, pp. 161–176, 2019.

[146] J. Lee and B. Park, "Development and evaluation of a cooperative vehicle intersection control algorithm under the connected vehicles environment," *IEEE transactions on intelligent transportation systems*, vol. 13, no. 1, pp. 81–90, 2012.

[147] A. A. Malikopoulos, C. G. Cassandras, and Y. J. Zhang, "A decentralized energy-optimal control framework for connected automated vehicles at signal-free intersections," *Automatica*, vol. 93, pp. 244–256, 2018.

[148] B. B. Elallid, M. Bagaa, N. Benamar, and N. Mrani, "A reinforcement learning based approach for controlling autonomous vehicles in complex scenarios," in *2023 International Wireless Communications and Mobile Computing (IWCMC)*, IEEE, 2023, pp. 1358–1364.

[149] U. Gunarathna, S. Karunasekara, R. Borovica-Gajic, and E. Tanin, "Intelligent autonomous intersection management," *arXiv preprint arXiv:2202.04224*, 2022.

[150] L. Muthugama, H. Xie, E. Tanin, S. Karunasekera, and U. Gunarathna, "Concurrent optimization of safety and traffic flow using deep reinforcement learning for autonomous intersection management," in *Proceedings of the 30th International Conference on Advances in Geographic Information Systems*, 2022, pp. 1–12.

[151] T. V. Baby, V. Bhattacharyya, P. K. Shahri, A. H. Ghasemi, and B. HomChaudhuri, "A suggestion-based fuel efficient control framework for connected and automated vehicles in heterogeneous urban traffic," *Transportation Research Part C: Emerging Technologies*, vol. 134, p. 103 476, 2022.

[152] M. A. S. Kamal, S. Taguchi, and T. Yoshimura, "Intersection vehicle cooperative eco-driving in the context of partially connected vehicle environment," in *2015 IEEE 18th International Conference on Intelligent Transportation Systems*, IEEE, 2015, pp. 1261–1266.

[153] W. Zhao, D. Ngoduy, S. Shepherd, R. Liu, and M. Papageorgiou, "A platoon based cooperative eco-driving model for mixed automated and human-driven vehicles at a signalised intersection," *Transportation Research Part C: Emerging Technologies*, vol. 95, pp. 802–821, 2018.

[154] M. Pourmehrab, L. Elefteriadou, S. Ranka, and M. Martin-Gasulla, "Optimizing signalized intersections performance under conventional and automated vehicles traffic," *IEEE Transactions on intelligent transportation systems*, vol. 21, no. 7, pp. 2864–2873, 2019.

[155] Y. Guo, J. Ma, C. Xiong, X. Li, F. Zhou, and W. Hao, "Joint optimization of vehicle trajectories and intersection controllers with connected automated vehicles: Combined dynamic programming and shooting heuristic approach," *Transportation research part C: emerging technologies*, vol. 98, pp. 54–72, 2019.

[156] H. Yao and X. Li, "Decentralized control of connected automated vehicle trajectories in mixed traffic at an isolated signalized intersection," *Transportation research part C: emerging technologies*, vol. 121, p. 102 846, 2020.

[157] C. Ma, C. Yu, and X. Yang, "Trajectory planning for connected and automated vehicles at isolated signalized intersections under mixed traffic environment," *Transportation research part C: emerging technologies*, vol. 130, p. 103 309, 2021.

[158] S. Wang, Z. Wang, R. Jiang, R. Yan, and L. Du, "Trajectory jerking suppression for mixed traffic flow at a signalized intersection: A trajectory prediction based deep reinforcement learning method," *IEEE Transactions on Intelligent Transportation Systems*, vol. 23, no. 10, pp. 18 989–19 000, 2022.

[159] M. Hajyan and A. Nikoofard, "Fuzzy control of autonomous vehicle at non-signalized intersection in mixed traffic flow," in *2022 9th Iranian Joint Congress on Fuzzy and Intelligent Systems (CFIS)*, IEEE, 2022, pp. 1–6.

[160] P.-C. Chen, X. Liu, C.-W. Lin, C. Huang, and Q. Zhu, "Mixed-traffic intersection management utilizing connected and autonomous vehicles as traffic regulators," in *Proceedings of the 28th Asia and South Pacific Design Automation Conference*, 2023, pp. 52–57.

[161] M. Klimke, B. Völz, and M. Buchholz, "Automatic intersection management in mixed traffic using reinforcement learning and graph neural networks," in *2023 IEEE Intelligent Vehicles Symposium (IV)*, IEEE, 2023, pp. 1–8.

[162] T. Niels, K. Bogenberger, N. Mitrovic, and A. Stevanovic, "Integrated intersection management for connected, automated vehicles, and bicyclists," in *2020 IEEE 23rd International Conference on Intelligent Transportation Systems (ITSC)*, IEEE, 2020, pp. 1–8.

[163] W. Wu, Y. Liu, W. Hao, G. A. Giannopoulos, and Y.-J. Byon, "Autonomous intersection management with pedestrians crossing," *Transportation research part C: emerging technologies*, vol. 135, p. 103 521, 2022.

[164] Z. Zhu and H. Zhao, "Learning autonomous control policy for intersection navigation with pedestrian interaction," *IEEE Transactions on Intelligent Vehicles*, 2023.

[165] C. E. Rasmussen, C. K. Williams, *et al.*, *Gaussian processes for machine learning*. Springer, 2006, vol. 1.

[166] P. J. Storm, M. Mandjes, and B. van Arem, "Efficient evaluation of stochastic traffic flow models using gaussian process approximation," *Transportation research part B: methodological*, vol. 164, pp. 126–144, 2022.

[167] Y. Yuan, Z. Zhang, X. T. Yang, and S. Zhe, "Macroscopic traffic flow modeling with physics regularized gaussian process: A new insight into machine learning applications in transportation," *Transportation Research Part B: Methodological*, vol. 146, pp. 88–110, 2021.

[168] Z. Cheng, X. Wang, X. Chen, M. Trépanier, and L. Sun, "Bayesian calibration of traffic flow fundamental diagrams using gaussian processes," *IEEE Open Journal of Intelligent Transportation Systems*, vol. 3, pp. 763–771, 2022.

[169] Z. Liu, C. Lyu, Z. Wang, S. Wang, P. Liu, and Q. Meng, "A gaussian-process-based data-driven traffic flow model and its application in road capacity analysis," *IEEE Transactions on Intelligent Transportation Systems*, vol. 24, no. 2, pp. 1544–1563, 2023.

[170] C. Zhang and L. Sun, "Bayesian calibration of the intelligent driver model," *IEEE Transactions on Intelligent Transportation Systems*, 2024.

[171] R. NEAL, "Bayesian learning for neural networks," *Lecture Notes in Statistics*, 1996.

[172] M. Titsias, "Variational learning of inducing variables in sparse gaussian processes," in *Artificial intelligence and statistics*, PMLR, 2009, pp. 567–574.

[173] H. Wackernagel, *Multivariate geostatistics: an introduction with applications*. Springer Science & Business Media, 2003.

[174] E. V. Bonilla, K. Chai, and C. Williams, "Multi-task gaussian process prediction," *Advances in neural information processing systems*, vol. 20, 2007.

[175] NGSIM, "Us highway 101 dataset," 2007. [Online]. Available: https://www.fhwa.dot.gov/publications/research/operations/07030/index.cfm.

[176] R. Krajewski, J. Bock, L. Kloeker, and L. Eckstein, "The highd dataset: A drone dataset of naturalistic vehicle trajectories on german highways for validation of highly automated driving systems," in *2018 21st International Conference on Intelligent Transportation Systems (ITSC)*, 2018, pp. 2118–2125. DOI: 10.1109/ITSC.2018.8569552.

[177] P. A. Lopez, M. Behrisch, L. Bieker-Walz, *et al.*, "Microscopic traffic simulation using sumo," in *2018 21st international conference on intelligent transportation systems (ITSC)*, IEEE, 2018, pp. 2575–2582.

[178] R. B. Gramacy and D. W. Apley, "Local gaussian process approximation for large computer experiments," *Journal of Computational and Graphical Statistics*, vol. 24, no. 2, pp. 561–578, 2015.

[179] British Columbia Ministry of Transportation and Highways, *Pedestrian crossing control manual for british columbia*, Accessed June 19, 2021, Highway Safety Branch, 1994. [Online]. Available: https://www2.gov.bc.ca/gov/content/home.

[180] S. Turner, L. Sandt, J. Toole, R. Benz, and R. Patten, "Federal highway administration university course on bicycle and pedestrian transportation," Tech. Rep. FHWA-HRT-05-133, 2006, Accessed June 19, 2021. [Online]. Available: https://www.fhwa.dot.gov/publications/research/safety/pedbike/05085.

[181] R. Walker, A. Winnett M.and Martin, and J. Kenndey, "Puffin crossing operation and behavior study," Tech. Rep. Report No. PPR239, 2005, Accessed June 19, 2021. [Online]. Available: https://content.tfl.gov.uk/puffin-behaviour-report.pdf.

[182] J. Hunt and G. Lyons, "Enhanced operating strategies to improve pedestrian amenity and safety at midblock signalled pedestrian crossings," PTRC, 1997.

[183] V. Gan, *Ask citylab: Do 'walk' buttons actually do anything?* Accessed June 19, 2021, Bloomberg CityLab, 2015. [Online]. Available: https://www.bloomberg.com/news/articles/2015-09-02/do-pedestrian-push-to-walk-buttons-actually-work.

[184] B. J. Campbell, C. V. Zegeer, H. H. Huang, and M. J. Cynecki, "A review of pedestrian safety research in the united states and abroad," Tech. Rep. FHWA-RD-03-042, 2004, Accessed June 19, 2021. [Online]. Available: https://www.fhwa.dot.gov/publications/research/safety/pedbike/03042.

[185] A. Ragusea, *Crosswalk buttons don't do anything! except when they do*, Accessed June 19, 2021, Radio Boston, 2010. [Online]. Available: https://www.wbur.org/radioboston/2010/05/10/walk-buttons.

[186] R. Van Houten, R. Ellis, and J.-L. Kim, "Effects of various minimum green times on percentage of pedestrians waiting for midblock "walk" signal," *Transportation research record*, vol. 2002, no. 1, pp. 78–83, 2007.

[187] N. Papola and G. Fusco, "Maximal bandwidth problems: A new algorithm based on the properties of periodicity of the system," *Transportation Research Part B: Methodological*, vol. 32, no. 4, pp. 277–288, 1998.

[188] R. P. Brent, *Algorithms for minimization without derivatives*. Courier Corporation, 2013.

[189] L. Breiman, "Random forests," *Machine learning*, vol. 45, no. 1, pp. 5–32, 2001.

[190] F. Pedregosa, G. Varoquaux, A. Gramfort, *et al.*, "Scikit-learn: Machine learning in python," *the Journal of machine Learning research*, vol. 12, pp. 2825–2830, 2011.

[191] *Average vehicle occupancy factors for computing travel time reliability measures and total peak hour excessive delay metrics*, Accessed June 19, 2021, Federal Highway Administration (FHWA), 2018. [Online]. Available: https://www.fhwa.dot.gov/tpm/guidance/avo_factors.pdf.

[192] X. J. Liang, S. I. Guler, and V. V. Gayah, "An equitable traffic signal control scheme at isolated signalized intersections using connected vehicle technology," *Transportation Research Part C: Emerging Technologies*, vol. 110, pp. 81–97, 2020.

[193] H. Yang, H. Rakha, and M. V. Ala, "Eco-cooperative adaptive cruise control at signalized intersections considering queue effects," *IEEE Transactions on Intelligent Transportation Systems*, vol. 18, no. 6, pp. 1575–1585, 2016.

[194] M. Tajalli and A. Hajbabaie, "Traffic signal timing and trajectory optimization in a mixed autonomy traffic stream," *IEEE Transactions on Intelligent Transportation Systems*, vol. 23, no. 7, pp. 6525–6538, 2021.

[195] H. Jiang, J. Hu, S. An, M. Wang, and B. B. Park, "Eco approaching at an isolated signalized intersection under partially connected and automated vehicles environment," *Transportation Research Part C: Emerging Technologies*, vol. 79, pp. 290–307, 2017.

[196] X. Huang and P. Lin, "Reservation-based dedicated lane method for mixed autonomous and human-operated vehicles at intersections," in *Journal of Physics: Conference Series*, IOP Publishing, vol. 1910, 2021, p. 012 006.

[197] R. Bautista-Montesano, R. Galluzzi, K. Ruan, Y. Fu, and X. Di, "Autonomous navigation at unsignalized intersections: A coupled reinforcement learning and model predictive control approach," *Transportation research part C: emerging technologies*, vol. 139, p. 103 662, 2022.

[198] L. M. Hulse, "Pedestrians' perceived vulnerability and observed behaviours relating to crossing and passing interactions with autonomous vehicles," *Transportation research part F: traffic psychology and behaviour*, vol. 93, pp. 34–54, 2023.

[199] T. P. Lillicrap, J. J. Hunt, A. Pritzel, *et al.*, "Continuous control with deep reinforcement learning," *arXiv preprint arXiv:1509.02971*, 2015.

[200] G. Tesauro, "Td-gammon, a self-teaching backgammon program, achieves master-level play," *Neural computation*, vol. 6, no. 2, pp. 215–219, 1994.

[201] H. Wei, G. Zheng, H. Yao, and Z. Li, "Intellilight: A reinforcement learning approach for intelligent traffic light control," in *Proceedings of the 24th ACM SIGKDD international conference on knowledge discovery & data mining*, 2018, pp. 2496–2505.

[202] R. S. Sutton and A. G. Barto, "Reinforcement learning: An introduction," *Robotica*, vol. 17, no. 2, pp. 229–235, 1999.

[203] V. Feinberg, A. Wan, I. Stoica, M. I. Jordan, J. E. Gonzalez, and S. Levine, "Model-based value estimation for efficient model-free reinforcement learning," *arXiv preprint arXiv:1803.00101*, 2018.

[204] D. Silver, T. Hubert, J. Schrittwieser, *et al.*, "Mastering chess and shogi by self-play with a general reinforcement learning algorithm," *arXiv preprint arXiv:1712.01815*, 2017.

[205] V. Mnih, K. Kavukcuoglu, D. Silver, *et al.*, "Playing atari with deep reinforcement learning," *arXiv preprint arXiv:1312.5602*, 2013.

[206] V. Mnih, A. P. Badia, M. Mirza, *et al.*, "Asynchronous methods for deep reinforcement learning," in *International conference on machine learning*, PMLR, 2016, pp. 1928–1937.

[207] D. Gettman, L. Pu, T. Sayed, S. G. Shelby, S. Energy, *et al.*, "Surrogate safety assessment model and validation," Turner-Fairbank Highway Research Center, Tech. Rep., 2008.

[208] J. C. Hayward, "Near miss determination through use of a scale of danger," 1972.

[209] T. Sayed, G. Brown, and F. Navin, "Simulation of traffic conflicts at unsignalized intersections with tsc-sim," *Accident Analysis & Prevention*, vol. 26, no. 5, pp. 593–607, 1994.

[210] B. L. Allen, B. T. Shin, and P. J. Cooper, "Analysis of traffic conflicts and collisions," Tech. Rep., 1978.

[211] D. P. Kingma and J. Ba, "Adam: A method for stochastic optimization," *arXiv preprint arXiv:1412.6980*, 2014.